Developing a methodology for the assessment of wave energy along the South African Coast

by

Bafana Gweba

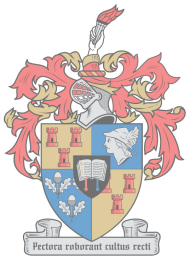

UNIVERSITEIT
iYUNIVESITHI
STELLENBOSCH
UNIVERSITY

Thesis presented in partial fulfilment of the requirements for the degree of Master of Science in Applied Mathematics in the Faculty of Science at Stellenbosch University

Supervisors:

Dr. G.P.J. Diedericks
Dr. J. Wilms
Dr. C. Rautenbach

March 2018

Declaration

By submitting this thesis electronically, I declare that the entirety of the work contained therein is my own, original work, that I am the sole author thereof (save to the extent explicitly otherwise stated), that reproduction and publication thereof by Stellenbosch University will not infringe any third party rights and that I have not previously in its entirety or in part submitted it for obtaining any qualification.

Date: March 2018

Abstract

Ocean wave energy can become one of the alternative energy resources for fossil-fuelled power generation in South Africa. Due to global warming, several studies about the generation of wave energy have been done to find cleaner and sustainable renewable energy resources. An array of Wave Energy Converters (WECs) in a form of a wave farm may be used to harness the energy resource to generate electricity. Nearshore wave field effects due to the presence of a wave farm must be investigated particularly at the coastline as it will be affected. The principal objective of this thesis is to investigate the impacts induced by a wave farm on the nearshore wave field region through numerical modelling. Another objective is to give guidance about some of the parameters and input conditions for numerical modelling of wave transformations.

In the present study, wave conditions have been assessed at selected locations of the South African coast. The JONSWAP model, which is the most frequently used spectral model to describe wind-generated waves, was used to represent wave energy spectrum along chosen locations. The JONSWAP model was fitted into the measured data along the coast to obtain the peak enhancement factor (gamma) values for chosen locations. The measured data was found to consist of bimodal spectra, local winds and distant storms and also multiple peaks in the spectra were observed. The spectral decomposition method was then applied to split the data into wind sea and swell to assess a more realistic description of the wave system. It was found that the method is effective in splitting bimodal spectra but is not successful in multi-peaked spectra.

Saldanha Bay was chosen as the case study for installation of a wave farm due to its abundance of wave energy. A nested numerical wave model, referred to as SWAN (Simulating WAves Nearshore), was used to simulate the nearshore wave field conditions in Saldanha Bay. The obtained gamma value for Saldanha Bay was used to set the wave model. Two model simulations in the study were considered, model simulations in the presence of a wave farm and model simulations in the absence of a wave farm. The difference in significant wave height and wave energy spectrum with and without the wave farm was assessed.

The results show a reduction in significant wave height and a change in wave energy spectrum at the selected output locations. A gradual redirection of waves induced by the presence of wave farm has been observed for all selected boundary wave direction conditions. The overall results of the study indicate the change in the nearshore wave field during the presence of wave farm. A sensitivity assessment was conducted to investigate the change in wave energy due to the orientation of the original wave farm layout and the addition of two devices in the original wave farm layout.

A proposed methodology for the assessment of wave energy was presented to evaluate the wave energy resource along the South African coast. The proposed methodology is based on analysis that was conducted in the study.

Uittreksel

Oseaangolfenergie kan een van die alternatiewe energiebronne op fossielbrandstowwe word vir kragopwekking in Suid-Afrika. Aardverwarming het meegebring dat verskeie studies oor die benutting van golfenergie gedoen is ten einde skoner en meer volhoubare hernubare energiebronne te vind. Daar is bevind dat 'n versameling golfenergie-omsetters (GEOs) in 'n golfplaas aangewend kan word as energiebron vir die opwekking van elektrisiteit. Die effek van sulke golfplase op die golfveld van die aangrensende kuslyn word in hierdie proefskrif ondersoek ten einde te bepaal hoe die kus geraak sal word. Die hoofdoel van hierdie proefskrif is om die impak van so 'n golfplaas op die omliggende golfveld van die kuslyn te ondersoek.

In die huidige proefskrif is 'n beraming van golftoestande op geselekteerde plekke aan die Suid-Afrikaanse kus gedoen. Die JONSWAP model, wat die mees gebruikte spektrale model vir die beskrywing van windgegenereerde golwe is, is gebruik om golfenergie spektra te verteenwoordig by die gekose liggings. 'n Afskatting vir die piekverbeteringsfaktor-waardes is verkry deur gemete golfdata met die JONSWAP model te pas. Die gamma waarde vir Saldanhabaai is gebruik om die golfmodel vir hierdie studie op te stel. As gevolg van verafgeleë storms en plaaslike winde, is die gemete data bimodaal of multimodaal van aard. 'n Spektraleontbindingsmetode is toegepas om die data in wind- en deiningskomponente te verdeel ten einde 'n meer realistiese beskrywing van die golfstelsel te bekom. Die ontbindingsmetode was egter slegs suksesvol vir die ontbinding van bimodale golfstelses aangesien multimodale data met geen dominante piek nie verdeel kon word nie.

Gebasseer op hierdie studie asook vorige studies oor golfenergie aan die Suid-Afrikaanse kus, is Saldanhabaai gekies as 'n potensiële terrein vir die installering van 'n golfplaas. 'n Geneste numeriese golfmodel, SWAN (Simulating WAves Nearshore), is gebruik om die nabygeleë golfveldtoestand na te boots. Twee model- simulasies is in die studie oorweeg: Model simulasies in die teenwoordigheid van 'n golfplaas en model simulasies in die afwesigheid van 'n golfplaas. 'n Beraming van die verskil in beduidende golfhoogte en die golfenergiespektrum met en sonder die golfplaas is gedoen.

Die resultate toon ’n vermindering in beduidende golfhoogte en ’n verandering in golfenergiespektra by die geselekteerde plekke. ’n Geleidelike verandering in golfrigting is waargeneem vir alle geselekteerde grensgolfrigting-voorwaardes. Die resultate van die studie dui op ’n verandering in die kusgolfveld weens die teenwoordigheid van ’n golfplaas. Die motivering vir die studie is om ’n metodologie vir die installering van GEOs langs die Suid-Afrikaanse kus met baie golfenergie daar te stel.

Acknowledgements

I would like to express my sincere gratitude to my supervisor Dr Hardus Diedericks from the Applied Mathematics division at Stellenbosch University who was always there for me when I had questions to ask and when I needed guidance during my thesis.

Special thanks to my co-supervisors Dr Josefine Wilms from Council for Scientific and Industrial Research (CSIR) and Dr Christo Rautenbach from University of Cape Town who guided me while I was at the CSIR. I am grateful to the CSIR community who provided me with the wave data and facilities, such as the library, articles and books.

I would also like to thank people within the CSIR (Coastal Systems and Mathematical Digital Science research groups) and Stellenbosch University, Applied Mathematics Division who helped me with specific problems and questions. Ursula Von St Ange who helped me with the processed data and Louise van der Merwe from the library at the CSIR who was always there when I wanted articles and books that are relevant to this thesis. I personally thank Dr Susan Taljaard, who was one my mentors throughout the period of my masters.

I would like to acknowledge the wave data supplied by the CSIR, Stellenbosch, which was collected on behalf of the Transnet National Port Authority (TNPA).

And finally, I want to thank the CSIR for funding me during my masters and the Coastal Systems and Mathematical Digital Science research groups for encouraging me during my masters.

Contents

List of Figures

List of Tables

Nomenclature

Constants

$g = 9.81\,\mathrm{m\,s^{-2}}$

$\alpha_{PM} = 0.0081$

$\alpha_P = 0.0074$

$\sigma_a = 0.07$

$\sigma_b = 0.09$

$\rho = 1025\,\mathrm{kg\,m^{-3}}$

Standard symbols

a	Wave amplitude	[m]
a_i	Wave amplitude of the wave component	[m]
C_w	Wave steepness constant	[ ]
C	Wave propagation speed	[m/s]
C_b	Bottom friction coefficient	[ ]
C_g	Group speed	[m/s]
C_{g_0}	Group speed at deep water	[m/s]
C_{g_s}	Group speed at deep water	[m/s]
C_x	Propagation velocity in x-space	[m/s]
C_y	Propagation velocity in y-space	[m/s]
C_θ	Propagation velocity in θ-space	[ ]
C_σ	Propagation velocity in σ-space	[ ]
C_{ds}	Turnable coefficient for wave energy dissipation	[ ]
C_p	Phase speed	[m/s]
C_{p_0}	Phase speed at deep water	[m/s]
D_w	Duration of the wave component	[m]
D_{tot}	Total rate of energy dissipation	[rad]
$D(\theta)$	Directional spreading	[rad]
$D(f,\theta)$	Energy spreading function	[rad]

$E(f)$	Variance energy density	$[\mathrm{m}^2/\mathrm{Hz}]$
$E_{swell}(f)$	Variance energy density for swell	$[\mathrm{m}^2/\mathrm{Hz}]$
$E_{sea}(f)$	Variance energy density for wind sea	$[\mathrm{m}^2/\mathrm{Hz}]$
$E(f,\theta)$	Directional energy spectrum	$[\mathrm{m}^2/\mathrm{Hz}/\mathrm{rad}]$
E_{tot}	Total wave energy	$[\mathrm{J}]$
E_p	Potential energy	$[\mathrm{J}]$
E_k	Kinetic energy	$[\mathrm{J}]$
$\bar{E}$	Total energy density	$[\mathrm{J}/\mathrm{m}^2]$
$E_P(f)$	Phillips spectrum	$[\mathrm{m}^2/\mathrm{Hz}]$
$E_{PM}(f)$	Pierson-Moskowitz spectrum	$[\mathrm{m}^2/\mathrm{Hz}]$
$E_{JP}(f)$	JONSWAP spectrum	$[\mathrm{m}^2/\mathrm{Hz}]$
$E_B(f)$	Bretscheider spectrum	$[\mathrm{m}^2/\mathrm{Hz}]$
$E_{OB}(f)$	Ochi-Hubble spectrum	$[\mathrm{m}^2/\mathrm{Hz}]$
$E_{TMA}(f)$	TMA spectrum	$[\mathrm{m}^2/\mathrm{Hz}]$
$\mathbf{f}$	External forces of the fluid	$[\mathrm{N}]$
f	Wave frequency	$[\mathrm{Hz}]$
f_s	Separation frequency in a wave spectra	$[\mathrm{Hz}]$
f_u	Upper frequency of a wave spectra	$[\mathrm{Hz}]$
f_{p_w}	Wave steepness peak frequency	$[\mathrm{Hz}]$
$f_{p_{ws}}$	Swell peak frequency	$[\mathrm{Hz}]$
$f_{p_{sw}}$	Wind sea peak frequency	$[\mathrm{Hz}]$
f_l	Lower frequency of a wave spectra	$[\mathrm{Hz}]$
$G(f)$	JONSWAP spectrum additional term	$[\,]$
$G(s)$	Gamma function for directional spreading	$[\,]$
H	Wave height	$[\mathrm{m}]$
H_o	Deep water wave height	$[\mathrm{m}]$
H_{max}	Maximum wave height	$[\mathrm{m}]$
H_{mo}	Significant wave height	$[\mathrm{m}]$
$H_{1/3}$	Significant wave height	$[\mathrm{m}]$
$H_{s_{nof}}$	Significant wave height without the wave farm	$[\mathrm{m}]$
$H_{s_{wif}}$	Significant wave height with the wave farm	$[\mathrm{m}]$
J	Energy flux	$[\mathrm{kW}/\mathrm{m}]$
k	Wave number	$[1/\mathrm{m}]$
K_s	Shoaling coefficient	$[\,]$

K_s	Shoaling coefficient	[ ]
K_r	Refraction coefficient	[ ]
K_d	Diffraction coefficient	[ ]
$\tilde{k}$	Mean wave number	[1/m]
L	Wavelength	[m]
L_o	Deep water wavelength	[m]
m_n	n^{th} order spectral moment	[ ]
$m_{0_{ws}}$	zeroth order spectral moment for swell	[ ]
$m_{0_{sw}}$	zeroth order spectral moment for wind sea	[ ]
N	Action density	[ ]
n	Group and phase speed ratio	[ ]
n_o	Deep group and phase speed ratio	[ ]
P	Pressure of the fluid	[Pa]
P_w	Wave power	[kW/m]
P_{w_o}	Deep water wave power	[kW/m]
P_{ds}	Turnable coefficient for wave energy dissipation	[ ]
Q_b	Fraction of breaking waves	[ ]
s	Energy directional distribution	[ ]
$\tilde{s}$	Overall wave steepness	[ ]
S_{tot}	Source term that represents physical processes	[ ]
S_{ds}	Wave energy dissipation source term	[ ]
$S_{ds,b}$	Depth-induced breaking source term	[ ]
$S_{ds,b}$	Bottom friction source term	[ ]
$S_{ds,w}$	White-capping source term	[ ]
S_{in}	Energy input by wind source term	[ ]
S_{nl}	Non-linear wave-wave interaction source term	[ ]
S_{nl3}	Triad wave-wave interaction source term	[ ]
S_{nl4}	Quadruplet wave-wave interaction source term	[ ]
$\tilde{s}_{PM}$	Steepness value of Pierson-Moskowitz	[ ]
t	Time	[s]
T	Wave period	[s]
T_p	Peak period of the wave spectra	[s]
T_{m01}	Mean wave period	[s]
T_{m02}	Zero-crossing period	[s]

T_{m-10} or T_e	Energy period	[s]
$\underline{\mathbf{u}}$	vector velocity	[m/s]
$\vec{U}$	Ambient current	[m/s]

Greek symbols

ω^2	Dispersion relation	[$1/s^2$]
α	Wave angle between the wave crest and shoreline	[rad]
α_{in}	Initial linear wave growth	[ ]
α_{BJ}	Proportionality constant of Battjes and Janssen	[ ]
α_o	Deep water wave angle between the wave crest and shoreline	[rad]
β	Exponential growth term	[ ]
δ	Turnable coefficient for wave energy dissipation	[ ]
Δf	Frequency interval of the wave component	[Hz]
ε_i	Phase angle	[rad]
η_t	Sea surface elevation of harmonic wave components	[m]
$\overline{\eta_t^2}$	Average squared sea surface elevation	[ ]
γ_{BJ}	Breaking parameter coefficient	[ ]
Γ_{KJ}	Stepnees parameter coefficient	[ ]
γ	Peak enhancement factor	[ ]
$\Gamma(.)$	Gamma function	[ ]
ω	Angular frequency	[rad/s]
ρ	Sea density	[kg/m^3]
ϕ	Potential function	[ ]
σ	Relative or intrinsic frequency	[Hz]
$\tilde{\sigma}$	Mean relative frequency	[ ]
σ_{η_t}	Standard deviation of the sea surface elevation	[ ]
θ	Wave direction	[rad]
θ_m	Mean wave direction	[rad]
$\xi(f)$	Wave steepness parameter	[ ]
μ	Kinematic viscosity of the fluid	[m^2/s]

Abbreviations

JONSWAP JOint NOrth Sea WAve Project

CSIR Council for Scientific and Industrial Research

NRE Natural Resource and the Environment

CRSES Center for Renewable and Sustainable Studies

TNPA Transnet National Port Authority

NDBC National Data Buoy Center

CDIP Coastal Data Information Program

EMEC European Marine Energy Centre

WECs Wave Energy Converters

SWEC Stellenbosch Wave Energy Converter

LIMPET Land Installed Marine Powered Energy Transformer

PTF Power Transfer Function

SWAN Simulating WAves Nearshore

SNL-SWAN Sandia National Laboratories - Simulating WAves Nearshore

SWASH Simulating WAves till SHore

FFT Fast Fourier Transformer

GPS Global Positioning System

HF High Frequency

VHF Very High Frequency

SWL Still Water Level

CD Chart Datum

SSER Sea Swell Energy Ratio

ID Intermodal Distance

WD Wave Dragon

Chapter 1

Introduction

1.1 Background

Ocean wave energy appears to be one of the most promising and sustainable renewable energy resources (Liberti *et al.*, 2013). The World Energy Council has estimated the global potential wave energy that could be harvested from the world oceans to be 2 TWh/yr [1], making this resource one of the renewables that has a capacity to produce large amounts of energy to society. Due to global warming concerns, induced by air pollution, several studies have been conducted to find better ways for electricity generation to replace fossil-fuelled energy production and, in doing so, reduce greenhouse gas emissions.

Ocean energy has many forms of renewable energy resources that could be utilised for the production of electricity. These forms include thermal gradient, salinity gradient, ocean current, tides and wave energy. The focus of this study is wave energy. Wave energy is predominantly highest between 30° and 60° temperate latitudes in both hemispheres on the west coasts of Scotland, Portugal, Chile, New Zealand, Australia and South Africa due to the prevailing wind direction and long fetches where storms occur (CRSES, 2015). The areas that have the highest wave energy potential are shown in Figure 1.1. Studies have shown that the South African coast is one of the most energetic wave condition areas for the extraction of wave energy for electricity generation (Joubert, 2008; CRSES, 2015).

Electricity generation in South Africa is dominated by coal-fired power stations which play a major part in the economy but contribute to global greenhouse gas emissions (McDonald, 2012). South Africa has the highest greenhouse gas emissions on the African continent, due to the dependency on coal-fired power stations for electricity production. Further research and development in renewable energies, such as ocean

[1] Terawatt (TW) is equal to a trillion watt

wave energy could help address one of the most serious threats to the environment by reducing South Africa's dependence on coal-fired power stations.

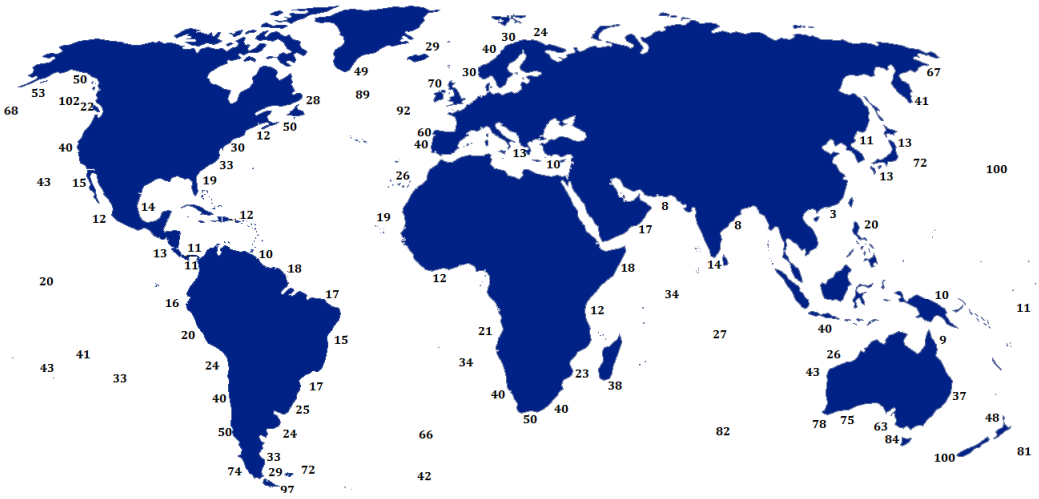

Figure 1.1: Approximate global wave power in Kilowatts per meter (kW/m) (Parry *et al.*, 2007).

The Centre for Renewable and Sustainable Energy Studies (CRSES) investigated the wave power resources along the South African coast through the analysis of measured and modeled wave data (CRSES, 2015; Joubert, 2008). The results of the investigation indicate that South African oceans are suitable for the implementation of Wave Energy Converters (WECs). However, installation of wave farms could have a potential environmental impact on the nearshore coastal dynamics such as sediment transport and beach profiles (Brooke, 2003). A wave farm is defined as an array of WECs arranged in rows and/or columns to extract wave energy and produce electricity.

Ocean waves are one of the main factors determining coastal morphological changes on the shoreline as waves have the ability to reshape beach profiles. They are responsible for coastal dynamics such as coastal erosion, accretion and the transport of sediments (Davidson-Arnott, 2010; Benassai, 2006). As the waves approach the shore, they are subjected to all types of transformations induced by the seabed such as shoaling (as the water depth decreases), refraction (due to the changing seabed contours), bottom friction and ultimately wave breaking (Benassai, 2006; Holthuijsen, 2010; Pecher and Kofoed, 2017). Furthermore, waves play a crucial role in influencing the planning and design of harbours and installation of marine structures, such as breakwaters, jetties and offshore oil platforms (Benassai, 2006). Thus, understanding and predicting the mechanisms and transformation of waves are of importance for assessing the impacts of wave farms.

Several studies such as Brooke (2003), Bento *et al.* (2014) and Smith (2008), found that the presence of wave farms resulted in reduced wave heights. The purpose of this

study is to investigate the changes in dominant wave parameters (height, period and propagation direction) due to the installation of wave farms focusing on a nearshore region along the South African coast. In doing so, a methodology will be provided for the computation of energy extracted from nearshore areas by WECs.

1.2 Overview of waves characteristics

1.2.1 Generation and propagation of ocean waves

Waves are generated by wind action on the water surface, as illustrated in Figure 1.2. The wind blows across the ocean surface and the waves are generated. Waves are fluctuations of the water level that are accompanied by local currents and pressure fluctuations (Kamphuis, 2010).

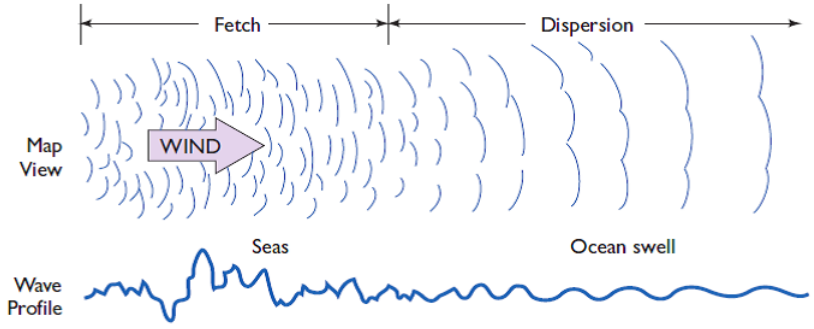

Figure 1.2: Ocean wave generation induced by wind action (Pinet, 2012).

These waves appear as a periodic oscillation of the water surface above and below the still water level (SWL). They are characterized by the following parameters: the vertical distance, H, of the wave that is the distance between the crest and trough, and it is twice the amplitude a, the horizontal distance between successive wave crests is the wavelength, L, the period T is the time interval between successive crests passing a particular location as illustrated by Figure 1.3. The frequency f is the inverse of the wave period. The waves propagate with the speed C which is the distance travelled by a wave per unit time and is sometimes referred to as the phase speed.

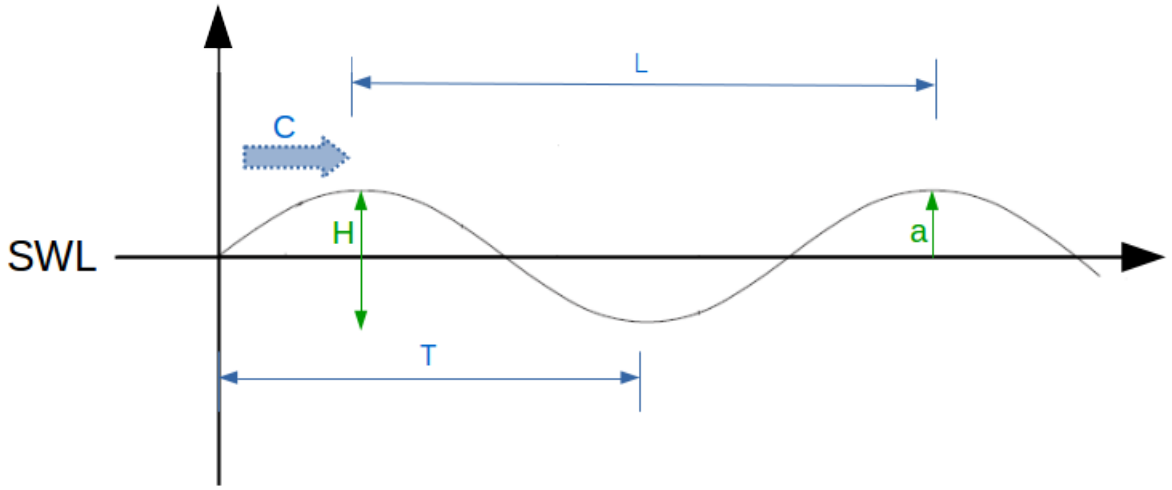

Figure 1.3: Periodic oscillation of the water surface, adapted from Bosboom and Stive (2012).

The height of the waves depends on the distance which the wind blows over the ocean surface (known as the fetch), the duration of how long the wind blows and the speed of the wind over the ocean surface (Davidson-Arnott, 2010). The greater the wind speed, the longer it blows and the longer the fetch, the bigger the waves. Figure 1.4 shows different types of waves that are found in the ocean as a function of wave period. It also shows the relative amount of energy that the ocean contains at each frequency (or period) and shows that wind-generated waves are the most energetic ocean waves.

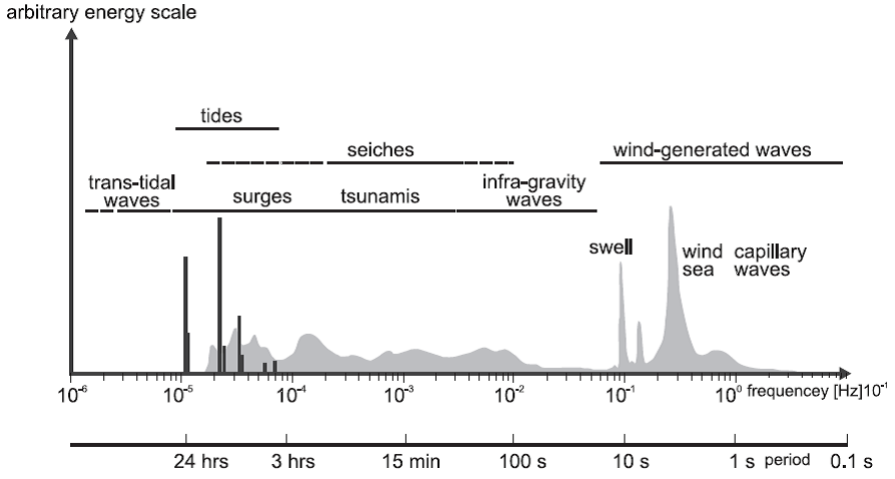

Figure 1.4: Different types of ocean waves. The figure shows various types of ocean waves which are classified according to their periods and frequency (Holthuijsen, 2010).

Ocean waves can vary in size, from small ripples to bigger waves. These waves propagate the energy supplied by the wind to the nearshore. According to Holthuijsen (2010) and Benassai (2006), wind-generated waves are divided into short and long waves which are classified in terms of periods as shown in Figure 1.4. The short waves have periods less than 20 s and long waves have periods ranging from 20 to 30 s (Benassai, 2006).

1.2.2 Nearshore wave energy

The wave climate conditions at the nearshore location depend on the offshore wave climate induced by factors such as prevailing winds and local bottom topography. As a result of these factors the nearshore wave energy resource tends to be smaller compared to the offshore energy resources. Studies have shown that even though the offshore areas have high energy levels, the installation and maintenance of marine structures are more expensive due to severe wave conditions and long sub-sea cables that will complicate maintenance. Thus, the modelling of nearshore wave energy resource is considered in this study. To model the nearshore wave energy resource, it is essential to evaluate the transformation of wave energy from deep to shallow waters (Soares, 2015).

1.3 Shoreline changes induced by wave farms

The movement of sediments induced by the action of waves and wind can be divided into cross-shore and longshore sediment transport (Kamphuis, 2010). This movement of sediment can result in accretion and erosion which can cause coastal modifications. Cross-shore and longshore sediment transport are very important to understand as they play key roles in shaping the coastline. Cross-shore sediment transport can be defined as the displacement of sediment particles perpendicular to the shoreline. Longshore transport is defined as the movement of beach sediment along the coast induced by action of tides, wind, currents and waves (Bosboom and Stive, 2012; Davidson-Arnott, 2010).

The stability of the shoreline depends on the balance between the sediment available in the area and the cross-shore and longshore sediment transport (Sorensen, 2005). The shoreline can remain in equilibrium, erode or accrete. If the shore is in equilibrium, this means that the shoreline is stable over a certain period of days, months or years (Sorensen, 2005). Factors such as an oblique angle of waves and wave breaking at the shore have an influence on the stability of the shoreline. The variation of the nearshore bathymetry tends to affect both wave height and wave direction and as a result wave breaking can cause changes in the longshore sediment transport. These changes can affect the shoreline stability and shape.

Coastal structures such as WECs have a potential of affecting the local wave climate and consequently lead to changes in sediment dynamics which can result in coastal modifications (Benassai, 2006). Abanades Tercero (2017) conducted a study on beach morphodynamics induced by WECs. A coupled numerical system XBeach (Roelvink *et al.*, 2010) and SWAN (Booij *et al.*, 1999) was used to determine the sediment

transport patterns. The effect of the wave farm was determined based on various wave scenarios at different water depths. It was concluded that locating the wave farm near or further from the shoreline might control the beach profile. In this thesis, modelling of sediment transport is not considered. Only the wave field changes will be modelled since changes in local wave conditions can change the sediment transport dynamics which can lead to shoreline changes.

1.4 Modelling the impacts of wave energy converters

Research and development of wave energy devices for harnessing wave energy has emerged since the oil crisis in the 1970s (Erselcan and Kükner, 2014). Several full scale individual wave energy devices have successfully been operational in real-sea conditions, for example, Pelamis, PowerBuoy, Wave Dragon and Oyster (Smith *et al.*, 2012). According to Margheritini *et al.* (2012), a large number of wave energy devices are available worldwide and are listed by the European Marine Energy Centre (EMEC), which is an energy device testing site (Venugopal and Smith, 2007). These devices differ in design and working principles (Zanopol *et al.*, 2014). According to Smith *et al.* (2012), installation of individual wave energy devices will not produce enough power. To become commercially competitive with other renewable energy resources in the energy sector, a large number of energy converters must be installed collectively in a wave farm to harness sufficient power. Both power production and cost are dependent on the wave farm layout (Diaconu and Rusu, 2013).

According to Greenwood *et al.* (2013), the impact of large wave farms on the environment is unknown, since there are no large-scale commercial clusters of wave energy devices that have been installed. However, several studies investigated the environmental impact due to energy devices and it was noticed that there are changes in the significant wave height. Based on these studies, the concern is changes in the nearshore region that are influenced by the wave field dynamics induced by energy devices. It is, therefore, necessary to model the impacts of wave farms as they could affect the longshore and cross-shore sediment transport which could result in beach erosion and shoreline changes.

The assessment of coastal dynamics in the nearshore region, due to the presence of wave farms, has been done using numerical model simulations and laboratory experiments (Smith, 2008; O'Dea *et al.*, 2014). These numerical wave models can predict the wave energy, depending on the weather and the location. They can also evaluate or measure the changes in wave energy and the direction of the waves as they approach the nearshore region. MIKE 21 BW (Kofoed-Hansen *et al.*, 2005), MILDwave (Radder and Dingemans, 1985) and SWAN (Booij *et al.*, 1999) are the most popular numerical

models for the assessment of wave farm effects, with SWAN being the most frequently used wave model (Folley *et al.*, 2004).

1.5 Aims and objectives

The aim of this study is to assess changes in dominant wave parameters (height and propagation direction) due to the installation of wave farms focusing on a nearshore region along the South African coast. This will be achieved through the following objectives:

- Obtaining the peak enhancement factor (γ) typically for South African wave conditions by fitting the JOint North Sea WAve Project (JONSWAP) model to a set of measured data.
- Obtaining the input boundary conditions for the numerical wave model using offshore wave data.
- Simulating the changes in the dominant wave parameters due to the installation of wave farms on a nearshore area along the South African coast using Saldanha Bay as the case study.
- Proposing a methodology for the assessment of wave energy along the South African coast.

1.6 Research method

The peak enhancement factor (γ) is an important input parameter for numerical wave modelling (e.g. SWAN). This parameter controls the sharpness of the spectral peak and has no effect on the other parts of the spectrum. The default value for γ in the numerical wave model SWAN is 3.3 which is based on North Sea wave conditions (Hasselmann *et al.*, 1973). To obtain the γ value for South African wave conditions, available measured wave data from Datawell Waverider buoys were used. The JONSWAP model was fitted to the measured data using MATLAB. Several mathematical models are used to describe the sea state conditions by wave energy spectra. The JONSWAP model is chosen because it is a well established mathematical model that is incorporated in SWAN. Also, the JONSWAP model is regarded as a good representation for open and short crested seas or fetch-limited conditions and is the most used model in laboratory, oceanography and marine engineering applications (Holthuijsen, 2010). The SWAN wave model is the most used spectral model for assessing the impacts of wave farms based on the literature (Folley, 2016). For this reason, it was chosen for this study. SWAN requires offshore wave boundary conditions as part of its input parameters. For

this study, offshore wave data from the National Centers for Environmental Prediction (NCEP) was used to derive the input boundary conditions. Transmission and reflection coefficients representative of WECs which form part of the numerical wave model, is obtained from literature (Diaconu and Rusu, 2013).

1.7 Outline of the thesis

Chapter 1 presents the background and motivation for this study. The chapter introduces the previous and current state of the wave energy power generation using WECs. A brief overview of wind-generated waves are provided to familiarise the reader with the concepts such as wave generation and propagation. A literature study is done on the modelling of the effects of WECs. This is important to investigate since these changes could modify the coastline.

In Chapter 2, ocean wave spectra are discussed. This includes the measurements of ocean wave spectra by Datawell Waverider buoys and the analysis of the data. In this chapter, the spectral analysis technique and the statistical description of ocean waves are explained and the measured wave spectra are shown as an illustration. In Chapter 3 the South African wave climate conditions, induced by weather patterns along the chosen locations, are explained. Wave generation, propagation, and dispersion will be further discussed in the chapter. In Chapter 4, the estimation of the JONSWAP spectral parameters using the South African wave conditions is explained. The JONSWAP model will be fitted into a set of measured data to provide the values of the model parameters, specifically the peak enhancement factor which will be used as an input parameter for SWAN simulations.

In Chapter 5, a review of the characteristics of various WECs are presented. The location, types and mooring systems of WECs will be discussed. The discussion includes the power take-off systems of WECs which are defined as the process that extracts wave energy and transforms it into electricity using a linear generator, hydraulic and air turbines and high-pressure oil hydraulic systems. In Chapter 5, the SWAN model simulations are presented to assess the effects induced by a wave farm on the nearshore region using Saldanha Bay as the case study.

Based on the results of this study, a proposed methodology for assessing the wave energy along the South African coast is presented in Chapter 6. Finally Chapter 7 provides a general summary and conclusions, as well as future work.

Chapter 2

Ocean wave spectra

2.1 Introduction

The measurement of ocean waves is generally conducted for several reasons such as calibration and validation of wave models and coastal engineering applications (Young, 1999). An ocean wave climate for a specific area can be defined as the distribution of wave conditions such as wave height, period and propagation direction (Denny and Gaines, 2007). Waves can be measured in various ways using several techniques. These techniques can be divided into *in situ* (e.g. wave buoys or poles) and remote sensing techniques (e.g. radar) (Holthuijsen, 2010).

This study focuses on the use of *in situ* measurements. The most common *in situ* instruments that were used to obtain wave record data that is used in this study, are floating wave buoys that are located at specific areas of interest in the ocean. According to Holthuijsen (2010), the buoys follow the three-dimensional motion of the water particles at the sea surface and measure the vertical and horizontal acceleration of the water surface in either deep or shallow water. The measured vertical acceleration is integrated twice to obtain sea surface elevation, as shown in Figure 2.1. The water surface is measured by the onboard mounted accelerometer in the Datawell Waverider buoys (CDIP, 2015).

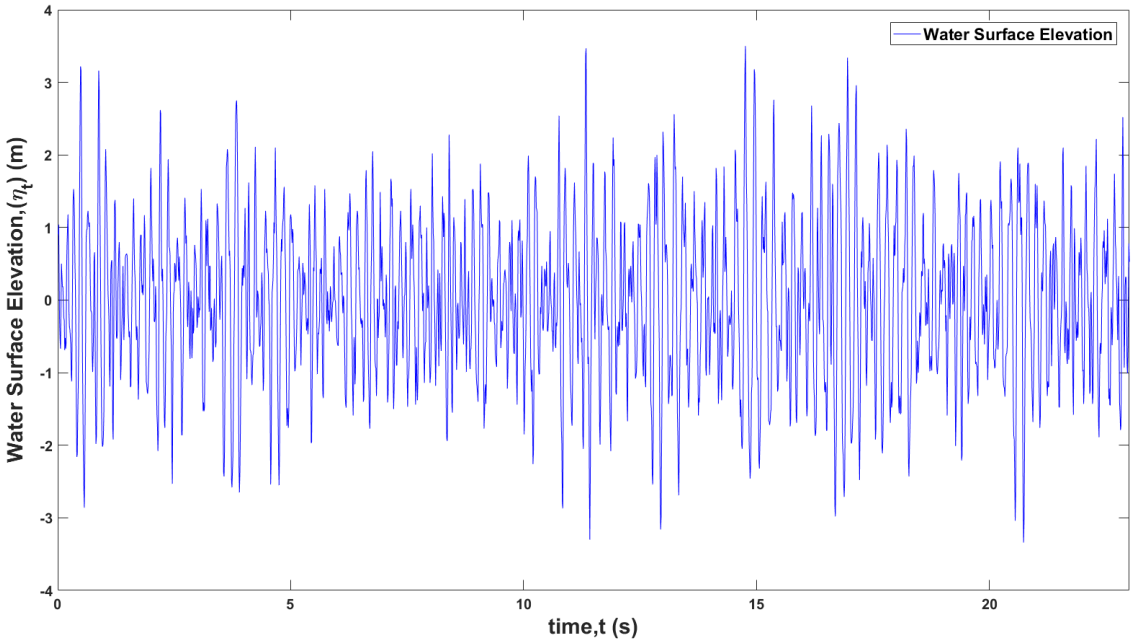

Figure 2.1: Sample of the wave record data from the sea surface elevation time series.

The Datawell Waverider buoys have diameters of 0.9 m, 0.7 m and 0.4 m respectively. The wave data set is collected at various locations along the South African coast. Before the year 2000, the non-directional Waverider buoys were mainly used. Due to the growing need for more information about the wave direction, the Council for Scientific and Industrial Research (CSIR) developed a directional buoy called 3D buoy (CSIR, 2015). The Datawell directional Waverider Mark III and non-directional Waverider buoys, for example the buoy shown in Figure 2.2, are the most common buoys used to measure ocean waves along the South African coast.

The sea surface elevation time series data is often analysed to determine the statistical representation of ocean waves. The most common method used to analyse ocean waves is spectral analyses. The objective of this chapter is to describe the sea surface elevation data measured by Datawell Waverider buoys and the technique used to analyse the data from the time to frequency domains. Wave parameters estimated from the spectra are briefly discussed and, lastly, the wave energy and power equations are introduced.

Figure 2.2: Datawell Waverider buoy which measures the sea surface elevation (CDIP, 2015).

2.2 Spectral analysis

The objective of this section is to describe the technique that is used to analyse sea surface elevation time series data as a stochastic process which leads to a variance energy spectrum or energy density spectrum. In the application of spectral analysis, the sea surface elevation is assumed to be stationary over a period of 30 min since the statistical properties such as mean and variance do not change over this interval. It should be noted that this assumption is not always appropriate for local seas (Holthuijsen, 2010; Bosboom and Stive, 2012). A spectral analysis uses a Fast Fourier Transform (FFT), which was introduced by Cooley and Tukey (1965), to decompose the sea surface elevation into a series of wave components with various amplitudes, phases and directions (Holthuijsen, 2010; Davidson-Arnott, 2010).

Essentially, an FFT transforms the sea surface elevation record from the time domain to the frequency domain. The result will be the statistical distribution, given as $E(f)$, which is a function of frequency and is called the energy density spectrum. The concept of a wave spectrum is explained in the next section. Spectral analysis is an important concept in analysing the sea surface time series as it reveals the energy content of the wave field system.

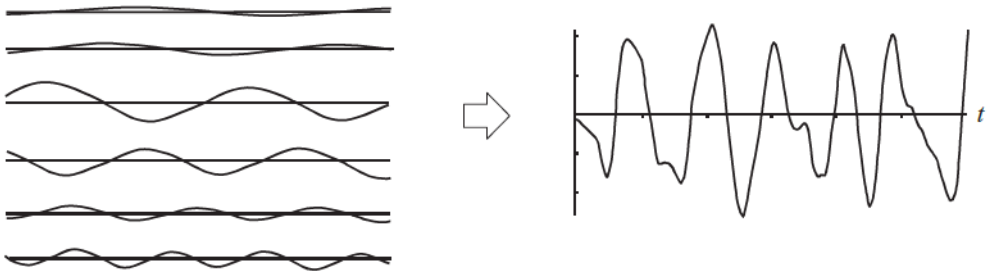

Figure 2.3: The summation of harmonic wave components which results in a sea surface elevation, adapted from Holthuijsen (2010).

The sea surface elevation can be decomposed into a large number of harmonic wave components, as illustrated by the left side of Figure 2.3. Each component has a defined frequency and amplitude and can be expressed mathematically as

$$\eta_t = \sum_{i=1}^{N} a_i \sin(2\pi f_i t + \varepsilon_i). \tag{2.2.1}$$

In Equation (2.2.1), N is the number of wave components and a_i, f_i and ε_i are the amplitude, frequency and phase angle of the i^{th} propagating wave component, respectively. The frequency $f_i = i/D_w$ (for $i = 1,2,3,...$), where D_w is the duration of the wave record and the frequency interval is given as $\Delta f = 1/D_w$.

The spectral analysis decomposes the sea surface elevation time series into frequency bands. This provides the expected value of the amplitude as a function of frequency which is referred to as the amplitude spectrum as shown in Figure 2.4.

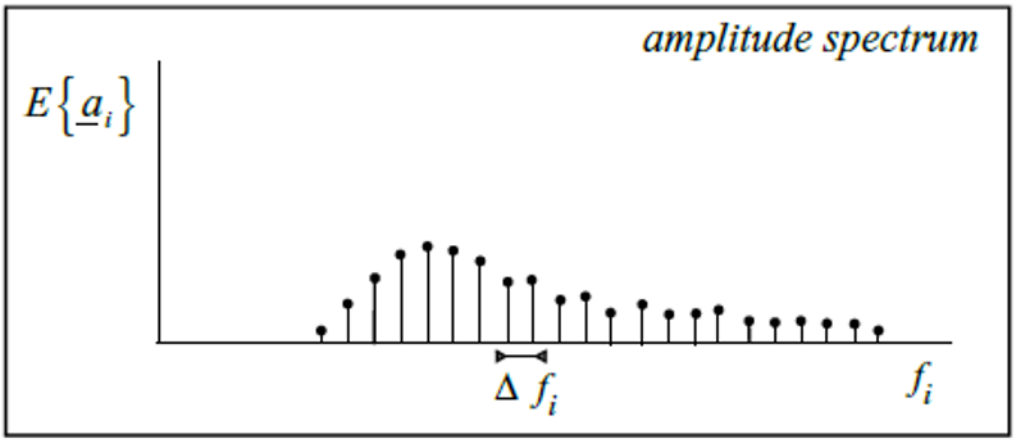

Figure 2.4: The amplitude spectrum, adapted from Holthuijsen (2010).

According to Bosboom and Stive (2012) and Holthuijsen (2010), the expectation or mean and variance of the sea surface elevation is 0 and $\frac{1}{2}a_i^2$, respectively. The variance of the sea surface elevation by definition, is the average squared sea surface elevation (Holthuijsen, 2010). The variance of the harmonic wave component with amplitude a is $\overline{\eta_t^2} = \frac{1}{2}a^2$. The variance of the harmonic wave components can be summed up to give $\underline{\overline{\eta_t^2}} = \sum_{i=1}^{N} E\{\frac{1}{2}\underline{a}_i^2\}$, where $E\{\overline{\eta_t}\} = 0$. The symbol $E\{.\}$ denotes the expected value, the amplitude $\underline{a}$ represents the random variable and the under-bar in $\underline{\eta_t^2}$ represents the time-averaging (Holthuijsen, 2010). The amplitude squared can be plotted against the frequency to give the variance spectrum which is discrete at each frequency, as shown in Figure 2.5.

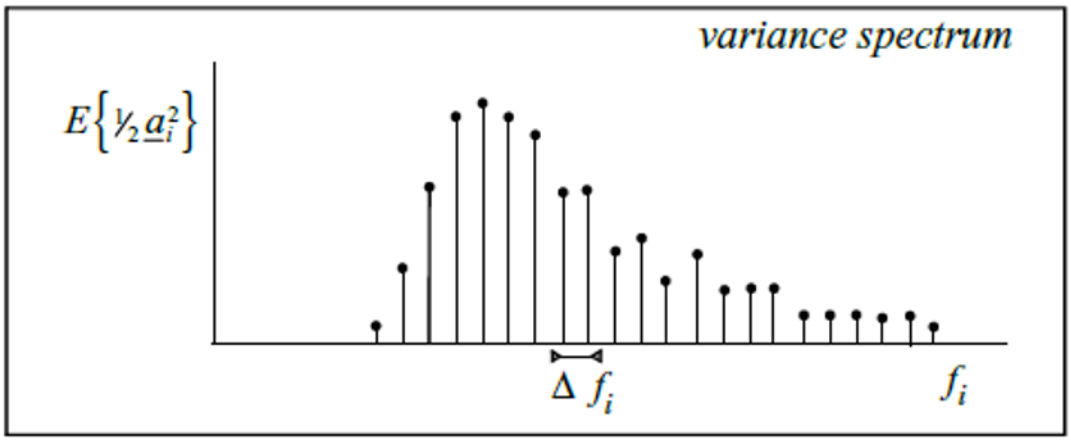

Figure 2.5: The variance spectrum, adapted from Holthuijsen (2010).

The variance associated with amplitude is then distributed over frequencies, $\Delta f_i = 1/D_w$, to give the variance density spectrum $\frac{1}{2}\underline{a}_i^2/\Delta f_i$, shown in Figure 2.6.

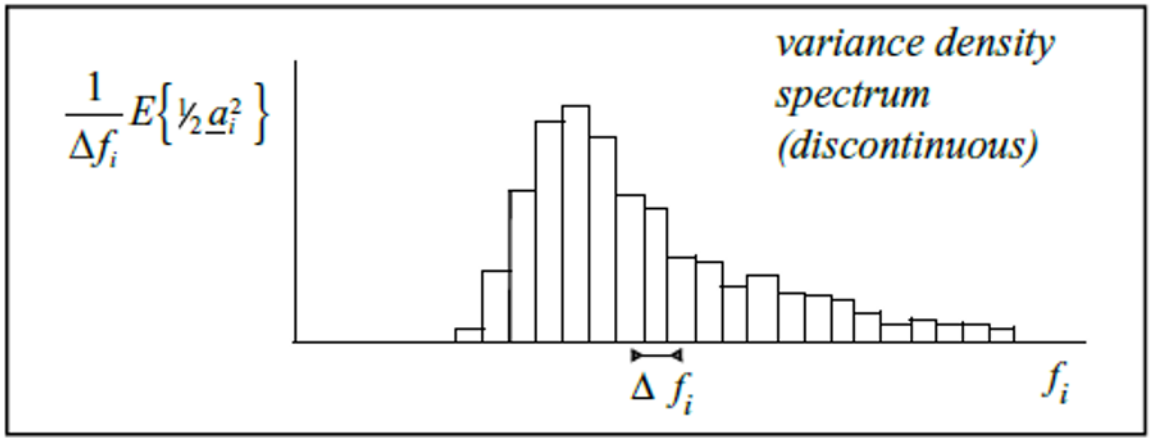

Figure 2.6: The variance spectrum (discontinuous), adapted from Holthuijsen (2010).

The drawback is that the value of the variance over frequencies jumps from one frequency band to another. To overcome this problem, the limit of the frequency interval ($\Delta f \to 0$)

is taken to give

$$E(f) = \lim_{\Delta f \to 0} \frac{1}{\Delta f} E\{\frac{1}{2}\underline{a}^2\}. \tag{2.2.2}$$

Thus, Equation (2.2.2) is the continuous variance density spectrum by definition and is illustrated by Figure 2.7.

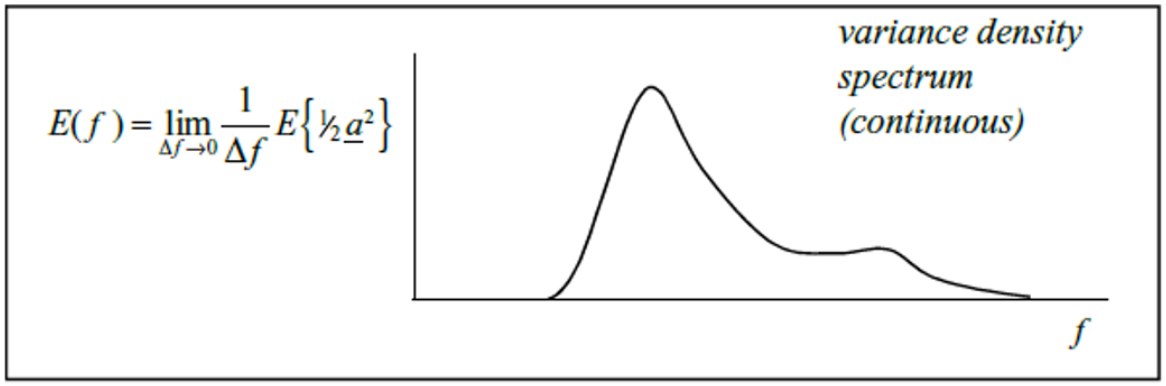

Figure 2.7: The continuous variance density spectrum, adapted from Holthuijsen (2010).

The variance density spectrum describes the contribution of a wave component to the total variance. Based on linear wave theory (Holthuijsen, 2010), the variance of the sea surface elevation is proportional to the total energy per unit area. The variance density spectrum is therefore transformed to an energy density spectrum:

$$E_{energy}(f) = \rho g E_{variance}(f). \tag{2.2.3}$$

The only difference between the energy and variance is the quantity ρg. The variance density spectrum describes the statistical features of the waves, whereas the energy density spectrum describes the physical features of the waves (Holthuijsen, 2010). This result shows a one-dimensional frequency spectrum which denotes the distribution of energy at various frequencies. It follows that the statistical characteristics of the wave field can be described by the energy spectrum and it is one of the most important phenomena in the concept of ocean wave analysis.

2.3 Wave energy spectrum

The wave energy spectrum is based on the assumption that the sea surface elevation time series can be represented as a Fourier series of wave components that consists of different frequencies, directions and amplitudes, as mentioned in Section 2.2. The spectrum can also be represented by a mathematical or graphical representation to show the wave energy distribution at various frequencies. The wave components are split into different frequencies. When the distribution of wave energy is plotted against frequency, it is called a wave energy spectrum, as shown in Figure 2.8. A wave energy

spectrum is usually referred to as the wave energy density spectrum or variance energy density, where the energy density is the amount of energy stored at each frequency and is expressed in m^2/Hz or m^2s (see Equation (2.2.3)).

An example of the wave energy spectrum, $E(f)$, computed from the wave data observed at the Cape Point station, is shown in Figure 2.8. The energy spectrum illustrates the distribution of energy at each frequency. The significant wave height, H_{m0}, which is the most frequently used spectral parameter, defines the sea state severity. It is equal to four times the square root of the area under the curve in the wave spectrum. The significant wave height of the spectrum shown in Figure 2.8(b) is 2.98 m and the wave energy is concentrated around a frequency of 0.085 Hz, which is the peak frequency of the spectrum. The observed spectrum shows that the wave energy is distributed between the frequency ranges of 0.05 to 0.3 Hz and has a relatively high variance at lower frequencies.

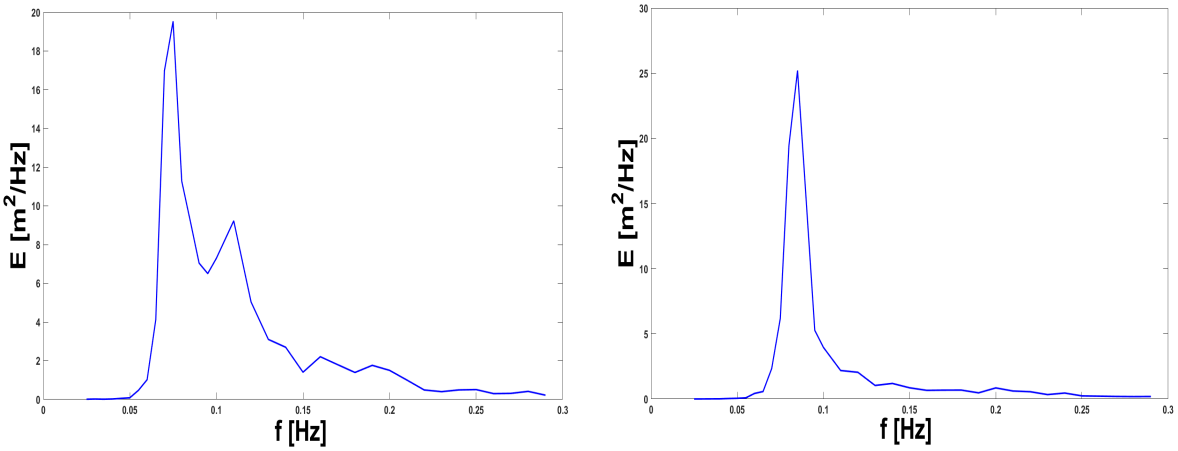

(a) Bimodal spectrum **(b)** Unimodal spectrum

Figure 2.8: An example of the Cape Point measured single and double peaked spectrum.

The measured spectrum at a particular location sometimes contains two wave systems, which is known to be a bimodal spectrum as indicated by Figure 2.8(a). For example a spectrum will often have double spectral peaks corresponding to low and high frequency components. Low frequencies denote the swell domain, whereas high frequencies denote the wind sea domain.

2.3.1 Wave parameters estimated from the ocean spectra

The sea surface elevation of the sea state can be described by several wave parameters. These parameters are usually estimated from the spectrum by expressing them in terms of the spectral moments. The general n^{th} order spectral moment is defined by

$$m_n = \int_0^\infty f^n E(f) df. \tag{2.3.1}$$

Where n= 0,1,2,....

The zeroth-order spectral moment explains the variance of the wave system, where m_0 is the zeroth-order moment that represent the area under the spectral curve. To estimate the wave height from the spectrum, m_0 is used to compute the significant wave height as

$$H_{m0} = 4\sqrt{m_0}. \tag{2.3.2}$$

However, from a time record the significant wave height can be denoted as $H_{1/3}$, where $H_{1/3}$ is defined as the average of the highest one-third of waves in a wave record (Holthuijsen, 2010). This parameter is often used for coastal engineering applications (Bosboom and Stive, 2012).

In a similar manner, wave periods can be estimated from the spectrum using the spectral moment definition. For instance, the peak period, T_p is the inverse to f_p, where f_p is the peak frequency of a wave spectrum. The mean period, T_{m01}, corresponds to the mean frequency of the wave spectrum and is given by

$$T_{m01} = \frac{m_0}{m_1}. \tag{2.3.3}$$

The zero-crossing period,T_{m02}, which is equivalently to zero-downcrossing period T_z is given as

$$T_{m02} = \sqrt{\frac{m_0}{m_2}}. \tag{2.3.4}$$

The energy period, denoted by T_{m-10} or T_e, is given as

$$T_{m-10} \equiv T_e = \frac{m_{-1}}{m_0}. \tag{2.3.5}$$

The energy period, T_e, is frequently used in the deep water wave power computation (Brooke, 2003). The wave power equation is given as

$$J = \frac{\rho g^2}{64\pi} H_{m0}^2 T_e. \tag{2.3.6}$$

2.4 Directional wave spectra

In many practical applications and activities (e.g. installation of WECs and construction of harbours etc) in the ocean, knowledge of the direction of the waves is an important factor. A directional wave spectrum shows how the variance of the sea surface elevation is distributed over frequencies and directions (Holthuijsen, 2010). The expression for the variance of the sea surface elevation in different directions and frequencies is given as

$$\bar{\eta}_t = \int_0^{\infty} \int_0^{2\pi} E(f,\theta) d\theta df. \tag{2.4.1}$$

$E(f,\theta)$ represents the energy distribution in both frequency and direction, f is the wave frequency (in Hz) and θ is the wave direction (in radians). The sea state can be characterised by the mean wave direction θ_m, which is defined as the mean of all individual wave directions in wave spectra. $E(f,\theta)$ is called the directional wave spectrum or two-dimensional energy spectrum. A graphical representation of the spectrum is given in Figure 2.9 and can be represented by the product of the one-dimensional spectrum $E(f)$ and the directional energy spreading function $D(f,\theta)$, generally expressed as

$$E(f,\theta) = E(f)D(f,\theta). \tag{2.4.2}$$

$E(f)$ is the non-directional wave spectra. The spreading function, $D(f,\theta)$, gives the magnitude of the directional spreading of the wave energy (Goda, 2010).

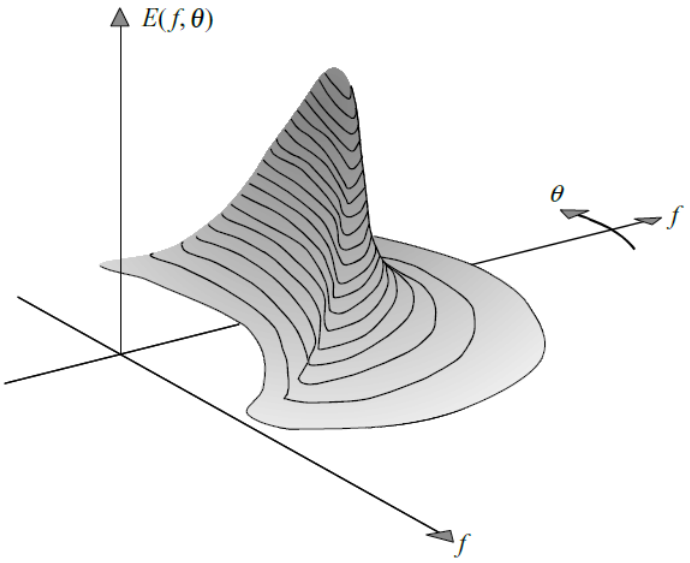

Figure 2.9: The directional wave spectrum that shows the distribution of energy at various frequencies and directions (Holthuijsen, 2010).

Several expressions regarding the directional spreading have been used to describe the term $D(\theta)$ (Holthuijsen, 2010). According to Mitsuyasu *et al.* (1975), Goda (2010) and Holthuijsen (2010), the most used expression for directional spreading is the $cos^{2s}\theta$ distribution. The directional spreading is expressed as

$$D(\theta) = G(s)cos^{2s}\left(\frac{\theta}{2}\right), \tag{2.4.3}$$

for $-\pi < \theta \leq \pi$, where $G(s)$ is expressed as

$$G(s) = \frac{\Gamma(s+1)}{[\Gamma(2s+1)\sqrt{\pi}]}, \tag{2.4.4}$$

where s controls the width of the distribution, as shown in Figure 2.10, and $\Gamma(.)$ is the gamma function.

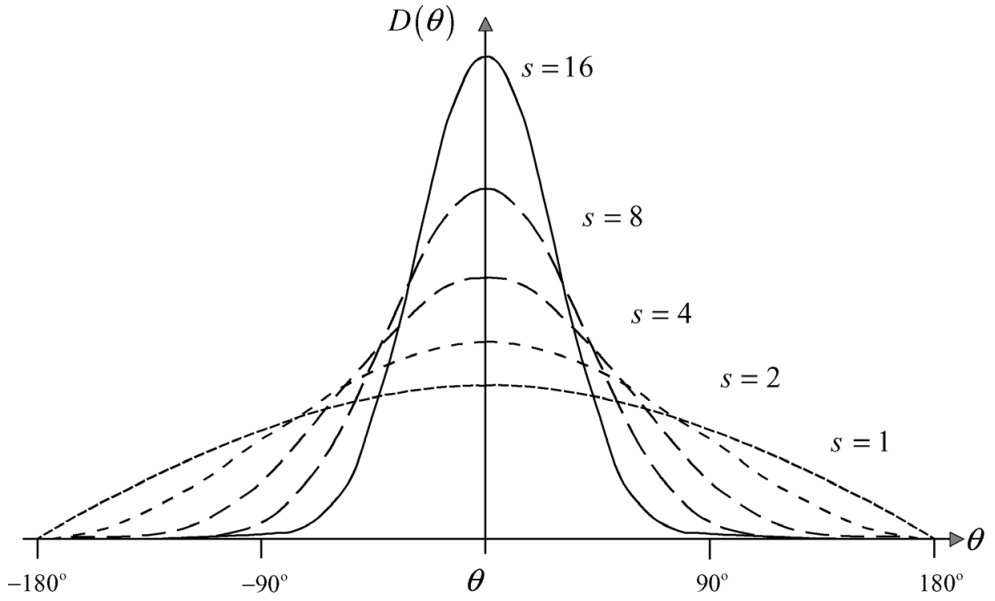

Figure 2.10: The $cos^{2s}\theta$ model that shows the directional energy distribution under idealized conditions and s describes the energy directional distribution around the mean direction θ_m (Holthuijsen, 2010).

According to Mitsuyasu *et al.* (1975), the higher frequency components of the energy spectra have a wider angular spread of the energy. This energy is more focused in the dominant direction of the peak frequency. Directional spreading is an important input parameter for numerical wave modelling (e.g. SWAN). It has been shown that to install some WECs, it is important to know the dominant directional spreading of the energy for power capture. According to Carballo *et al.* (2014), there is no information that has been published with regards to the effect of wave direction on the WECs.

2.5 Wave energy and power

The movement of the water surface is made up of two energy contributions, the potential (E_p) and kinetic energy (E_k). The potential energy is associated with the work done against gravity. Kinetic energy is the part associated with the orbital motion of the of the water velocity. According to Davidson-Arnott (2010) and CEM (2002), the potential and kinetic energy of the waves propagating in the same direction is defined as the total energy per wave crest expressed as

$$E = E_k + E_p = \frac{\rho g H^2 L}{8}. \tag{2.5.1}$$

The total energy density, $\bar{E}$, per unit distance is expressed as

$$\bar{E} = \frac{E}{L} = \frac{\rho g H^2}{8}. \tag{2.5.2}$$

Where L is the wavelength and ρ is sea water density. The rate at which the wave energy is transmitted in the direction of energy propagation is called the wave power level and is given as

$$P_w = \frac{\rho g H^2}{8}\frac{C_p}{2}\left\{1 + \frac{2kd}{\sinh(2kd)}\right\}, \tag{2.5.3}$$

where C_p is the wave celerity and is given by Equation (A.1.11) in Appendix A. The wave number is given as $k = \frac{2\pi}{L}$. In deep water and shallow water, Equation (2.5.3) simplifies to

$$P_{w_o} = \frac{1}{2}E_o C_{p_0}, \tag{2.5.4}$$

and

$$P_w = EnC_p, \tag{2.5.5}$$

where subscript "o" represent the deep water (CEM, 2002) and $n = \frac{1}{2}\left\{1 + \frac{2kd}{\sinh(2kd)}\right\}$ is the ratio between group speed and phase speed. In deep water, $n \approx \frac{1}{2}$ but the value of n increases as the waves approach the intermediate depth to shallow water. In shallow water, $n = 1$ since $kd < 1$ and $\sinh = 2kd$. More information about the application of power equations can be found in CEM (2002).

2.6 Summary

The chapter introduces the concept of wave energy spectra, measurement techniques and methods used to analyse ocean waves. There are several methods used to characterize ocean waves. A spectral analysis is one of the most common methods used for ocean waves analysis. The method uses a Fast Fourier Transform (FFT) to decompose the sea surface elevation into a series of wave components that contain various amplitudes, phases and directions. The numerical method transforms the sea surface elevation from a time domain to frequency domain, as a result, the statistical distribution of wave energy given by $E(f)$ and $E(f,\theta)$ and associated wave parameters will be estimated.

Wave energy spectra distribution along the South African coast is the most important concept in this study. This chapter is the starting point in understanding the wave system components that exist in a spectrum. These include wind sea and swell components. The shape of the spectrum defines sea state severity. At times, the sea state will contain both wind sea and swell components and sometimes a very complex spectrum containing wind sea and several swells. In these cases, it is difficult to interpret such spectrum. Characterization and classification of frequencies are often used to comprehend complex wave systems. To see the wave energy contribution for wave system components, the decomposition of a spectra methods are used. The decomposition concept will be explained in Chapter 4.

A brief description of the directional wave spectrum and the directional spreading function, which is an important input parameter in numerical wave model (e.g. SWAN), is discussed.

Chapter 3

South African wave conditions

3.1 Introduction

Wave conditions at various locations along the South African coast are continuously measured and analysed by the Council for Scientific and Industrial Research (CSIR) in Stellenbosch. The entire length of the coast is about 3 000 km long and stretches from the Orange River mouth down to the south coast up to subtropical Mozambique at the north-eastern border. The coastline is exposed to harsh wave conditions, strong ocean currents and tides. These extreme wave conditions are mainly influenced by various weather systems. They include a low-pressure system passing along the Southern Atlantic and tropical cyclones along the east coast of the South African coastline (Van der Borch van Verwolde, 2004; Rossouw *et al.*, 2013). Generally, wave conditions along the South African coast are bimodal in nature and consist of local seas and swells. The local seas being generated locally by local winds and swells that are generated by strong south westerly winds (Walker, 2012).

Typically, the mean period range for South African wave conditions that are swell dominated is 9 s to 16 s and the peak period is 13 s (with a peak frequency of 0.0769 Hz). For low energy wind sea, the wave peak period is in the range of 5 s to 8 s (Van Tonder, 1994). The wave spectra associated with these wave conditions are typically narrow band and can be represented by various mathematical equations. In this study the JONSWAP spectral model, which is discussed in Chapter 4, will be used to represent the wave spectra along the South African coast.

The objective of this chapter is to describe the wave conditions at the chosen locations along the South African coast. This will include a brief introduction to the weather systems that are causing these wave conditions. A brief description of the wave generation, propagation and dispersion and wave transformation is also included.

3.1.1 Weather systems

In order to describe the wave conditions along the South African coast, a brief background is given in this section of the prevailing weather systems causing the wave conditions. The wave conditions along the South African coast are the result of severe weather conditions (MacHutchon, 2006). These weather conditions are mainly induced by low-pressure systems associated with cold fronts passing along the South Atlantic and Indian Oceans (Van der Borch van Verwolde, 2004). This is mainly caused by atmospheric temperature differences over the ocean surface and over the land.

According to Rossouw (1989), the main source of extreme waves affecting the coastline is due to these low-pressure and cold fronts. Tropical cylones may also generate extreme wave conditions along the coast. These are mainly created by circular motion of the warm ocean surface which may lead to strong wind fields and heavy rains.

3.1.2 Wave directions

The annual and seasonal wave roses at various locations along the South African coast are given in Appendix B. These figures show the dominant wave directions and significant wave heights. It can be seen from the figures that the main wave directions along the west coast are predominantly from the south west both seasonally and annually with a 60% occurrence, as illustrated by Figures B.1 and B.2. The dominant wave direction along the west coast is mainly coming from the south west at both the Saldanha Bay and Cape Point locations.

Along the east coast, offshore of Ngqura (Algoa Bay), the dominant wave direction, with 60% occurrence, is coming from the south west as shown in Figure B.3. In East London, most of the waves are coming from the south with wave heights around 3.5 m to 4 m as shown in Figure B.4. At Durban and Richards Bay, most of the waves are coming from south of south east with other small percentages of waves coming from south east to east of north east, as shown by Figures B.5 and B.6. Based on Figure B.1, it is not possible to identify the wave system components such as swell and wind that exist at the coast. These can be identified by the spectra of these locations in Chapter 4.

3.2 Wave generation

Wind action over the sea surface is the most common external force that generates waves, as illustrated in Figure 1.2. The atmospheric pressure fluctuations over the sea surface induce the small waves (sometimes referred to as capillary waves, short-period

or high-frequency waves) with short wavelengths. Due to the continuous action of the wind, waves will grow in height and length and will propagate in the direction of the wind. Wave characteristics such as wave height, period and propagation direction depend on the duration for which the wind is blowing and the fetch, as mentioned in Section 1.2.1. Thus, wave formation and growth depend on the wind speed and fetch.

During this process, there is a transfer of energy from the wind to the ocean surface. The energy is then transferred from high-frequency to low-frequency waves. The wave height and period will increase with respect to the fetch. As the wind and wave speed increase, the transfer of wind energy to the ocean surface will eventually cease and the waves and the wind will reach an equilibrium. At this point, the sea state is said to be fully developed sea (Pierson and Moskowitz, 1964).

3.2.1 Wave propagation and dispersion

Linear wave theory is often used to understand the motion of the waves in oceanography and ocean and coastal engineering (CEM, 2002). The propagation of waves is dispersive (e.g. waves of different wavelengths tend to disperse since they propagate at different speeds) (Bosboom and Stive, 2012). The speed at which the wave propagates is termed phase speed or "wave celerity" and is given by

$$C_p = \frac{L}{T}. \tag{3.2.1}$$

Equation (3.2.1) can also be expressed as $C_p = \frac{\omega}{k}$, where ω is the angular wave frequency $(2\pi/T)$ and k is the wave number $(2\pi/L)$. The wavelength, L, is given by $L = \frac{gT^2}{2\pi}\tanh\left(\frac{2\pi d}{L}\right)$. According to linear wave theory (CEM, 2002), the parameters are related by

$$\omega = \sqrt{gk\tanh(kd)}. \tag{3.2.2}$$

Equation (3.2.2) is called the dispersion relation and is a function of the water depth d and the gravitational acceleration g (Bosboom and Stive, 2012). The phase speed differs at various locations in the ocean and expressions for it are given by Equation (A.1.16) and (A.1.17) in Appendix A.

The name "dispersive relation" is based on the fact that for a given ω and k, the waves will propagate faster in deep water compared to shallow water. If the waves propagate as a group with various wavelengths and speeds, there will be a separation between short period waves and longer period waves. Eventually, the longer period waves will propagate faster. During this process, the wave field will disperse hence Equation (3.2.2) is termed a dispersion relationship. When the group of waves propagate through a medium, the speed of the overall amplitude of the waves is called group speed. It is

not the same as the individual speed of the waves. The expression for the group speed of the wave train is given by

$$C_g = nC_p. \tag{3.2.3}$$

The expression for C_g in Equation (3.2.3), is derived in Appendix A. According to Bosboom and Stive (2012) and CEM (2002), the group speed in deep water is half the phase speed. According to Pecher and Kofoed (2017), ocean waves are generally dispersive in nature since the wave energy does not propagate with the same speed as the wave profile.

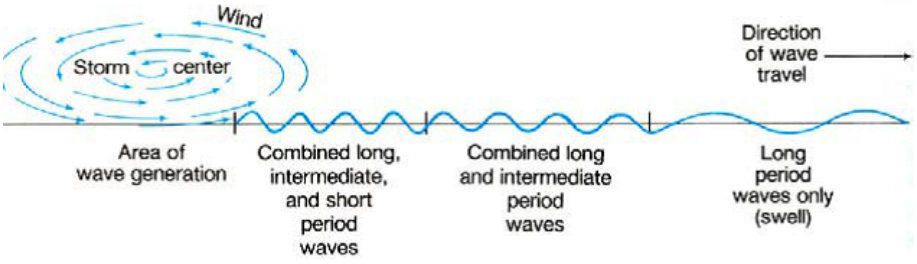

Figure 3.1: Transformation of the wind sea to swell waves propagating towards shallow water (Bosboom and Stive, 2012).

Figure 3.1 shows the transformation of ocean waves as they change to longer, faster swell waves from the initial area of generation. Figure 3.1 also shows that the waves can travel at different speeds and the wavelengths will spread out due to dispersion.

3.3 Wave transformation

Ocean waves are subjected to various types of transformations as they propagate from deep into intermediate and shallow water. The interaction with bottom topography changes the shape and the motion of waves, as a result the wave height, wavelength and direction will transform until the waves break (Bosboom and Stive, 2012). These changes that occur as the waves propagate towards the shallow water from deep water region are referred to as wave transformation.

Due to the changes that surface waves undergo as they enter the shallow water region, the wave spectra will change and be significantly different from deep water spectra. Thus, it is important to understand the wave transformation in the nearshore region. The spectral models such as SWAN (Booij *et al.*, 1999) and MIKE 21 SW (Warren and Bach, 1992*a*) can model the effects of wave conditions in the nearshore and can model wave transformation in shallow water (Davidson-Arnott, 2010).

3.3.1 Wave shoaling

As the waves propagate towards an area of decreasing depth as shown in Figure 3.2, the wave speed and the wavelength will decrease and wave height will increase (Bosboom and Stive, 2012). In the shallow water region, wave transformation processes such as shoaling, refraction and diffraction can take place simultaneously (Dhanak and Xiros, 2016). These processes are related to wave heights by the following expression given as

$$\frac{H}{H_o} = K_s K_r K_d, \tag{3.3.1}$$

where H is the wave height in shallow water, H_o is the deep water height. Parameters K_s, K_r and K_d are shoaling, refraction and diffraction coefficients, respectively. Assuming that there is no dissipation of energy as the waves propagate to shallow water, the shoaling coefficient is given as

$$K_s = \sqrt{\frac{n_o L_o}{nL}}, \tag{3.3.2}$$

where n and n_o represents the ratio of the group and phase speeds in shallow and deep water conditions, respectively. The ratio will reduce to $n_0 \approx \frac{1}{2}$ in deep water and $n \approx 1$ for shallow water as mentioned in Section 2.5. The expression is derived in Appendix A. Parameters L and L_o are the shallow and deep water wavelengths, respectively. These processes will cause the wavelength to decrease and the amplitude will grow until the waves break and this process is called wave shoaling.

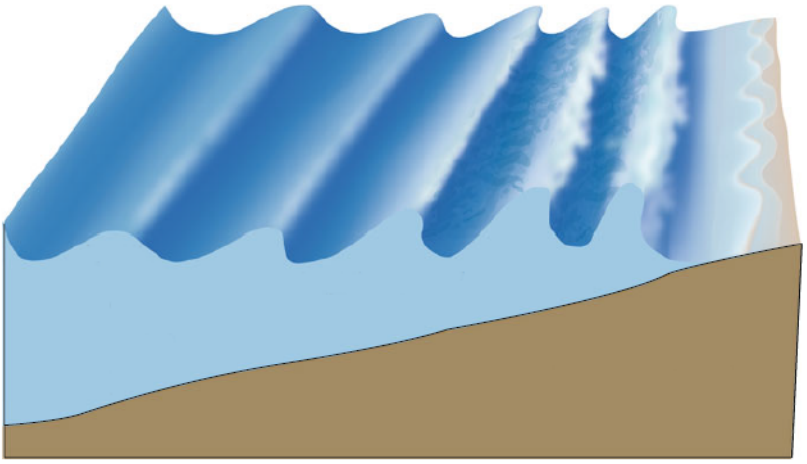

Figure 3.2: The change in the wave shape as the waves approach the shore induced by water depth, adapted from Pecher and Kofoed (2017).

3.3.2 Wave refraction

The waves are affected by the bottom topography as they approach the shallow water region. This will cause the orbital motion of the waves to change. The waves will

bend and change direction as shown in Figure 3.3. This is called wave refraction that is analogous to the refraction of light waves. This process is described by Snell's law, with the refraction coefficient given as

$$K_r = \sqrt{\frac{cos\alpha_o}{cos\alpha}}, \tag{3.3.3}$$

where α is the angle between the wave crest and the shoreline and α_o is the deep water angle. The angles can be found by applying Snell's law expressed as

$$\frac{sin\alpha}{sin\alpha_o} = \frac{C_p}{C_{p_o}}, \tag{3.3.4}$$

where C_p and C_{p_o} are the phase speeds at shallow water and deep water regions, respectively (Bosboom and Stive, 2012; Davidson-Arnott, 2010; Kamphuis, 2010).

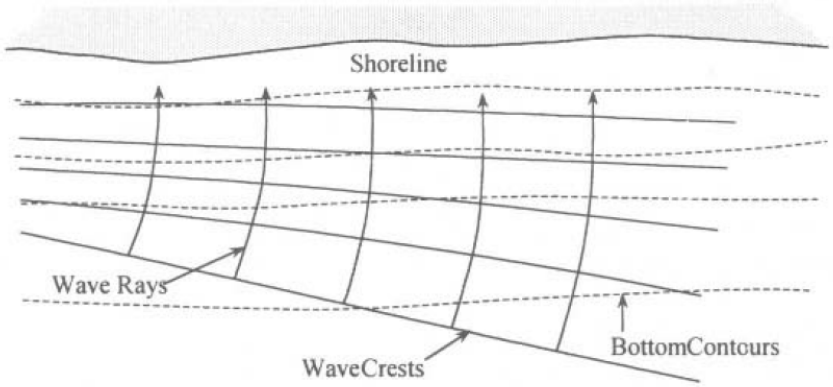

Figure 3.3: Wave refraction induced by bottom topography close to the shore (Kamphuis, 2010).

3.3.3 Wave diffraction

The wave diffraction phenomenon is the process of obstruction of the wave propagation induced by obstacles such as offshore island, headlands, rocks, reefs, and breakwaters as shown by Figure 3.4. During this process, the wave energy spreads sideways when the waves are in contact with one of the obstacles and the rest of the waves will be reflected towards the sea (Bosboom and Stive, 2012). Diffraction is also analogous to the physical phenomena in sound and light wave motion.

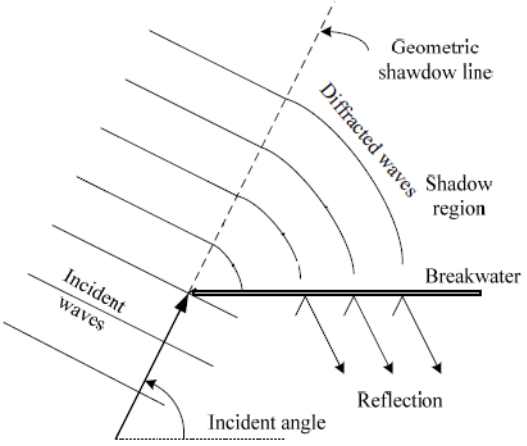

Figure 3.4: Wave diffraction induced by a breakwater (Rasmeemasmuang and Weesakul, 2009).

3.3.4 Wave reflection

Ocean waves are either partially or totally reflected by man-made structures such as breakwaters as shown in Figure 3.4 or natural objects such as sea walls and cliffs. Waves bounce back from these objects and can cause interference with other approaching waves which may result in standing waves (Reeve *et al.*, 2004).

3.3.5 Wave breaking

Wave breaking occurs when the front face of the waves become steeper which will lead into the slow motion of the wave crest. During this process, the orbital motion of the waves will change because of the seabed. This will cause the lower part of the wave to decrease its speed and eventually the wave crest will be unstable and the wave will start to break. According to Bosboom and Stive (2012) and Davidson-Arnott (2010), the wave breaking condition in deep water is limited by the wave steepness ratio $\frac{H_o}{L_o}$ and occurs when the wave crest interior angle is 120°. There are three categories considered as the basic types for wave breaking and these are illustrated in Figure 3.5.

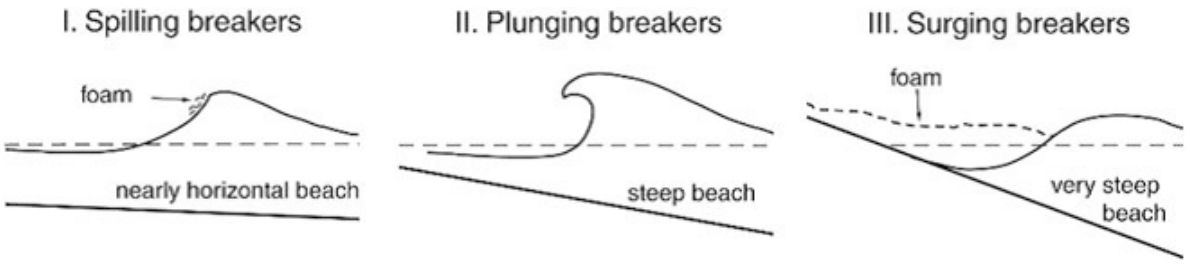

Figure 3.5: The classification of wave breaking types into categories and they all depend on wave steepness (Pecher and Kofoed, 2017).

3.4 Wave measurements along the South African coast

The understanding of the marine environment along the South Africa coastline requires an accurate observation of the sea state. Wave measurements are conducted and monitored by the CSIR in Stellenbosch on behalf of Transnet National Port Authority (TNPA).

Wave measurements have been collected on South African oceans since 1949 (Rossouw, 1984). Various measurement instruments are still used along the South African coast. The instruments that are used for the wave data collection include the wave clinometer observations, Datawell Waveriders, Directional 3D buoys and Datawell accelerometer buoys. The first Datawell accelerometer buoy was installed off the coast close to Mossel Bay in 1969. Datawell Waverider buoys are still one of the main sources of data for the South African coast. These measuring instruments provide vital information for coastal planning and management for ports and the public.

The Datawel Waverider buoy follows the motion of the water by floating on the surface. It records the wave profile by measuring the vertical acceleration of the buoy using an on-board accelerometer. It uses radio communication to send signals to a land based receiving station. According to Holthuijsen (2010), the method has become the most reliable for measuring surface waves and their direction. Other buoys can communicate via satellite by using remote sensing systems such as Global Positioning System (GPS) to measure waves (Holthuijsen, 2010). The buoys do not only measure the wave heights but they can also measure the wave direction. Further information about the South African wave measurement history can be found in Rossouw (1984) and CSIR (2015).

3.5 Description of wave stations

The wave stations considered in this study along the South African coast are shown in Figure 3.6. The stations have been chosen specifically to understand the variability of wave energy along the coast with Saldanha Bay as the case study for assessing the impact of a wave farm on the nearshore area. The energy spectra of these locations will be discussed in Chapter 4. In this section, the objective is to briefly describe the wave conditions at the chosen locations along the coast and the measurement instruments used to collect the wave data. Table 3.1 shows the wave recording stations and the measurement instruments.

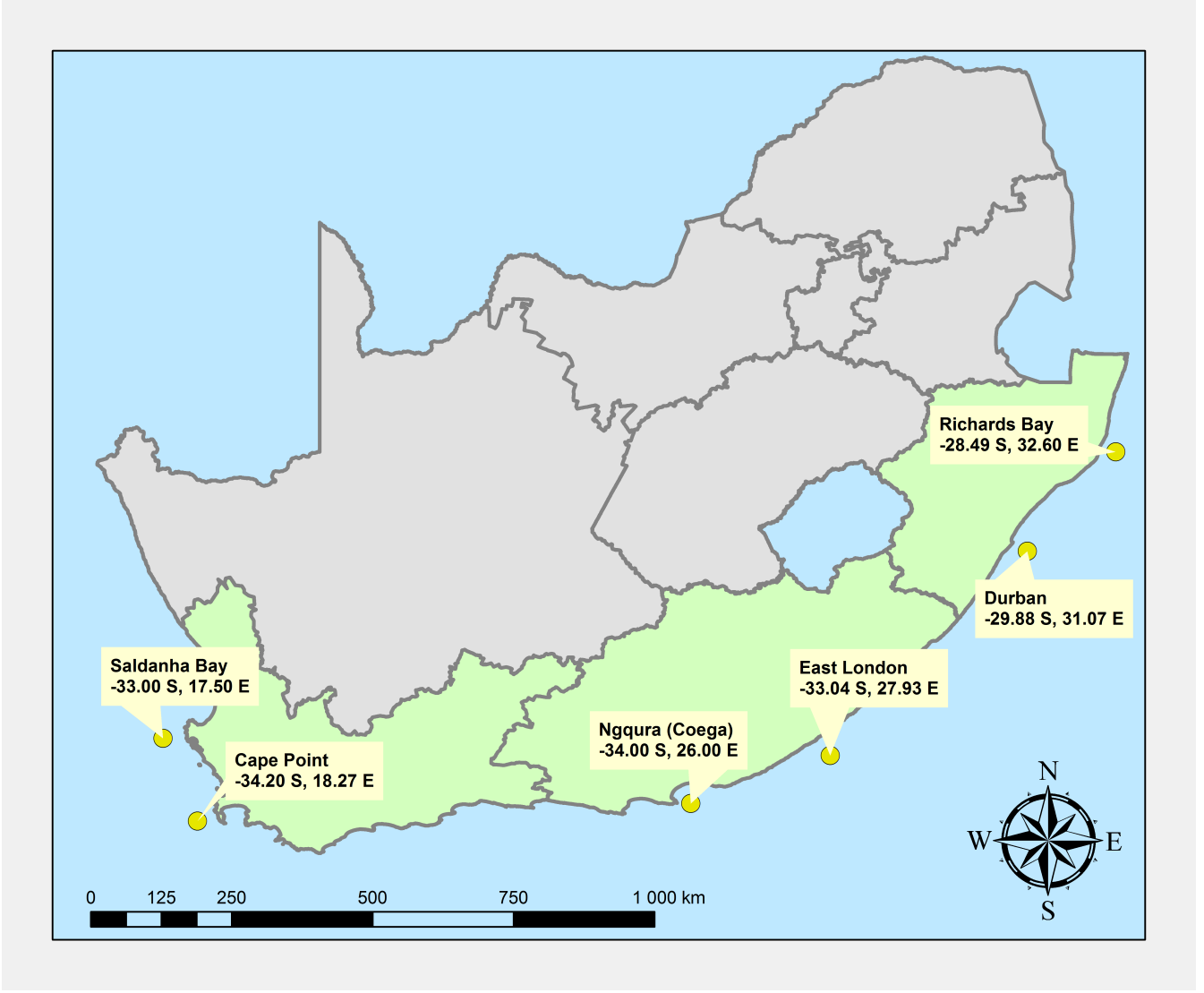

Figure 3.6: The wave data stations chosen in this study around the South African Coast.

The CSIR operates a real-time wave monitoring system which provides hourly updates on the wave conditions and weather at various locations around the South African coast on behalf of TNPA (CSIR, 2015). Rossouw (1984) conducted a study that contains a detailed wave climate conditions along the South African coast. The study provides a database of wave power resources, especially for the south-west coast of the country.

Table 3.1: Selected wave recording stations along the South African coast .

Wave stations			
Station name	Instrument	Water depths (m)	Long Lat coordinates
Saldanha Bay	Non-directional Datawell Waverider Buoy	23	-33.00S, 17.50E
Cape Point	Directional Datawell Waverider Buoy	70	-34.20S, 18.27E
Ngqura	Directional Datawell Waverider Buoy	21	-34.00S, 26.00E
East London	Directional Datawell Waverider Buoy	27	-33.04S, 27.93E
Durban	Directional Datawell Waverider Buoy	30	-29.88S, 31.07E
Richards Bay	Directional Datawell Waverider Mk 4 Buoy	22	-28.49S, 32.60E

3.5.1 Saldanha Bay

Saldanha Bay is approximately 100 km north of Cape Town. It is situated in the southern Benguela upwelling system on the Atlantic west coast of South Africa. The bay has a wide entrance. It is one of the natural harbours in the southern part of the African continent. The climate in this area is mild and influenced by the cold Benguela current that moves up the west coast of Southern Africa.

The CSIR maintains a non-directional Datawell Waverider buoy for TNPA. It is situated in 23 m water depth, approximately 2 km south west of the Port of Saldanha jetty. It monitors the surface waves continuously at the entrance of Saldanha Bay. Wave energy propagation in Saldanha Bay is subjected to wave processes such as refraction that result in decreased wave heights. The stations is chosen as the case study in this thesis due to high wave energy levels for wave power generation (Joubert, 2013).

3.5.2 Cape Point

The Cape Point wave station is situated near the second most south-westerly tip of the African continent. The station uses a directional Waverider buoy which is located at a water depth of 70 m approximately 7 km southwest of Kommetjie (Rossouw, 1984). The station is the most south-westerly located and is exposed to the dominant south-westerly winds. The dominant wave direction for this station is from South-west with 60% of significant wave height occurrence annually, as shown in Figure B.2.

3.5.3 Ngqura (Coega)

The Port of Ngqura is the port located on the shores of Algoa Bay on the east coast. The Port is 20 km northeast of Port Elizabeth in the Eastern Cape. Algoa Bay is subjected to extreme winds predominantly from the west of the south west and can affect ships entering the Port and cargo operations (Rossouw *et al.*, 2013). Understanding wave climate conditions in this area is of vital importance for wave energy analysis.

The port falls under the authority of the TNPA, which is responsible for wave measurements in this area. The directional Datawell Waverider buoy used to collect the data is situated at 21 m water depth, approximately 2 km from the breakwater (CSIR, 2015).

3.5.4 East London

The East London port is located about 600 km south of Durban. The wave climate conditions at the port are influenced by the hydrodynamic processes such as wave-driven longshore currents and the Agulhas current. Predominantly, the wave direction is from the south of south-west shown in Figure B.4. The directional Waverider buoy, which is situated about 1.2 km off the breakwater, at 27 water depth is used to record the wave data (CSIR, 2015).

3.5.5 Durban

The Durban port is located 178 km south of Richards Bay port, off the coast of KwaZulu-Natal. The mechanisms that are responsible for wave generation include the frontal system

(low pressure) passing along the South African coast. The system is responsible for the storm events all over the South African coast (Rossouw, 1989).

There are two directional Datawell Waverider buoys that are measuring the waves off the Durban coast. The Waverider buoy from the eThekwini municipality is situated 1.5 km from the shore, off the mouth of Umgeni River at 15m water depth. The CSIR Waverider buoy is situated 1.7 km from the shore at 30 m water depth, (CSIR, 2015).

3.5.6 Richards Bay

The Richards Bay wave station is located at the most northerly port on the South African coast. Waves in that area are generated by tropical cyclones and cold fronts that are more from west to east off the coast of KwaZulu-Natal. The Directional Datawell Waverider Mk 4 buoy is situated 1.4 km off the southern breakwater at 22 m water depth (CSIR, 2015).

3.6 Wave data records

The CSIR has been collecting wave data since 1961 along the South African coast (Rossouw, 1984). As a result, a wave research group called the National Mechanical Engineering Research Institute (NMERI) was established (CSIR, 2015). The objective of the group was to collect and statistically analyse the wave climate condition along the South African coast. Since then, the wave data has been continuously collected on the eastern and western parts of the coast.

The measured spectra data along the coast is continuously collected and analysed by CSIR on behalf of TNPA. For the purpose of the analysis, the period between 1 June 2014 to 31 May 2015 was selected. The selected period is the same for all the stations in Figure 3.6. Wave parameters such as significant wave height (H_{mo}), mean direction (θ_m) and the peak period (T_p) have been estimated from the wave spectra data which has been discussed in Chapter 2.

3.7 Summary

The objective of this chapter is to explain the generation of the ocean wave climate conditions along the South African coast. South African weather systems which have been considered as the main cause for wave generation along the coast, are briefly discussed. In this study, it is therefore important to understand the foundation of ocean waves and why we have energetic wave conditions along the coast. Further information about weather systems responsible for wave climate conditions along the coast can

be found in Rossouw (1989); Van der Borch van Verwolde (2004) and MacHutchon (2006).

Generation, propagation, and dispersion of ocean waves have been explained to understand the mechanism of waves as they approach the shallow water from deep water region. Also, wave transformation types have been introduced. This is also important to know due to wave energy dissipation induced by these transformations. Wave spectra changes depend on these wave transformations. This will be illustrated in Chapter 6 where the spectra of the output locations of the Saldanha Bay wave model will be plotted to see the variability of the spectra at different water depths. The spectral shape will show the amount of energy available with and without the WECs.

A brief overview of the wave conditions at chosen locations along the South African coast is given. Instruments used to measure wave energy at the chosen locations are listed in Table 3.1. The measured spectra data will be used in Chapter 4 to obtain one of the JONSWAP spectral parameters for South African wave conditions which will be used as the input parameter for wave simulations.

Chapter 4

Estimation of JONSWAP model parameters

4.1 Introduction

The analyses of sea states have led to the mathematical description of wave spectra. The spectral models of the sea surface elevation describe a frequency domain of the random process of the sea state (Lakhan, 2003). Several spectral formulations have been developed for the optimal mathematical description of wave spectra (Torsethaugen *et al.*, 2004; Soares, 1991; Hasselmann *et al.*, 1973). Some of these spectral models were derived to describe unimodal spectra. However, the sea state consists of the wind sea and one or more swell systems. Depending on the climatic conditions and the nature of the sea state, spectral models may consist of multiple peaks.

Various spectral models were proposed based on the marine environmental conditions for engineering and prediction purposes. Some of them were empirically derived by applying fitting techniques to measured data sets. For example, the spectral model called JONSWAP (Hasselmann *et al.*, 1973), was fitted to measured wave spectra data to provide values of the model parameters and their relationship to each other (Aranuvachapun, 1987). This spectral model was accepted as the standard model for wind-generated waves. It was formulated in 1968 and 1969 during an extensive measurement program in the North Sea, between the Island Sylt in Germany and Iceland (Hasselmann *et al.*, 1973). The JONSWAP model is also referred to as the modified Pierson-Moskowitz (PM) spectral model (Pierson and Moskowitz, 1964).

The objective of this chapter is to describe the theoretical background of the JONSWAP spectral model. This model will be fitted to a set of locally measured data to obtain the parameter values using South African sea state conditions, specifically the peak enhancement factor values. The basis of this model was formulated by Phillips (1958)

using dimensional analysis as basis, which will be further discussed in the Section 4.1.1.

4.1.1 Phillips spectrum

The spectral models for the description of the wind wave spectrum were developed in the field of physical oceanography by various researchers such as Phillips (1958), Pierson and Moskowitz (1964) and Hasselmann *et al.* (1973). These researchers investigated the influence of the wind on the wave growth with the intentions of deriving a mathematical expression that will describe ocean wave spectra.

Phillips (1958), investigated the growth of wind-generated waves. He, introduced the idea of an equilibrium range and assumed that the high-frequency part of the spectrum is limited by wave breaking process and gravity is the determining factor. Because of gravity, he concluded that the energy density at high frequencies depends on the frequency and the gravitational acceleration g (Holthuijsen, 2010). Dimensional analysis led to the expression of the wave spectrum at high frequencies given as

$$E_P(f) = \frac{\alpha_P g^2}{(2\pi)^4} f^{-5}, \tag{4.1.1}$$

where $\alpha_P = 0.0074$ is the Phillips proportionality constant and f is the wave frequency. The value of α_P, was obtained based on the wind wave measurements that were conducted in Middlesex, England. A capacitance wire recorder instrument was used to record the high-frequency components of the wave system (Phillips, 1958). The Phillips spectrum, which is described by Equation (4.1.1), denotes the high frequency side of the spectrum which is limited by wave breaking (Parente *et al.*, 2002).

4.1.2 Pierson - Moskowitz spectrum

Pierson and Moskowitz (1964) assumed that if the wind blew steadily for a long period of time over a large area, the waves and the wind would reach equilibrium. This is described as fully developed seas. This assumption led them to propose a mathematical expression that represents fully developed seas for the low-frequency part of the spectrum and introduced an exponential term to the Phillips Equation (4.1.1) which led to

$$E_{PM}(f) = \frac{\alpha_{PM} g^2}{(2\pi)^4} f^{-5} \exp\left\{ -\frac{5}{4}\left(\frac{f_p}{f}\right)^4 \right\}. \tag{4.1.2}$$

Here f_p, is the peak frequency of the wave spectrum and $\alpha_{PM} = 0.0084$ is the proportionality constant, which was obtained based on wave measurements (Pierson and Moskowitz, 1964). According to Parente *et al.* (2002), fully developed seas are very rare in nature since a steady wind blowing over a surface is required over a large area and a long

period. Further investigations were conducted by Hasselmann *et al.* (1973) to clarify wind wave growth under fetch limited conditions, which is discussed in Section 4.1.3.

4.1.3 JONSWAP spectrum

Wave measurement analysis was conducted in the North Sea in a quest to understand the growing seas under fetch limited conditions, where the number of wave record stations were carefully chosen and installed along the German coast (Hasselmann *et al.*, 1973). It was found that the sea state is never fully developed as was assumed during the analysis by Pierson and Moskowitz (1964). It continues to develop through nonlinear wave-wave interactions even for a very long time and over long distances. Hence, an extra term was introduced to the Pierson and Moskowitz spectrum in order to improve the fit of their model. This led to the formulation of the JONSWAP spectral model. The JONSWAP model is, therefore, a modification of the Pierson and Moskowitz spectrum.

Hasselmann *et al.* (1973), derived an expression for the frequency spectrum for the fetch-limited waves, where waves continue to grow until they reach the land, with an additional term, $G(f)$, given as

$$G(f) = \gamma^{\exp\left\{\frac{-(f-fp)^2}{2(\sigma fp)^2}\right\}}, \tag{4.1.3}$$

where σ is the width of the spectrum and γ is the peak enhancement factor.

The JONSWAP spectral model is one of the most widely used models in ocean and coastal engineering applications (Lakhan, 2003). It has been accepted as a spectral model for wind-generated waves both in laboratory and design experiments (Sorensen, 2005). This model has been used to approximate single-peaked spectra. Estimation of its parameters has been approached by different authors, for example Saulnier and Le Crom (2013); Young and Verhagen (1996); Aranuvachapun (1987); Kumar and Kumar (2008) and Mansard and Funke (1991), using different estimation techniques. The JONSWAP model is given as

$$E_{JP}(f) = \frac{\alpha_{PM} g^2}{(2\pi)^4} f^{-5} \exp\left\{-\frac{5}{4}\left(\frac{f_p}{f}\right)^4\right\} \gamma^{\exp\left\{\frac{-(f-fp)^2}{2(\sigma fp)^2}\right\}}, \tag{4.1.4}$$

with

$$\sigma = \begin{cases} \sigma_a = 0.07 & f \leq f_p \\ \sigma_b = 0.09 & f > f_p \end{cases}$$

- γ is the peak enhancement factor, which is used to describe a wind-wave growth of the sea state.

- α_{PM} is the proportionality constant as mentioned in Section 4.1.2.
- f_p is the peak frequency of the wave spectrum.
- σ is the width of the spectrum, σ_a being used for lower frequencies and σ_b for frequencies greater than f_p.

The values for spectral widths and the peak enhancement factor parameters in the JONSWAP data were found to be $\sigma_a = 0.07$, $\sigma_b = 0.09$ and $\gamma = 3$. In this study, it is assumed that the spectral widths values will change as the spectra develops depending on the wave conditions of the area of interest. The spectral width accounts two sides of the spectral peak (Hasselmann *et al.*, 1973).

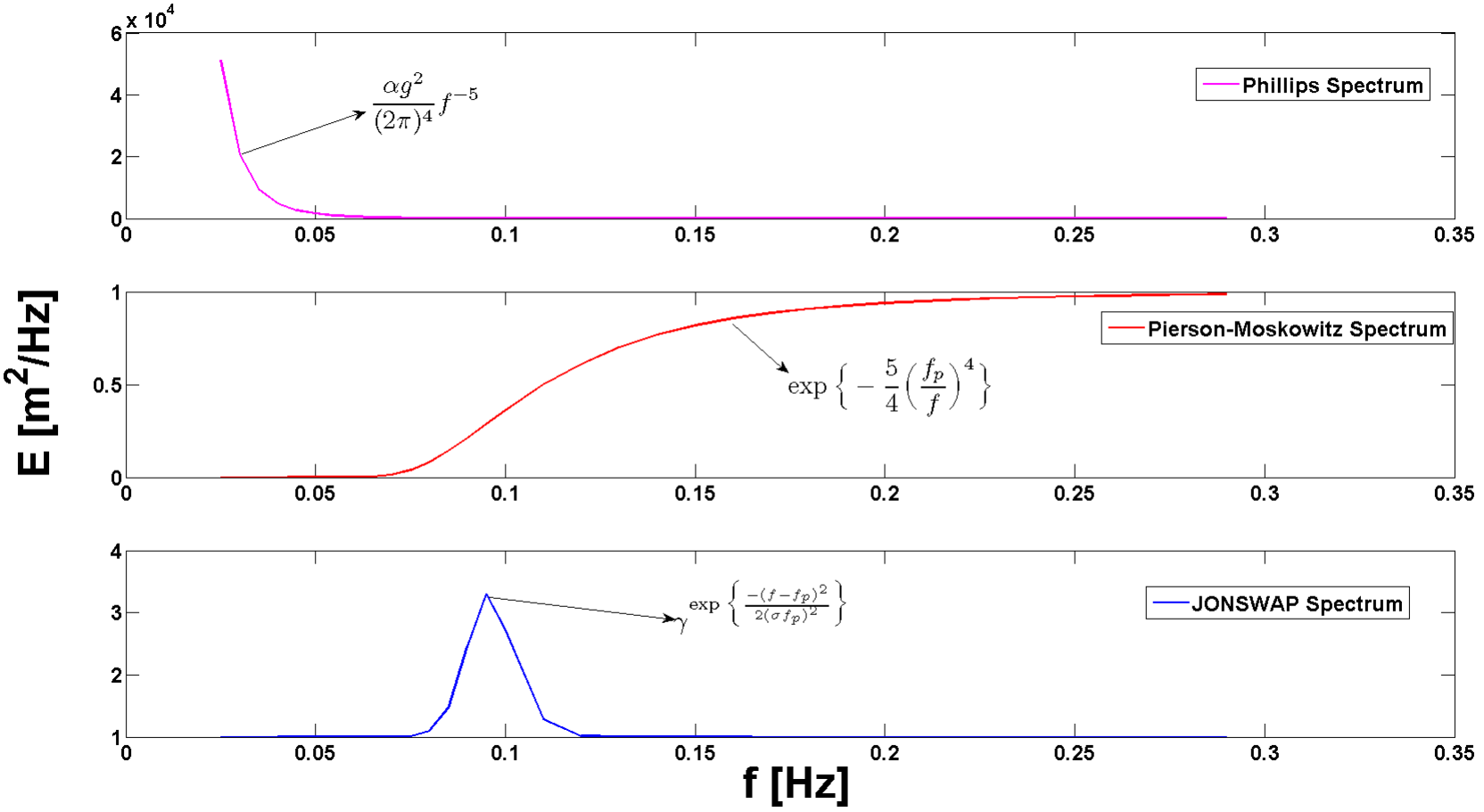

Figure 4.1: An illustration of the contributions to the JONSWAP spectrum. High frequency tail that was suggested by Phillips (1958), the smooth low frequency suggested by Pierson and Moskowitz (1964) and the γ parameter to enhance the peak of the spectrum suggested by Hasselmann *et al.* (1973).

The JONSWAP spectrum is a five parameter model with scale parameters (α and f_p) and shape parameters (γ, σ_a and σ_b). Figure 4.1 shows the effect of individual spectral shapes of Equations (4.1.1), (4.1.2) and (4.1.3) in the JONSWAP model represented by Equation (4.1.4). The propositionally constant $\alpha_{PM} = 0.0084$ and peak enhancement factor $\gamma = 3.3$ were used in the figure. The function of the parameter γ, is to enhance the peak of the spectrum as illustrated in Figure 4.1 of the bottom panel (Hasselmann *et al.*, 1973). If the value of the peak enhancement factor is higher, then, in general, the waves have strong wind as a forcing parameter. When $\gamma = 1$, the JONSWAP model reduces to Equation 4.1.2. The higher the values of γ, the narrower the spectrum will be around the peak frequency as shown in Figure 4.2.

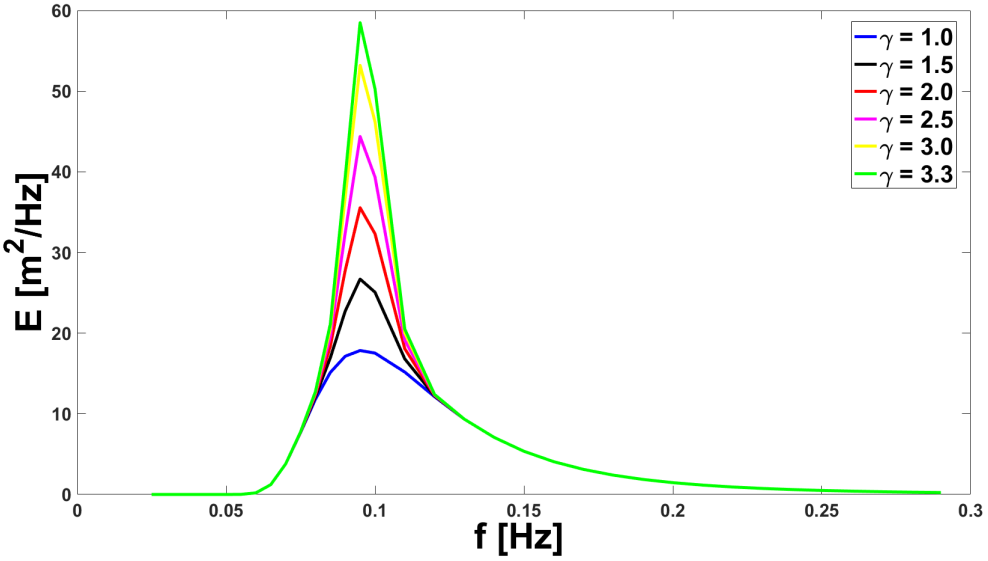

Figure 4.2: The JONSWAP Spectral model showing different gamma values.

4.1.4 Other spectral models

Several studies on the modelling of the sea state have been done. Most of them have addressed only the single peaked spectra. Models such as JONSWAP and Pierson-Moskowitz have been used to approximate single peaked spectra (Soares, 1999). However, it is not always the case that the sea states are single-peaked. Torsethaugen *et al.* (2004) and Ochi and Hubble (1977) developed spectral models that describe two-peaked spectra. These models include the swell and wind sea components. These two wave systems are separated in both frequency and direction (Holthuijsen, 2010).

The Torsethaugen spectrum is used to fit the spectral shape that represents the two wave system, where waves are influenced by local wind seas and swell waves. There are

other models used to define wave spectra in coastal and ocean engineering applications. The formulation of these models and how they are applied in the modelling of ocean waves are described in Appendix C.2. These spectral models are applied differently depending on the wave climate conditions of the area of interest.

4.1.5 Double and multiple peaked spectra

Various combinations of wave systems, wind sea and swell or more than one swell component from distant storms exist in the ocean. As a result, complex spectra with multiple spectral peaks will be present, as shown in Figure 4.3(c). The reason for this will be the meteorological conditions such as distant storms experienced within the area of interest. Due to these conditions, it is clear that the sea states cannot always be approximated by single-peaked spectral models.

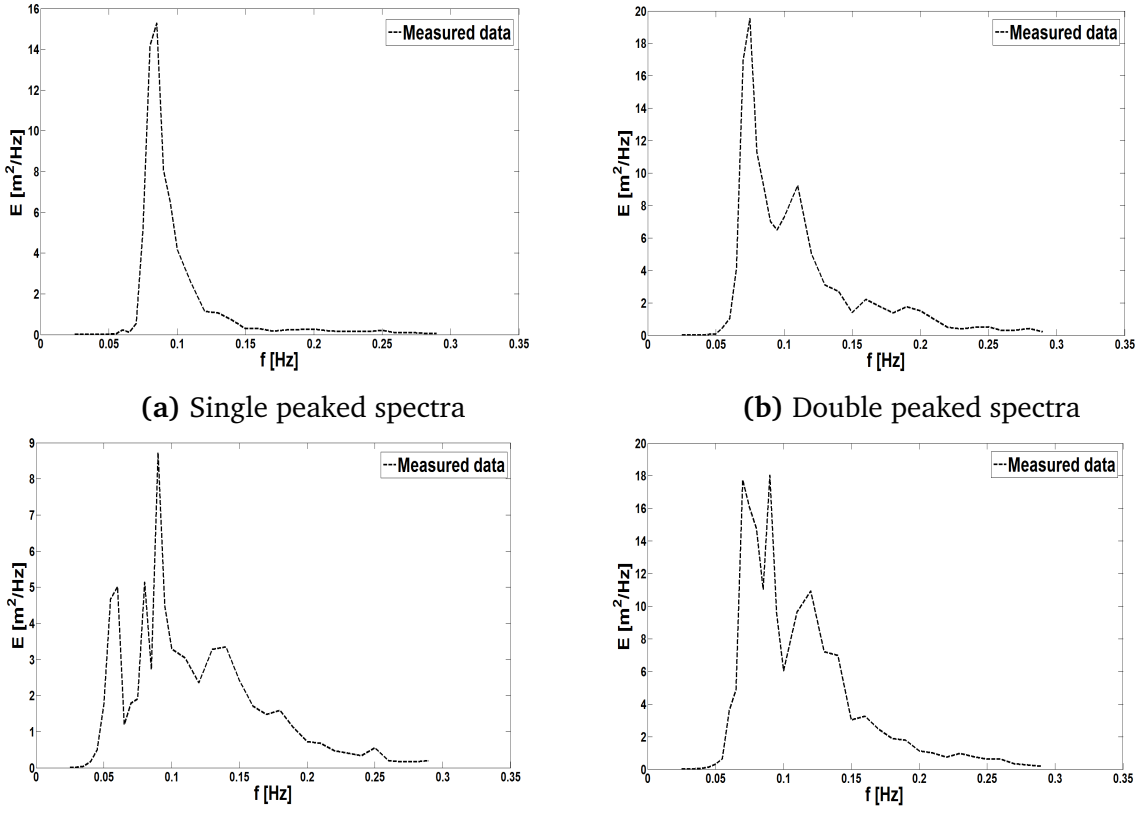

(a) Single peaked spectra

(b) Double peaked spectra

(c) Complex peaked spectra

(d) Multipeaked spectra

Figure 4.3: An example of the Cape Point measured data which represents single, double and multi-peaked spectra.

Lucas and Soares (2015) analysed a set of measured data of sea states and identified them according to classes of various spectral shapes of wave systems. For examples, spectral shapes shown in Figure 4.3. These classes include one-peaked spectra (see Figure 4.3(a)) with one wave system prevailing wind sea (class I) or swell (class II). The double-peaked spectra (class III, IV) which have two wave systems existing simultaneously and have a clear separation frequency that separates the two wave

systems (see Figure 4.3(b)). The multi-peaked spectra (class V) which contain complex wave systems with two or more swell systems are shown in Figures 4.3(c) and 4.3(d). Detailed information about the classification and characterization of the sea states is given by Soares (1999) and is further explained in Section 4.6. Wind sea and swell components are explained and discussed further in Section 4.2.

4.2 Wind sea and swell

The sea state generally consists of the combination of waves that are generated locally by wind and waves that propagated away from the area of generation as mentioned in Section 3.1. However, in deep water, as the waves move away from the area of generation the wave energy is transferred from higher (or shorter periods) to lower frequencies (higher periods). As the waves approach the shore, the wave height of the swell will slightly decay due to air resistance and bottom friction (Reeve *et al.*, 2004). Thus, the wavelength will decrease with distance. According to Reeve *et al.* (2004), there is no exact definition of the swell in a wave spectrum, but they can be characterized by long periods (lower frequencies).

It is not easy to identify these two wave systems due to the changing winds (in both magnitude and direction). A double-peaked spectrum can be associated with these two wave systems and they show a spectrum that is well separated as indicated in the Figure 4.4. However, if double peaks are very close to each other, then the wave systems can come from the same direction (Soares and Nolasco, 1992).

For multi-peaked spectra, several swell components can be present showing the dominance of a swell component at the location of interest, as indicated by the Figure 4.3(d). In this situation, it is difficult to analyze such a spectrum. However, for less complex wave systems, wave spectrum can be used to identify and separate the wave systems.

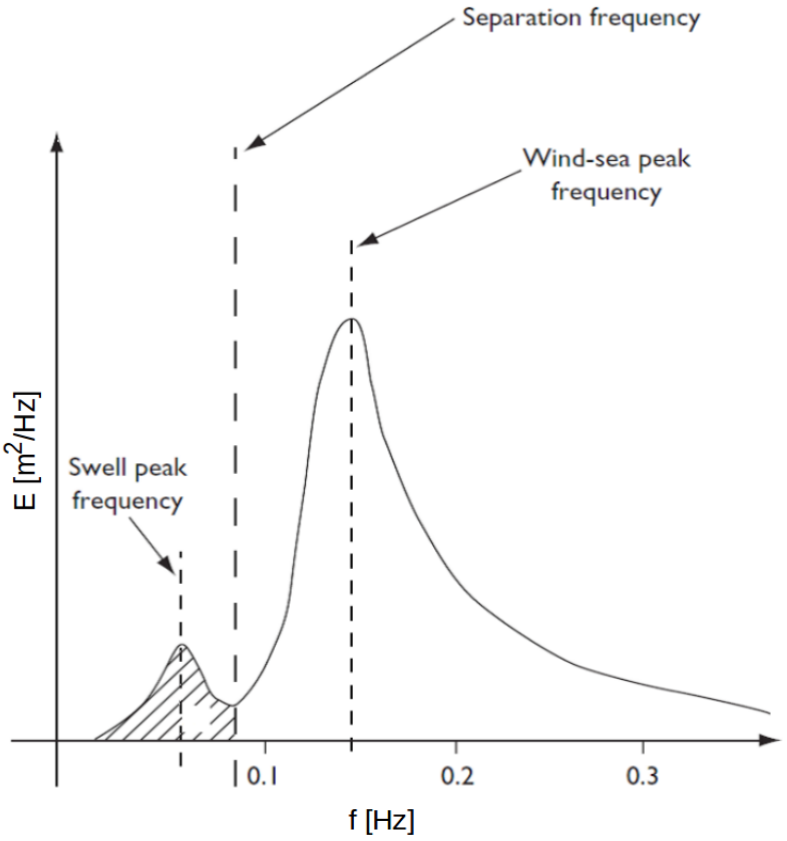

Figure 4.4: Representation of a bimodal spectrum, wind sea and swell components and the separation frequency that divides the two wave systems, adapted from Reeve *et al.* (2004).

4.3 Analysis of the measured data

This study makes use of data obtained from Datawell Waverider buoys, both directional and non-directional, which measures wave data along the South African coast. The wave records and number of frequency bins for each station are listed in Table 4.1. Saldanha Bay is the only station that uses a non-directional buoy as listed in Table 3.1. Various locations were selected to understand the variability of wave energy along the South African coast. Previous studies by Joubert (2008) and Brooke (2003) have shown that west coast of South Africa has the highest wave energy resource due to high wave conditions that exist.

Table 4.1: Wave records and the number of frequency bins for chosen locations.

Locations	Station code	Wave records	Frequency bins
Saldanha Bay	SB01	2866	35
Cape Point	CP01	2899	35
Ngqura	NG01	2799	35
East London	OL01	2825	35
Durban	DB08	2743	100
Richards Bay	RB01	2654	100

The wave energy spectra data from 1 June 2014 to 31 May 2015, at different water depths along the coast, were used for this study. The wave spectra data chosen is composed of the frequency (Hz), variance energy density (m^2/Hz), mean direction (°) and spreading factor (°) as variables. The measured spectra data as shown by Figures B.7, B.8, B.9 and B.11 in Appendix B.2, were plotted to observe the variability of wave energy for each data set.

Along the South African coast, single and double-peaked spectra were observed for the chosen locations, implying that the wave systems have two components, as mentioned in Section 4.2. Also, multiple and complex peaked spectra were observed, as shown in Figure 4.3. In this case, we can assume that the meteorological disturbances (e.g. frontal systems) were the result of the multiple and complex peaked spectra. The measured spectra for other stations, for example, Ngqura, show several peaks. Examples of such spectra are shown in Figure 4.5. These spectra show no clear separation between wind sea and swell. Such spectra are difficult to analyze since they show a complicated wave system with two or more swells present.

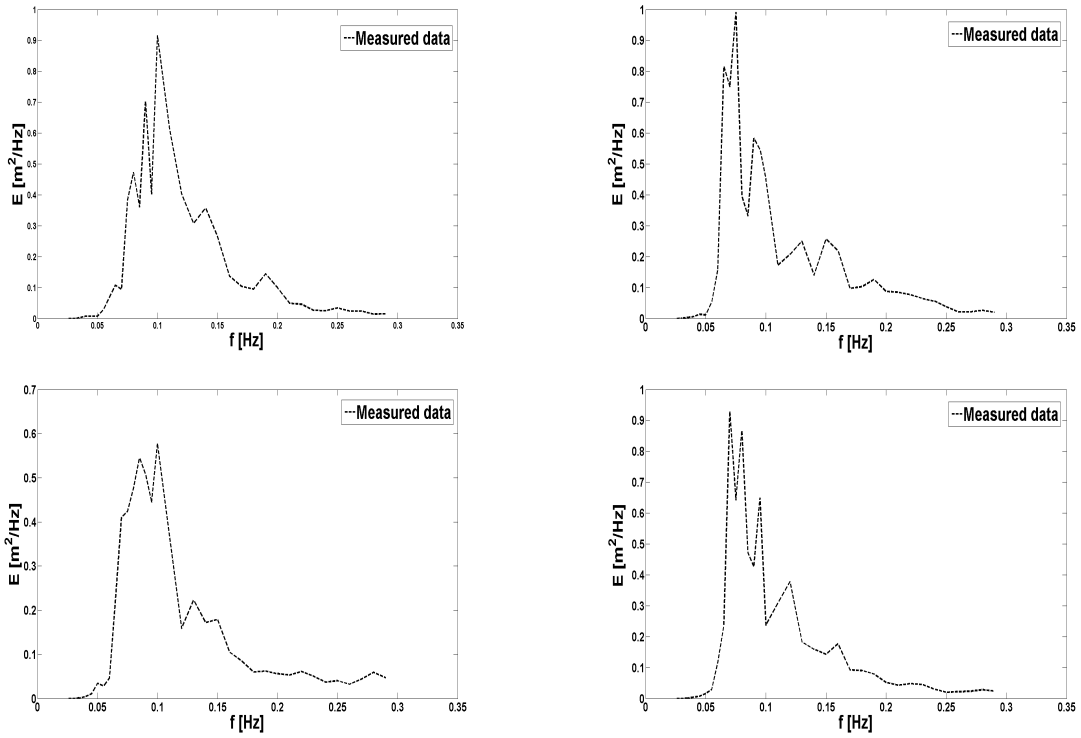

Figure 4.5: Measured spectra for Ngqura showing several spectral peaks.

4.4 The method for spectral fitting of JONSWAP spectra

The MATLAB function *fminsearch* which uses a direct search algorithm called the Nelder-Mead simplex algorithm, was used to estimate the JONSWAP model parameters in this study. The algorithm does not require any derivatives (Olsson and Nelson, 1975). Thus, it is suitable for non-smooth functions (e.g. JONSWAP model). The *fminsearch* function finds the minimum between the JONSWAP model and the data starting at given initial estimates.

In this study, the initial estimates were obtained from literature studies such as Hasselmann *et al.* (1973) and Pierson and Moskowitz (1964). The scale parameters (α_{PM} and f_p) and the shape parameter (γ) were estimated using *fminsearch* function. The parameters α_{PM} and f_p were kept constant. The usual choice for gamma is 3.3 which was obtained in the North Sea wave conditions. For the purpose of the analysis in this study, γ values in a range of $1.0 < \gamma < 7.0$ were chosen as initial estimates. With regards to the width of the model σ_a and σ_b, it was assumed that the values are the same as that suggested by Hasselmann *et al.* (1973). The width values are given in Equation (4.1.4).

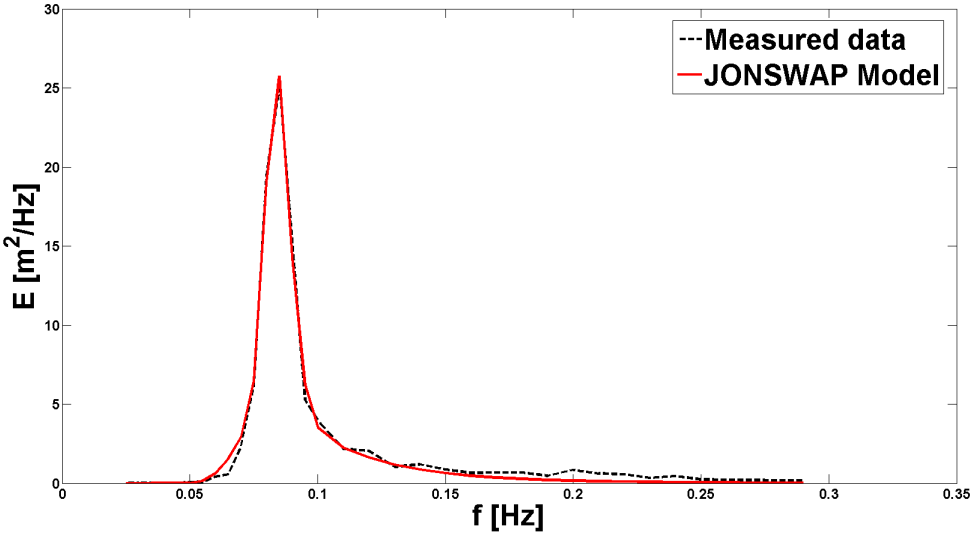

Figure 4.6: An example of the Cape Point spectral fitting of the measured single spectra.

The model was fitted at each 3-hour interval of the measured wave spectra for the chosen locations. Figure 4.6 shows one example of the JONSWAP model fitted to measured data. It can be seen from the figure that the model shows a good approximation for single peaked spectrum. The parameter estimates obtained for the model are listed in Table 4.2 were less than the standard parameter values of 0.0081 for α_{PM} and 3.3 for γ which are the default values in numerical wave models (e.g. SWAN).

Table 4.2: JONSWAP parameter values estimated from the measured data for all the locations.

Locations	α (mean)	γ (mean)	r^2
Saldanha Bay (SB)	0.000385	2.2191	91%
Cape Point (CP)	0.001671	2.1417	98%
Ngqura (NG)	0.001562	1.6966	96%
East London (EL)	0.001253	1.5922	94%
Durban (DB)	0.002638	1.4164	97%
Richards Bay (RB)	0.001821	1.4089	37%

To show how well the model approximates the observed data, the coefficient of determination r^2, was computed where the sum of squared errors between the model and the observed data were computed. The coefficient of determination values between the model and the data are listed in Table 4.2, deducing that the JONSWAP model shows a good approximation to the set of measured data from Saldanha Bay to Durban. With regards to Richards Bay, the JONSWAP model showed a poor approximation based on the coefficient of determination value. This may be due to severe storm conditions that were present and the observed data showed multi-peaked wave spectra. This can be

attributed to locally generated wind-waves coexisting with more than one swell, thus producing multi-peaked spectra.

As mentioned in Section 4.1.4, the JONSWAP model has been used to approximate single peaked spectra, not double or multi- peaked spectra. The model fails to approximate a double-peaked spectrum as shown in Figure 4.7. The models that can approximate double-peaked spectra are given in Appendix C.2. Due to unsatisfactory fitting of the model to the observed double and multi-peaked spectra, it was suggested that a spectrum must be decomposed in order to fit both JONSWAP and Pierson-Moskowitz models separately which will be discussed in the next sections.

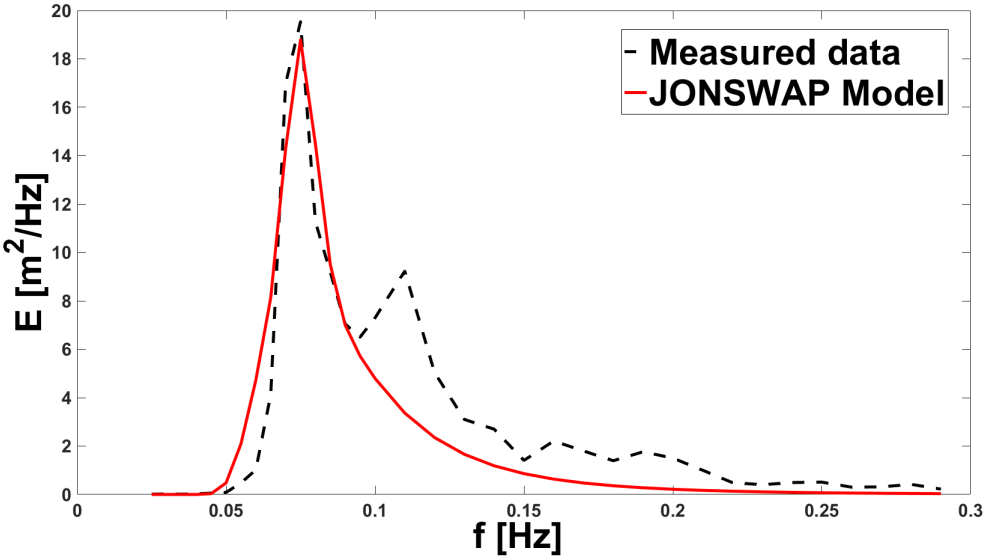

Figure 4.7: Cape Point measured double peaked spectra.

Soares and Nolasco (1992) studied wind-generated waves and noticed that the swell spectra are long-crested and narrow shaped and it will be appropriate to fit them with a JONSWAP model (Lakhan, 2003). The JONSWAP model was derived for single-peaked spectra and it cannot be used for double and multi-peaked spectra as shown by Figures 4.7 and 4.8. It must be noted that JONSWAP model was able to find the main peak correctly in a spectrum but it was unable to find secondary peaks.

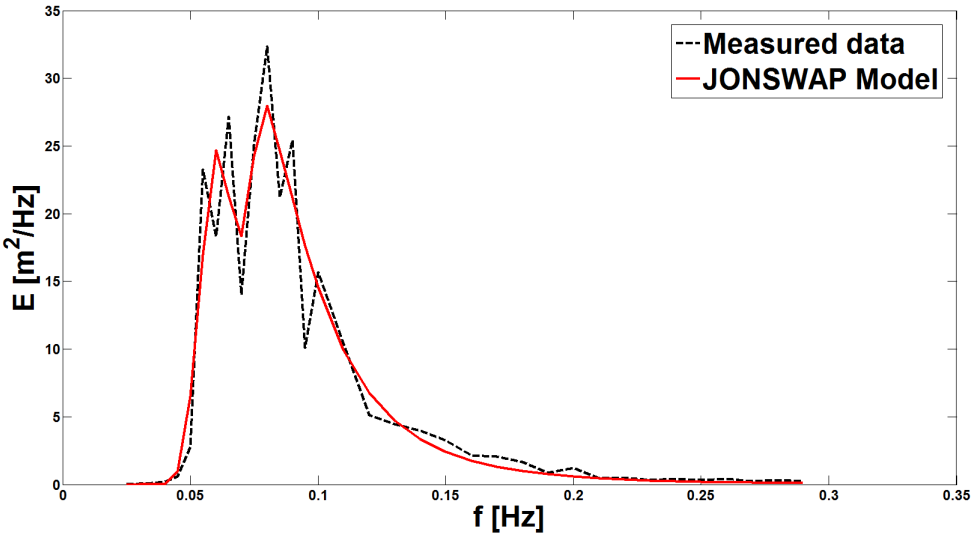

Figure 4.8: An example of the Cape Point fitted multi-peaked spectra.

4.5 Wave spectra decomposition method

The fitting of the JONSWAP model has been carried out in the study. It was found that the model is a good approximation for single-peaked spectra as shown in Figure 4.6. However, the model was unsatisfactory for double and multiple peaked spectra as illustrated by Figures 4.7 and 4.8, respectively. Several approaches by different authors have been proposed in the modelling of double and multiple spectra (Wang and Hwang, 2001; Aranuvachapun, 1987; Soares, 1999). These include characterization and classification of the sea state and spectral decomposition of the sea state.

Studies such as Wang and Hwang (2001), Ailliot *et al.* (2013) and Rashmi *et al.* (2013) have proposed a decomposition method to separate wave spectra into wind sea and swell. These methods are necessary for identifying spectral peaks of multi-modal wave spectra in order to examine how the energy is distributed in frequency and direction (Parente *et al.*, 2002). They make use of the separation frequency, f_s, which separates the wave spectra into two components, low and high-frequency corresponding to swell and wind sea, respectively as illustrated in Figure 4.4. According to Hwang *et al.* (2012), the methods usually follow two steps: identification of the spectral peaks and the combination of adjacent spectral peaks into a single ordinary wave system.

The most widely used method that applies to separation frequency is called the wave steepness method. The method was developed by the National Data Buoy Center (NDBC) (Gilhousen and Hervey, 2002). The method separates wind sea from swell with the knowledge that the wind seas are steeper than swell. The highest steepness occurs near the peak period of the wind sea component (Gilhousen and Hervey, 2002).

The wave steepness method uses the ratio between wave height and wavelength to compute the wave steepness parameter, $\xi(f)$, at a given frequency and is expressed as

$$\xi(f) = \frac{H_f}{L_f}, \tag{4.5.1}$$

where H_f is the wave height and L_f is the wavelength used for wave steepness computation. The wavelength is expressed as $L = \frac{gT_z^2}{2\pi}$ (in deep water) which is based on linear wave theory. The expression for H_f is the same as given by Equation (2.3.2). The parameter T_z, is the zero-crossing period given by Equation (2.3.4). The ratio is found by integrating from a lower to higher frequency of the wave spectrum. Substituting the wave height and period, we obtain the wave steepness parameter given as

$$\xi(f) = \frac{8\pi\left(\int_{f_l}^{f_u} f^2 E(f)df\right)}{g\sqrt{\int_{f_l}^{f_u} E(f)df}}, \tag{4.5.2}$$

where f_u and f_l are the upper and lower frequency limits in a spectrum, respectively. The separation frequency is computed as

$$f_s = C_w f_{p_w}, \tag{4.5.3}$$

where f_{p_w} is the peak frequency of the wave steepness parameter and $C_w = 0.75$ is the determined constant and was computed by Gilhousen and Hervey (2002). A detailed discussion about the separation method can be found in Wang and Hwang (2001).

4.6 Sea state characterization and classification

Soares (1999) conducted a series of studies in mixed sea states and concluded that sea state conditions can be classified as follows:

- Swell dominated sea states. The wave energy field is concentrated in the low-frequency part of the wave spectrum.
- Wind sea dominated sea states. The dominant wave energy field is confined to the high-frequency part of the wave spectrum.
- Sea states with similar influence from the wind sea and swell. The wave field energy is distributed equally over low and high-frequency ranges.

Based on these classifications, they proposed a method of characterizing sea states by using the concept of two related dimensionless parameters, Sea Swell Energy Ratio ($SSER$) and Intermodal Distance (ID) with the aim of identifying the energy distribution

and the spectral shape of the sea states (Rashmi *et al.*, 2013). The Intermodal Distance can be expressed as

$$ID = \left(\frac{f_{p_{ws}} - f_{p_{sw}}}{f_{p_{ws}} + f_{p_{sw}}} \right), \tag{4.6.1}$$

where ID is the separation frequency between the peak frequency, f_p, that corresponds to wind sea and swell components. The frequencies $f_{p_{ws}}$ and $f_{p_{sw}}$ are peak frequencies of the wind sea and swell, respectively. Using the ID dimensionless parameter, the sea states can be classified as follows:

(i) An ID value close to zero, is when a swell and wind sea spectral peaks are close to each other.

(ii) Sea states with double peaked spectra have spectral peak frequencies relatively separated.

(iii) An ID value close to 1.0, where both components (wind sea and swell) are well separated.

For the $SSER$ dimensionless parameter, which is the ratio of wave energies associated with each sea state, the parameter can be expressed as follows

$$SSER = \left(\frac{m_{0_{ws}}}{m_{0_{sw}}} \right), \tag{4.6.2}$$

were $m_{0_{ws}}$ and $m_{0_{sw}}$ are the zero order spectral moments of the wind sea and swell components. These spectral moments are based on the n^{th} order spectral moment given by Equation (2.3.1).

4.6.1 Wind sea and swell components from the measured data

In the present study, an automated method used to separate a wave spectrum into two wave systems, wind sea and swell was applied. The method was developed by Marx *et al.* (1993). The method was suggested because the JONSWAP model was unable to fit double and multiple peaked spectra as illustrated by Figures 4.7 and 4.8, respectively. Thus, it was necessary to separate these spectra. With separation of spectrum it is possible to identify which component contributes more to the energy concentration of the spectrum.

The method works as follows: all the wave energy lower than $f = 0.085$ Hz are assumed as swell component and above $f = 0.110$ Hz as wind sea component. The wave energy between 0.085Hz and 0.110 Hz at three discrete frequencies (namely: $f = 0.090$ Hz, $f = 0.095$ Hz and $f = 0.100$ Hz), is equally allocated between swell and

wind sea components. Following the procedure conducted by Marx *et al.* (1993), the method can be expressed by simple relationships given as

$$E(f)_{swell} = E(f) * \frac{F_1 * E(0.085)}{F_2 * E(0.090) + F_1 * E(0.085)}, \tag{4.6.3}$$

and

$$E(f)_{sea} = E(f) * \frac{F_2 * E(0.110)}{F_2 * E(0.090) + F_1 * E(0.085)}. \tag{4.6.4}$$

The measured spectra have discrete frequencies that are different from those proposed by Marx *et al.* (1993). This is due to the measured spectra that was used for the method. Table 4.3 provides the scaling frequencies used in Equations (4.6.3) and (4.6.4), respectively.

Table 4.3: Wind sea and swell frequency scaling.

Swell	Wind sea
$F_1 = 0.75$	$F_2 = 0.25$
$F_1 = 0.5$	$F_2 = 0.5$
$F_1 = 0.25$	$F_2 = 0.75$

A measured wave spectrum has been separated to examine how the wind sea growth modifies the pre-existing swells. A measured double-peaked spectrum as shown in Figure 4.7 was decomposed using the aforementioned method to see the distribution of wave energies as shown by Figures 4.9(a) and 4.9(b), respectively.

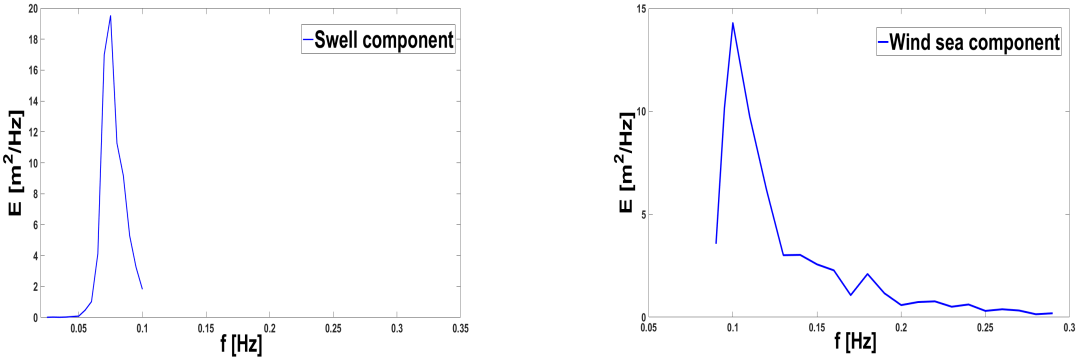

(a) Swell component **(b)** Wind Sea component

Figure 4.9: The decomposed double peaked spectrum.

The swell component was approximated with the JONSWAP model in Equation (4.1.4) due to its narrow shape and long-crest. The wind sea component was approximated with the Pierson-Moskowitz model in Equation (4.1.2) due to the broad shape and short-crest. This is illustrated by Figures 4.10(a) and 4.10(b), respectively.

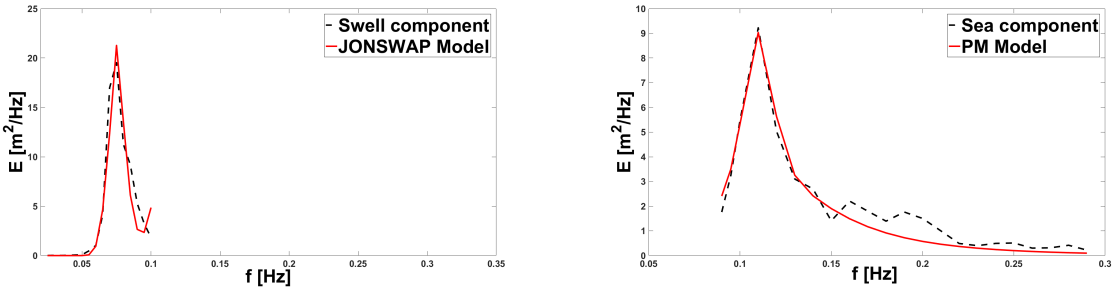

(a) Swell fitting **(b)** Wind Sea fitting

Figure 4.10: Fitted wind sea and swell components.

A similar procedure that was used in Section 4.4 for estimating the JONSWAP spectral parameters, was also used in this section to obtain the mean γ values for both wind sea and swell components as listed by Table 4.4. These stations were selected for the purpose of the analysis in this section. Table 4.4 shows the estimated mean values of three locations for the wave system components.

Table 4.4: Swell and sea parameter values estimated from the measured data for three locations using PM for sea and JONSWAP for swell component.

Locations	Wind Sea mean γ value	Swell mean γ value
Saldanha Bay	1.303	2.4963
Cape Point	1.308	1.3713
Ngqura	1.2032	1.9810

The measured wave spectra for the chosen locations showed outliers within the data. The outliers were removed as part of data analysis. The measured wave spectra showing several spectral peaks can be assumed as the possible reason for the outliers observed. According to Bosboom and Stive (2012), the swell component has more energy when comparing to wind sea due their long periods and larger wavelengths. It can be concluded that the γ values are higher for swell waves than wind seas as shown in Table 4.4.

4.7 Summary

The analysis of the measured wave spectra data at several locations along the South African coast has been conducted to see variability in wave energy distributions. Wave energy against frequency has been plotted to see spectral shapes and wave systems that exist along the coast. It has been found that the wave energy comprises two components, wind sea and swell. Swell being considered as a dominant wave system along the west coast and wind sea along the east coast. Based on these components, it was found that the swell component has more energy levels than wind sea. This is based

on the overall estimation of the peak enhancement factors for all the locations, as listed in Table 4.2. It was also found that the spectra of the west coast follow a JONSWAP spectral shape. The coefficient of determination values along the coast are listed in Table 4.2, implying that the model shows a good approximation for observed spectra along the coast, specifically for single-peaked spectra. The coefficient of determination value for Richards Bay was very low implying that the model showed a poor approximation to the observed data. This may be due to severe storm conditions mainly caused by weather systems (e.g. frontal systems or cyclones) that lead to multi-peaked spectra in Richards Bay.

Even though the JONSWAP model showed a good approximation for single-peaked spectra, it was noticed that the model is unsatisfactory for double and multiple peaked spectra. It is because of this reason that the automated algorithm to separate wave system components in spectra was applied. As expected, mean γ values for swell components were higher than wind sea components. The values will not be used as part of the input parameters for numerical wave model (e.g. SWAN). The objective of Section 4.6.1 was to fit both the JONSWAP and Pierson-Moskowitz models to spectra that have two wave systems present and the same time understand the contributions of wind sea and swell energies on the entire spectra.

A spectral decomposition method which is different to the one applied in this study is explained in Section 4.5 and is described further in Wang and Hwang (2001). The classification and characterization of the sea state have been explained in Section 4.6. The concepts for classification and characterization are important in the analysis of wave spectra due to their complexity when mixed sea states have been encountered at the location of interest.

Chapter 5

Characteristics of wave energy converters

5.1 Introduction

Wave energy devices are specifically designed to convert wave power into electricity and have parts that move due to the action of the waves (Jamasb *et al.*, 2006). Many of these devices are still under research and development but a small number of these have been tested and deployed at large scale in the UK (Drew *et al.*, 2009; Behrens *et al.*, 2012). Most have been invented in Japan, North America, and Europe (Clément *et al.*, 2002). According to Margheritini *et al.* (2012), about 56% of these devices are located in Europe. Most of these devices vary in design and are deployed at various locations in the ocean. These devices are not yet commercially viable but it is expected that in future they will be due to the rise of interest in renewable energy.

5.2 Location of wave energy devices

Wave energy devices are usually classified according to their placement on the ocean surface. These positions include the shoreline, nearshore (20 - 30 m water depths) and offshore (which are devices placed in more than 30 m water depths). The devices can also be classified according to their operational principle which will be discussed in Section 5.3

5.2.1 Shoreline devices

Shoreline devices are built or installed on rocky cliffs and others are integrated in breakwater-like structures. These devices are easy to install and maintain and they do not require long lengths of underwater electrical cables. One of the disadvantages of such devices is that they experience much less wave power resource due to the local

bathymetry and shoreline geology.

When the waves approach shallow water they break and lose energy before arriving at the device. The most common shoreline device for shallow waters is the Oscillating Water Column (OWC). It consists of a partially submerged concrete structure that is opened below the water surface and has trapped air on top of the water column. As the waves approach the device, they will cause the water column to rise and fall, compressing the air inside the device, and ultimately rotating the turbine that generates electricity to the grid. OWCs use a Wells turbine to drive the generator and these turbines rotate in the same direction irrespective of the air flow.

Several OWC devices have been installed worldwide, namely, on the shores of Scotland (Wavegen LIMPET, 500 kW), Portugal (Pico island, 400 kW), Japan (Sakata, 60 kW) and in breakwater-like structures in Spain (Mutriku, 300 kW) (Guedes Soares *et al.*, 2014; Jamasb *et al.*, 2006).

5.2.2 Nearshore devices

Nearshore devices are deployed in shallow water of 20 to 30 m depths, up to several kilometers away from the shoreline. Most of these devices are moored to the seabed and therefore stationary. At the nearshore, the wave power is higher than that at the shoreline. Installation and maintenance costs exceed those of shoreline devices. One example of a nearshore device is the Wavegen OSPREY which stands for Ocean Swell Powered Renewable EnergY and is of the OWC type (Brooke, 2003).

5.2.3 Offshore devices

Offshore devices are deployed at deepwater depths of 40 m or more. These devices are either floating or submerged in deep water. They can harvest a great amount of wave energy from the open seas. However, these devices are difficult to maintain due to extreme wave conditions. Durability and mooring systems are the major issues for these devices. Such devices need to be designed in a manner that they can endure the extreme wave conditions and salt-water corrosion that exist in open seas. Examples of these offshore devices are Archimedes Wave Swing (AWS) and the Pelamis, which are shown in Figures 5.1 and 5.2, respectively.

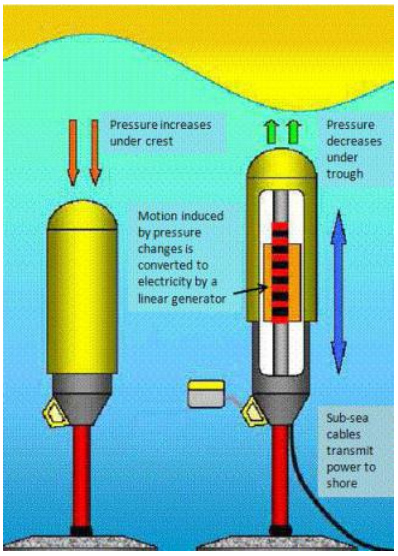

Figure 5.1: Archimedes Wave Swing (Parry *et al.*, 2007).

5.3 Wave energy device types and conversion systems

Based on the different designs and working principles, wave energy extraction can be categorized into three types: *floating or pitching*, *oscillating water column* and *overtopping*. Wave energy converters have been specifically designed to extract energy in different forms at different wave climate conditions.

5.3.1 Surface floats or pitching devices

Surface floating or pitching devices are devices that are floating on the ocean surface or fixed on the ocean floor to ensure the floating part of a device follows the harmonic motion of the waves to generate power. The Archimedes Wave Swing (AWS) device, illustrated in Figure 5.1, is a good example of such a device.

The device consists of a cylindrical shaped air-filled chamber (the floater). Due to the harmonic motion of the wave, the entrapped air from the floater swings up and down due to pressure differences caused by wave action. The floater is the only moving part of the device, as shown in Figure 5.1. This movement of the floater is used to generate power by a linear generator. The air floater has a diameter of 9.5 m and a height of 21 m (Salimullah *et al.*, 2014). The device was first tested at the Portuguese northern coast at the full-scale open water where it produced 2 megawatt (2 MW) of power.

Figure 5.2: Pelamis P2 device on site in Portugal (Pecher and Kofoed, 2017).

The Pelamis device, shown in Figure 5.2, is another promising surface floating device. It was developed by Pelamis Wave Power, formerly known as Ocean Power Delivery Ltd, in Scotland. This offshore attenuator device is a semi-submerged articulated cylindrical structure. It consists of 3.5 m diameter hollow steel segments, that are connected by four flexible joints and has a length of approximately 150 m (EMEC, 2015). The Pelamis device is tethered to the ocean bed so that it can swing perpendicularly to the incoming surface waves. The device points in the direction of the incoming waves. Waves travel down the length of the device and, in doing so, each of the long sections moves up and down and side to side. The movement is resisted by hydraulic rams. A hydraulic ram drives oil through a hydraulic motor which drives a generator that generates electricity (Tabak, 2009). The power is transmitted to the shore using standard sub-sea cables.

The first Pelamis P1 wave farm operated in 2008 at Aguçadoura 5 km off the Atlantic coastline of the Portuguese northwest coast, where it became the first offshore wave power converter to successfully generate electricity into the national grid. Due to the global financial crisis of 2008, the wave farm was removed. The second generation, Pelamis P2, was developed on the basis of Pelamis P1 (He *et al.*, 2013). Pelamis P2 is considered to be more efficient than Pelamis P1. The device has been manufactured and tested at the European Marine Energy Centre (EMEC) in Orkney Islands, Scotland, which is the only grid-connected test facility for wave and tidal energy converters in Europe (Bahaj, 2011). The P2 device has five sections, linked by four joints that have a diameter of 4 m and a length of 36 m. It has a power output of 750 kW and a total length of 180 m (Yemm *et al.*, 2012). The first of these devices, designated

P2-001 and P2-002, were installed in October 2010 and May 2012 respectively and have generated hundreds of megawatt hours (MWh) of electricity into the grid (EMEC, 2015). According to Polinder and Scuotto (2005), three units (2.25 MW) are being researched and developed and will be installed in Portugal.

Pelamis has reached the manufacturing stage and are constructing a wave farm that will be deployed in Scotland. It will consist of 40 Pelamis units with a maximum of 30 MW capacities in total, in a square kilometre array generating electricity to 20 000 homes.

5.3.2 Oscillating water column devices

Oscillating water column devices are built or installed into the shoreline and are easily maintained. They capture less energy compared to the nearshore and offshore devices. The reason is that as the waves move towards shore, the seabed interaction reduces the wave energy and less power will be generated to the grid.

These devices consist of a wave capture chamber with an open-air turbine. As waves approach the device, they enter the device from below, forcing the air through the turbine, as shown in Figure 5.3. The channelled air spins the turbine generator and power is generated. The OWC devices use a Wells turbine and they have the ability to spin in one direction regardless of the direction of the air flow. The only moving part is the Wells turbine which was named after its inventor Professor Wells (Smith, 2013). The turbine can easily be removed for maintenance. The OWC energy conversion systems are the most utilized in the field of wave energy conversion (Joubert, 2013). According to Jamasb *et al.* (2006), large numbers of OWCs have been built worldwide. A few examples are listed below:

- *The Wavegen LIMPET* is a 500 kW (2*250 kW counter rotating Wells turbines) plant installed on the island of Islay off the west coast of Scotland.
- *Japanese OWC device, kaimai* which was developed by Yoshio Masuda and who is regarded as the father of wave energy technologies (Guedes Soares *et al.*, 2014).
- *The European OWC Pilot Plant, Pico OWC* that is situated at the island of Pico.

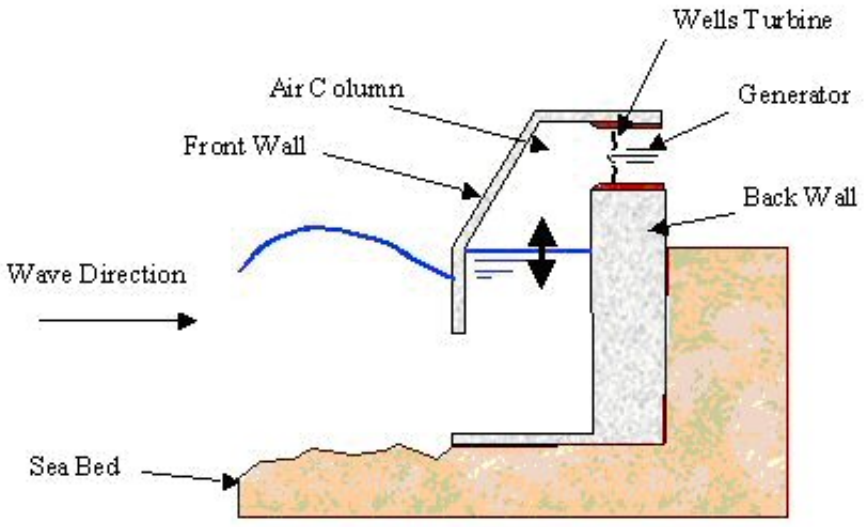

Figure 5.3: Schematic of the Oscillating Water Column Device (Thorpe, 1999).

The Land Installed Marine Powered Energy Transformer (LIMPET) OWC device, was the first shoreline commercial-scale wave device to be grid-connected. The first of its kind was installed in Hebridean island of Islay, off the southwestern coast of Scotland and became operational in November 2000 (Brooke, 2003). The device is fixed to a rocky cliff and is easy to maintain. The location for this device was specifically chosen due to the strong waves of the Atlantic Ocean at this position. The device was developed by Queens University in Belfast in partnership with Wavegen Ireland Ltd. It has been operating remotely since November 2000, producing electricity to the United Kingdom's electrical grid. There is another large OWC plant that is currently operating in Europe on the Island of Pico, Portugal.

The LIMPET device has three distinct components: namely, the OWC collector, a turbo generation unit and a control and monitoring station, as illustrated in Figure 5.3. The water columns are placed side by side and are made from steel-reinforced concrete with an external width of 21 m and a surface area of 170 m^2 (Brooke, 2003).

5.3.3 Overtopping devices (OTD)

Overtopping devices are generally large structures in the ocean that captures surface waves in a water reservoir. When the water level in the reservoir is high, the water leaves the reservoir through a number of low-head turbine outlets. This will drive the turbines as the water flows back out to the sea under gravity, which will generate electricity. According to Guedes Soares *et al.* (2014), the energy conversion system is similar to that used in hydro-power. Top and cross-sectional views of the wave dragon layout are illustrated in Figure 5.4. It was developed by Danish Wave Energy programme. Wave Dragon is an offshore and nearshore slack-moored energy overtopping

type device. It is a simple structure that has turbines as the only moving parts. The device consists of two wave reflectors that focus the incoming waves towards the ramp, a water storage reservoir for collecting the overtopping water and a set of low-head independent water turbines (Bevilacqua and Zanuttigh, 2011; Polinder and Scuotto, 2005; Christensen *et al.*, 2005; Diaconu and Rusu, 2013).

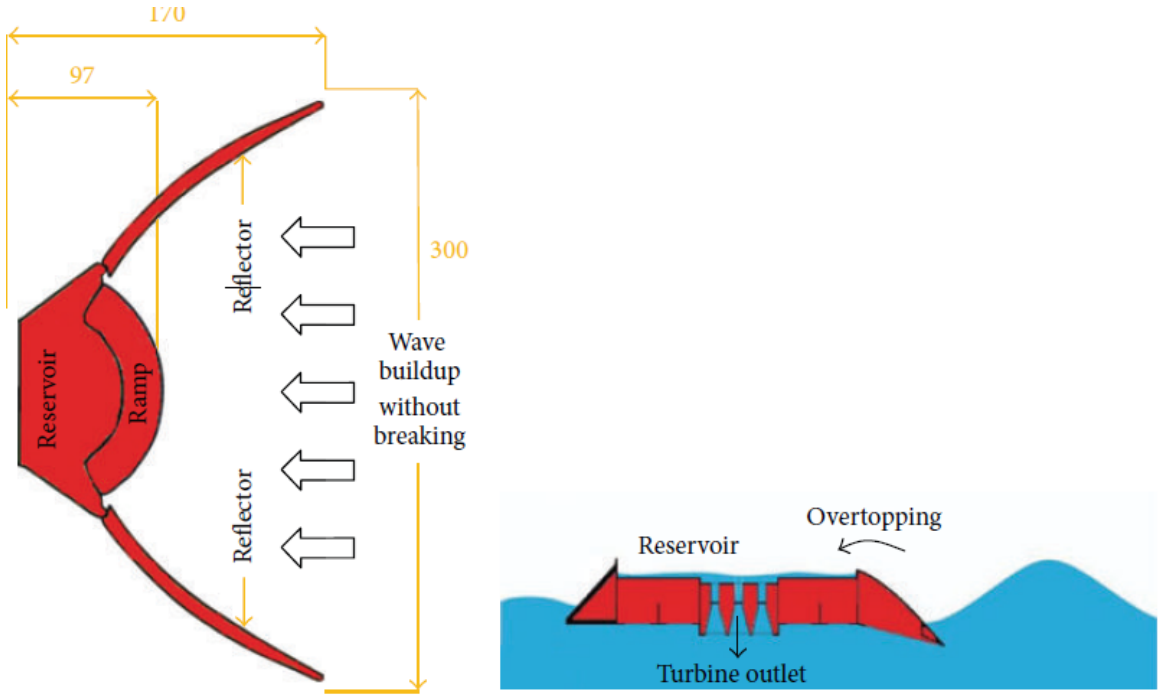

Figure 5.4: The basic principle of Wave Dragon device, ocean waves overtopping a ramp, water is stored in a reservoir and water falls through hydro turbines (Diaconu and Rusu, 2013).

The device is a unique converter as it uses the energy in the water directly via turbines. It has a capacity of 1.5 - 12 MW, depending on the wave climate, and is specifically designed so that it can swivel itself into coming waves. This device is moored in the deep water of more than 52 m to harness the waves before they reach the coastal area. It has a width of 260 - 390 m, with an arm length of 145 m. The distance between the tips of the arm is 300 m. The water reservoir storage contains approximately 8 000 m^3 of water and has a total weight of 54 000 tons (Joubert, 2008).

In Nissum Bredning, off the coast of Denmark, a 237 ton prototype was deployed, as shown in Figure 5.5. The device was equipped with 7 turbines, of 20 kW each. Each turbine generates electricity via a permanent magnet generator. The prototype is connected to the electrical network on the mainland via undersea cables since 27 of June 2003. At full scale, the device will generate 4 MW in a location with stronger wave climate conditions (Polinder and Scuotto, 2005). The long-term objective is to connect several units together in a wave farm along coastlines that will generate 80 to 100 MW (Christensen *et al.*, 2005).

Figure 5.5: Wave dragon in Nissum Bredning, coast of Denmark (Bevilacqua and Zanuttigh, 2011).

5.3.4 Stellenbosch Wave Energy Converter (SWEC)

According to CRSES in Stellenbosch, the oil crisis in 1970 led to research in renewable energy (Joubert, 2013). In 1985, Professor Deon Retief from Stellenbosch University designed an energy device called the Stellenbosch Wave Energy Converter (SWEC), as shown in Figure 5.6. The device was specifically designed for South African wave conditions (Du Plessis, 2012; CRSES, 2015; Joubert, 2008). The purpose of this development was to find alternatives for electricity generation due to the oil crisis. The project was funded by Murray and Roberts and Anglo American (Joubert, 2013).

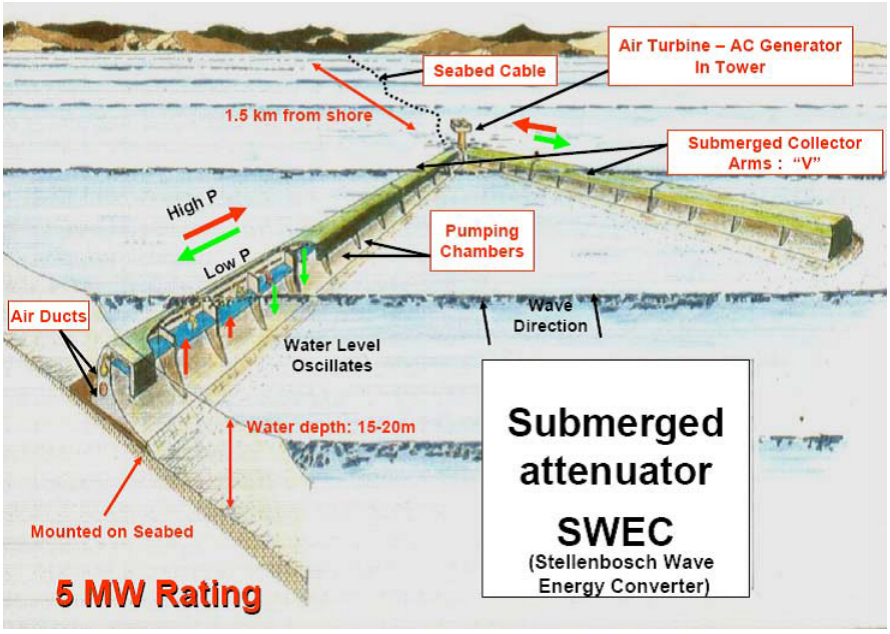

Figure 5.6: Schematic diagram of the Stellenbosch Wave Energy Converter (SWEC) (Joubert, 2008).

The SWEC is an OWC type converter and was developed specifically to harness the wave power that is found in the southwest of the South African coast (Joubert, 2013). The energy device has V-shaped submerged collector arms. It consists of 12 series of OWC chambers in which water level oscillations displace air via inlets. The outlet valves

go through to the low and high-pressure manifold systems which are connected to the air turbine in the tower (Joubert and Van Niekerk, 2009). According to Joubert (2013), there are features that differentiate this device from the typical OWC. These features include the collector arms which are fully submerged and the Power Take Off-system (PTO) mechanism with an air-turbine that can be optimized for airflow.

According to Joubert (2013), the generation potential of 10 chamber ShoreSWEC at the area of interest, on average is 6 kW for a 15 kW capacity system. The capacity is based on 11 years of hindcast wave data and experimental results given by Joubert (2013).

5.4 Mooring systems for wave energy converters

Most of the WECs need to be kept in position by mooring systems to protect the device against severe wave conditions. The mooring system is directly linked to the device's design and working principle (Harris *et al.*, 2004). The chosen location is also important for the mooring system of the devices. In literature on WECs, it has been shown that devices that are installed on the open seas have a potential of extracting more energy because of the higher energy density available. However, the installation costs and maintenance of the mooring systems are high.

According to Harris *et al.* (2004), there are two major requirements for mooring WECs: the capability of the device to withstand the environmental conditions and the durability of the loadings to keep it in position. These requirements are crucial for the device to be economically feasible. It is very important to provide a low-cost installation that has a reliable system and is easy to maintain.

5.5 Wave climate conditions for wave energy converters

Producing sufficient energy is one of the most important functions of WECs. According to Carballo *et al.* (2014), the energy that can be produced by a WEC device can be determined by the combination of a power matrix of the device and the bi-variate scatter diagram of the wave energy resource at the location of interest. The bi-variate scatter diagram depicts the distribution of wave energy available using a combination of significant wave height and wave period pairs. The power matrix is directly derived from the scatter diagram and it contains the power output efficiency of the energy devices. Power matrices of some devices are given by Silva *et al.* (2013). The power matrix provides the power output of the sea states which is indexed by the combination

of significant wave height and peak or energy period. Multiplying the bi-variate scatter diagram and power matrix produced by the device developer gives the total annual power output at the location of interest. WECs have a maximum efficiency in the higher ranges of H_{mo} and T_e, where T_e is the energy period, which can be related to the peak period, T_p, and H_{mo} is the significant wave height. These wave parameters have been explained in Section 3.3.1. The combination of these parameters is referred to as the energy bin.

Different combinations of H_{mo} vs T_e and H_{mo} vs T_p have been used to show the expected power output of energy devices. Most of the power matrices are produced by device developers and are not widely available. These include the efficiency and power output of the device for different sea states.

WECs with various working principles and sizes were studied for power absorption at different locations at the sea by Babarit *et al.* (2012). They computed power matrixes and scatter diagrams of the sea state, at the location of interest, for each device. It was noticed that the power absorption for each device, at various locations, are different. Furthermore, even if there is an increase in the wave power resource, it does not necessarily mean there will be an increase in annual power absorption. This was based on the two selected locations with longer waves compared to the other. For longer waves, the wave resource is larger but the power absorption of the two WECs out of eight was less due to their working principle. In this case, it can be assumed that the power absorption depends on the working principle and the size of the WEC, not the wave resource.

As mentioned in Chapter 1, to produce enough electricity, WECs must be deployed in a wave farm. The distance between the WECs in a wave farm is an important factor for sufficient energy production and it must be known. O'Dea *et al.* (2014) modelled a wave farm of 60 devices in two staggered rows and these devices were included in the spectral wave model SWAN. Each device had an 18 m diameter. Closely spaced arrays had a distance of 72 m (4 times the WEC diameter) between devices and rows. Widely spaced arrays had a distance of 180 m (10 times the WEC diameter) between devices and rows. According to this study, assessment on the spacing of devices both closely and widely spaced were simulated for each set of input wave conditions (significant wave heights, peak periods and directional spreading). It was concluded that the distance between the wave farm and the shore has an impact on the magnitude of the nearshore effects of the arrays (O'Dea *et al.*, 2014).

With regards to the energy range that ensures optimal performance and durability, the information is not yet published or available. These questions will be addressed

further in Chapter 6.

5.6 Modelling of the power transfer function of the WECs

WECs are complex marine structures when it comes to the power output. To predict the power output of WECs per wave crest at each frequency is one of the important characteristics of wave energy extraction. Generally, energy devices respond differently at differently sea states, depending on the type and design of an energy converter. The ability of WECs to extract power at each frequency is referred to as the response function or Power Transfer Function (PTF) (Smith *et al.*, 2012). According to Smith *et al.* (2012), PTFs of the energy devices are not yet available or published. They are determined experimentally and can be assigned to represent any type of energy device (O'Dea *et al.*, 2014).

Several studies Millar *et al.* (2007), O'Dea *et al.* (2014) and Smith *et al.* (2012), have used spectral models such as SWAN to investigate the nearshore effects of the wave field due to wave farms. These studies used the frequency dependent transmission coefficient through an obstacle, where energy absorption transmission coefficients were considered with the absence and presence of wave farm. Millar *et al.* (2007) studied a change of wave spectrum before and after the obstacle absorption rates using SWAN. Wave spectra changes induced by wave farms were assessed and it was noticed that there is a reduction in significant wave height. Further information about the response curves in front and behind the wave farm will be addressed in Chapter 6.

5.7 Summary

Wave energy devices of various design and working principles have been discussed. These include a Pelamis wave power device which was the first device to be commercialised. These devices vary in design and operate differently depending on the wave conditions they encounter and are deployed at various locations in the ocean. They generate electricity using various operational principles. There are advantages and disadvantages. Offshore devices have an advantage of extracting enough energy but the disadvantage is the high cost of maintenance and installation and long subsea cables. Nearshore and shoreline devices extract less energy compared to offshore and are not difficult to maintain. The devices are kept in a stationary position by mooring systems to withstand the extreme wave conditions.

The amount of energy that can be produced by WECs depends on the surrounding wave

Table 5.1: A list of few energy devices which have been deployed, tested and commercialized.

Device name and company	Country of origin	Location	Device capacity	Device status	Capture method	Water depth	Power take-off	Number of devices	Size of the device
AWS Ocean Energy	Scotland, (UK)	Offshore	2.5 MW	Operational	Surface following attenuator	70 - 150 m	Linear generator	12 devices	1,300 tonnes
LIMPET Island of Islay	Scotland, (UK)	Fixed shoreline	500 KW - 1 MW	Operational	OWC	5 - 15 m	Air turbine	N/A	N/A
Pico/Azores Wave power plant	Island of Pico/Azores, Portugal	Fixed shoreline	100 KW - 700 KW	Operational	OWC	5 - 15 m	Air turbine	N/A	N/A
Oceanlinx	Port Kembla, Australia	Near-shore and Offshore	N/A	Operational	OWC	5 - 15 m	Air turbine	N/A	3,000 tonnes
Sakata	Sakata, Japan	In Breakwater	N/A	Operational	OWC	5 - 15 m	Air turbine	N/A	N/A
Mutriku	Bay of Biscay, Spain	In Breakwater	N/A	Operational	OWC	5 - 15 m	Air turbine	N/A	N/A
OSPREY Plant	Dounreay, (UK)	Near-shore	2 MW	Operational	OWC	15 m	Air turbine	N/A	N/A
Pelamis Ocean power delivery	Agudoura Coast, Portugal	Offshore	750 KW	R and D	Surface attenuator	$>$ 50 m	Hydraulic ram	N/A	1,350 tonnes
Wave Dragon (WD)	Nissum Bredning, Denmark	Near-shore Offshore	140 KW	R and D	Overtopping	25 - 60 m	Hydroelectric	N/A	54,000 tonnes
CETO 5 Carnegie Wave power	Garden Island, Austria	Offshore	3 MW	Operational	Hydraulic generator	5 - 25 m	Pump to shore	3 devices	N/A
Oyster Aquamarine Wave power	Orknes, Scotland	Near-shore	Oyster1: 315 KW Oyster2: 2 MW	R and D	Oscillating wave surge	10 - 20 m	Hydroelectric turbine	3 devices	N/A
Power Buoy, Ocean power Technology	New Jersey, (U.S)	Offshore	150 KW	Operational	Buoy	30 - 60 m	Hydroelectric turbine	N/A	N/A

climate conditions. The energy that can be produced by a single device is determined by a power matrix of the device and the wave energy around the area of interest. The power matrix provides information about the sea state which is the combination of significant wave height and peak or energy period. The parameters in the power matrix table are referred to as the energy bins. WECs maximum efficiency can be viewed in this table and they show a power output of WECs at various ranges of H_{mo} vs T_e and H_{mo} vs T_p. Depending on the area of interest and the device, power absorption is different as explained in Section 5.5.

A large number of WECs must be deployed to produce enough power. The in-between distance and the distance between rows in a wave farm are important for energy absorption. According to Roberts *et al.* (2014), the distance of the wave farm to the shore has an impact in the nearshore wave field.

Chapter 6

Modelling the impacts of the WECs

6.1 Introduction

The extraction of wave energy will require large numbers of WECs in the form of a wave farm to be deployed (O'Dea *et al.*, 2014). In order to predict or estimate the power capture and impact induced by WECs, numerical models such as SWAN and MIKE 21 SW are used (Millar *et al.*, 2007; Venugopal and Smith, 2007; Smith *et al.*, 2012). Folley (2016) has outlined a brief history of the modelling techniques used to model the WECs in the frequency and time domains. Some of these techniques include the use of Computational Fluid Dynamics (CFD) in solving the Euler equations for incompressible flow around the WECs. In this study, changes in the average wave conditions are investigation and the SWAN wave model is used.

The objective of this chapter is to assess the nearshore wave field changes induced by WECs. The response curves and output locations will be shown. In this study, the response curves will be the wave energy spectra in front and behind the wave farm of the selected output locations.

6.2 Numerical wave propagation models

Numerical wave propagation models are generally classified into two types: phase-resolving time domain and phase-averaged spectral models. The phase-averaged models determine the change of the wave energy as a function of frequency and direction. These models solve the wave action balance equation. Phase-resolving models compute the sea surface elevation as a function of time by solving the time dependent conservation of mass and momentum equations.

A range of numerical wave propagation models, both phase-resolving and phase-averaging, has been developed and are outlined in Folley *et al.* (2004). These models include: a

nonlinear Boussinesq wave model (MIKE 21 BW), a linear mild-slope model (MILDwave) which is based on the Radder and Dingemans equations (Radder and Dingemans, 1985), a nonlinear potential flow model OceanWave3D and the spectral wave model SWAN. The latter being one of the most used spectral models in ocean and coastal applications. These numerical models play a vital role in understanding the impact of the WEC farms for both the near-and far-fields. Examples of the application of these models have been given in Section 1.4. These types of models are further discussed in the next sections.

6.2.1 Phase-resolving models

In phase-resolving models, the sea surface elevation is resolved over a small space and time (e.g., the surf zone at the coast or in a harbour) (Holthuijsen, 2010). These models resolve individual waves and they focus on a fine grid resolution with the aim of capturing the smallest wavelength or period. They are considered computationally expensive due to the reconstruction of the sea surface elevation in both space and time as they account for effects such as refraction and diffraction as explained in Booij *et al.* (1999). These models are usually based on the nonlinear equations such as Boussinesq equations (Madsen and Sørensen, 1992) and Hamiltonian formulation (Miles, 1981). Examples of such a model is REF/DIF (refraction/diffraction model) (Dhanak and Xiros, 2016) and MIKE 21 BW (Kofoed-Hansen *et al.*, 2005).

6.2.2 Phase-averaging models

The phase averaging models are also called spectral wave models. These models compute the wave energy evolution in both space and time of the sea state. The sea state according to these models depends on the wave frequency and direction and is defined by a wave energy spectrum (Folley *et al.*, 2004). In these models, the sea state is solved by applying the spectral action balance equation which includes several processes such as white-capping and bottom friction. These models are called third-generation spectral models and can be used for predicting sea state conditions for both regional and global applications (Komen *et al.*, 1996). SWAN (Booij *et al.*, 1999) and MIKE 21 (Warren and Bach, 1992*b*) are examples of phase-averaging models. In this study, the spectral wave model SWAN will be applied.

6.3 The SWAN wave model

The SWAN wave model was developed by the Delft University of Technology located in the Netherlands. It is an open source software which can be used to estimate wave field parameters in nearshore and coastal areas. This model determines the evolution of the

wave spectrum by using an Eulerian formulation of the action balance equation. The equation has a number of terms that define natural processes and accounts for effects of generation, dissipation and wave-wave interactions.

The purpose of this section is to give a theoretical background of the SWAN wave model and a more detailed discussion about the physical processes incorporated in SWAN and can be found in Holthuijsen (2010), Van der Westhuysen (2002) and Booij *et al.* (1999).

6.3.1 The action balance equation

The evolution of the action density, denoted by N, is described by the spectral action balance equation as

$$\frac{\partial N}{\partial t} + \nabla_{\vec{x}}.[(\vec{C_g} + \vec{U})N] + \frac{\partial C_\sigma N}{\partial \sigma} + \frac{\partial C_\theta N}{\partial \theta} = \frac{S_{tot}}{\sigma}. \tag{6.3.1}$$

The action density N is determined in space and time as $E(\sigma,\theta)/\sigma$, where E denotes the energy density spectrum which is explained in Chapter 2. The parameter σ is called the relative or intrinsic frequency. The parameter $\vec{C_g}$, is the group velocity which is derived in Appendix A and $\vec{U}$ is the ambient current which is assumed constant with respect to the vertical coordinate. The quantities C_σ and C_θ are propagation velocities in spectral space. The source term S_{tot} represents physical processes such as generation, dissipation and nonlinear wave-wave interactions of wave energy. For Cartesian coordinates, in the absence of ambient current $\vec{U}$, Equation (6.3.1) simplifies to

$$\frac{\partial N}{\partial t} + \frac{\partial C_x N}{\partial x} + \frac{\partial C_y N}{\partial y} + \frac{\partial C_\sigma N}{\partial \sigma} + \frac{\partial C_\theta N}{\partial \theta} = \frac{S_{tot}}{\sigma}. \tag{6.3.2}$$

The action balance Equation (6.3.2) provides a statistical description of the evolution of the sea state. A more detailed derivation of Equation (6.3.2) can be found in Komen *et al.* (1996).

6.3.2 Source terms

The energy source term S_{tot} is expressed as

$$S_{tot} = S_{in} + S_{nl} + S_{ds}, \tag{6.3.3}$$

or

$$S_{tot} = \underbrace{S_{in} + S_{nl4} + S_{ds,w}}_{\text{deep water}} + \underbrace{S_{nl3} + S_{ds,br} + S_{ds,b}}_{\text{shallow water}}. \tag{6.3.4}$$

Here S_{in} represent the energy input by the wind action, S_{nl} represent a non-linear wave-wave interactions (S_{nl3} and S_{nl4}) and S_{ds} represents the wave energy dissipation and has three contributions, namely: $S_{ds,w}(\sigma,\theta)$ for white-capping, $S_{ds,b}(\sigma,\theta)$ for bottom

friction and $S_{ds,br}(\sigma,\theta)$ for depth-induced breaking. According to Young (1999), these processes are not the only factors that have an influence on the evolution of the wave spectrum. However, they are the major factors that influence the energy in the spectrum.

6.3.2.1 Generation by wind

The mechanism of energy transfer from the wind to the ocean surface in SWAN is modelled by the source term $S_{in}(\sigma,\theta)$. This mechanism is described by both a linear growth mechanism (Phillips, 1957) and an exponential growth mechanism (Miles, 1957). The source component S_{in}, is expressed by the combination of these mechanisms and is given as

$$S_{in}(\sigma,\theta) = \alpha_{in} + \beta E(\sigma,\theta), \tag{6.3.5}$$

where α_{in} indicates the initial linear wave growth and β the exponential growth term and $E(\sigma,\theta)$ is described by Equation (6.3.1). The linear growth coefficient α_{in} can be determined by the empirical expression formulated by Cavaleri and Rizzoli (1981). For the exponential growth term β, two expressions are used to determine the coefficient in SWAN and can be found in Komen *et al.* (1984).

6.3.2.2 Non-linear wave-wave interaction

In SWAN, the non-linear interactions of wave energy are modelled by two wave-wave interactions: firstly, the (*four-wave*) quadruplet wave-wave interactions S_{nl4}, which dominates the evolution of the wave spectrum in deep water and secondly, the (*three-wave*) triad wave-wave interactions S_{nl3} in shallow water. These interactions are incorporated in SWAN and expressed as

$$S_{nl}(\sigma,\theta) = S_{nl3} + S_{nl4}. \tag{6.3.6}$$

6.3.2.3 Wave energy dissipation

The wave energy dissipation in SWAN is modelled by three processes and are represented by a source term S_{ds} given as

$$S_{ds}(\sigma,\theta) = S_{ds,w}(\sigma,\theta) + S_{ds,b}(\sigma,\theta) + S_{ds,br}(\sigma,\theta). \tag{6.3.7}$$

According to Booij *et al.* (1999), white-capping is generally controlled by the steepness of the waves and the energy is assumed to be proportional to the wave steepness (wave height over wavelength). The source term for this processes is given as

$$S_{ds,w}(\sigma,\theta) = -\Gamma_{KJ}\tilde{\sigma}\frac{k}{\tilde{k}}E(\sigma,\theta), \tag{6.3.8}$$

where $\tilde{\sigma}$ and $\tilde{k}$ represent the mean frequency and mean wave number, respectively. The coefficient Γ_{KJ} represents the steepness and its expression is given in Appendix C.1.1. The value of the coefficient has been estimated by Komen *et al.* (1984).

Wave energy dissipation due to bottom-induced dissipation in SWAN is modelled by the source term $S_{ds,b}$ given as

$$S_{ds,b}(\sigma,\theta) = -C_b \frac{\sigma^2}{g^2 \sinh^2(kd)} E(\sigma,\theta), \tag{6.3.9}$$

where C_b is the bottom friction coefficient. In SWAN there are three types of formulations for the bottom friction dissipation. The default bottom-induced dissipation based on the JONSWAP bottom friction scheme (Hasselmann *et al.*, 1973) will be used in this study.

Depth-induced breaking occurs when waves propagate into shallow water. As water depth decreases, it causes the waves to become unstable and break. According to Van der Westhuysen (2002), wave breaking in the shallow water region is the most dominant process compared to other processes such as shoaling, refraction and diffraction. In SWAN, the depth-induced breaking can be modelled by the expression of Battjes and Janssen (1978) which is given as

$$S_{ds,br}(\sigma,\theta) = \frac{D_{tot}}{E_{tot}} E(\sigma,\theta), \tag{6.3.10}$$

where E_{tot} is the total wave energy and D_{tot} is the total rate of energy dissipation induced by wave breaking. As the waves approach shallow water, the total rate of energy dissipation D_{tot}, depends on the water depth and the maximum wave height. The expression for D_{tot} is given in Appendix C.1.2.

6.4 Wave farm layout

The layouts of wave farms are mostly done by device developers after they have been experimentally tested. The devices in a wave farm are arranged in such a way that they do not affect other neighbouring devices for power absorption. The wave farm layout used for this thesis was based on tested farm configurations studied by Beels *et al.* (2010). According to Beels *et al.* (2010), there are several aspects that are considered in the layout of the wave farm. These include the distance between devices in a row, in-between distances of the rows, the number of rows and mooring configurations. The illustration of the wave farm layout that was used for this study is given in Figure 6.1. The layout and the spaces between devices in Figure 6.1 are suitable for maintenance vessel movement around the devices.

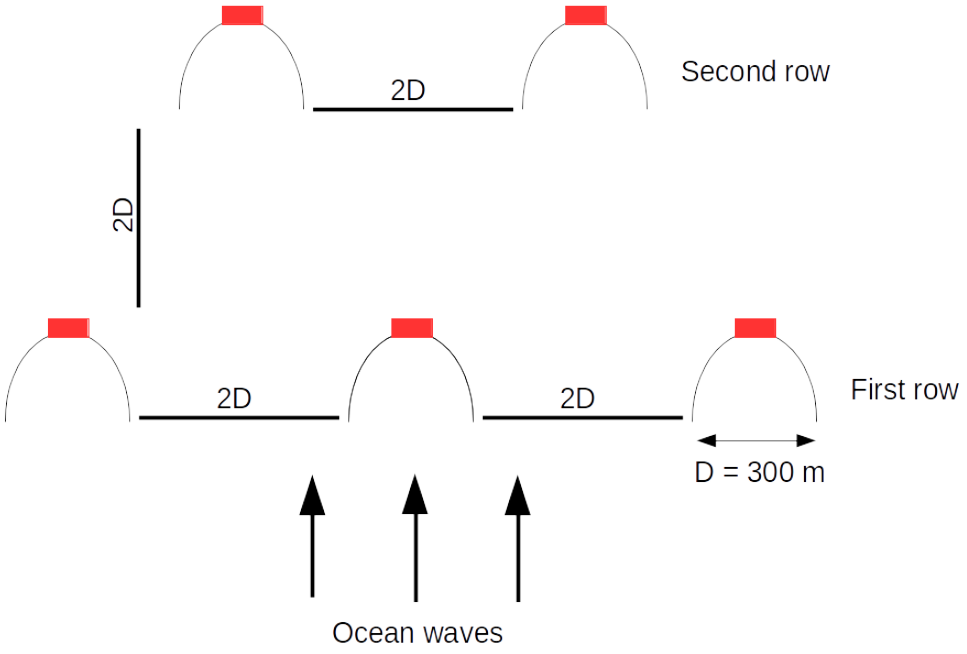

Figure 6.1: Wave farm layout of the wave dragons, adapted from Beels *et al.* (2010).

In Figure 6.1, D is the length between wave reflectors of a Wave Dragon (WD) and twice this length has been used as the in-between distance within the units in a row. The length of wave reflectors is illustrated in Figure 5.4. In this study, the Wave Dragon was chosen, based on its ability to extract energy due to the long wave reflectors that focus on the incoming waves towards the ramp. Further information about the Wave Dragon device is given in Section 5.3.3.

Saldanha Bay, specifically the Outer Bay, was chosen as the potential area for deployment of the wave farm. The choice of Saldanha Bay was based on studies that were done by Joubert (2008, 2013), who identified the wave power levels to be high along the west coast of South Africa.

Table 6.1, lists the characteristics of two types of converters that were deployed, tested and commercialized. The estimated distances are based on the length of each device. The rated power capacity for both a single device and a wave farm are given in Table 6.1 and is generally provided by device developers.

Table 6.1: WECs specifications showing location, distances and estimated capacity for a single WEC and a wave farm.

Device name	Estimated distance from the shore	Device length	Estimated distance between units in a farm	Device capacity	Water depth
Wave dragon	2.5 km	1×WEC: 300 m 5×WEC: 2.25 km	600 m	1×140 kW 5×140 kW	30 m
Pelamis	5 to 10 km	1×WEC: 150 m 5×WEC: 700 m	120 m	1×750 kW 5×750 kW	> 50 m

6.5 Model domain

The SWAN wave model used for this study was validated and calibrated by Van Ballegooyen *et al.* (2002). It was used to model the offshore to nearshore wave conditions.

Figure 6.2: The area of interest for the hypothetical wave farm that was modelled.

The bay is divided into two bays which are referred to as Big Bay and Small Bay (Joubert, 2013). The potential area for the wave farm is represented by the yellow rectangular box shown in Figure 6.2. The wave farm is facing the dominant wave direction, which is mostly coming from a west of south west inside the Outer Bay.

6.5.1 Computational grid

The computational grid domain for this study is shown in Figure 6.3 and is represented by three computational grids, namely: coarse, medium and fine grids. The medium and fine grids are nested in the coarse grid to simulate the wave energy propagation from the offshore to nearshore region. Both these grids have been generated from the coarse grid. Grid properties such as orthogonality and refinement have been applied to compute accurate results at high resolution inside the area of interest. The WECs were placed in the fine grid region where the resolution is high enough to accurately resolve effects induced by WECs.

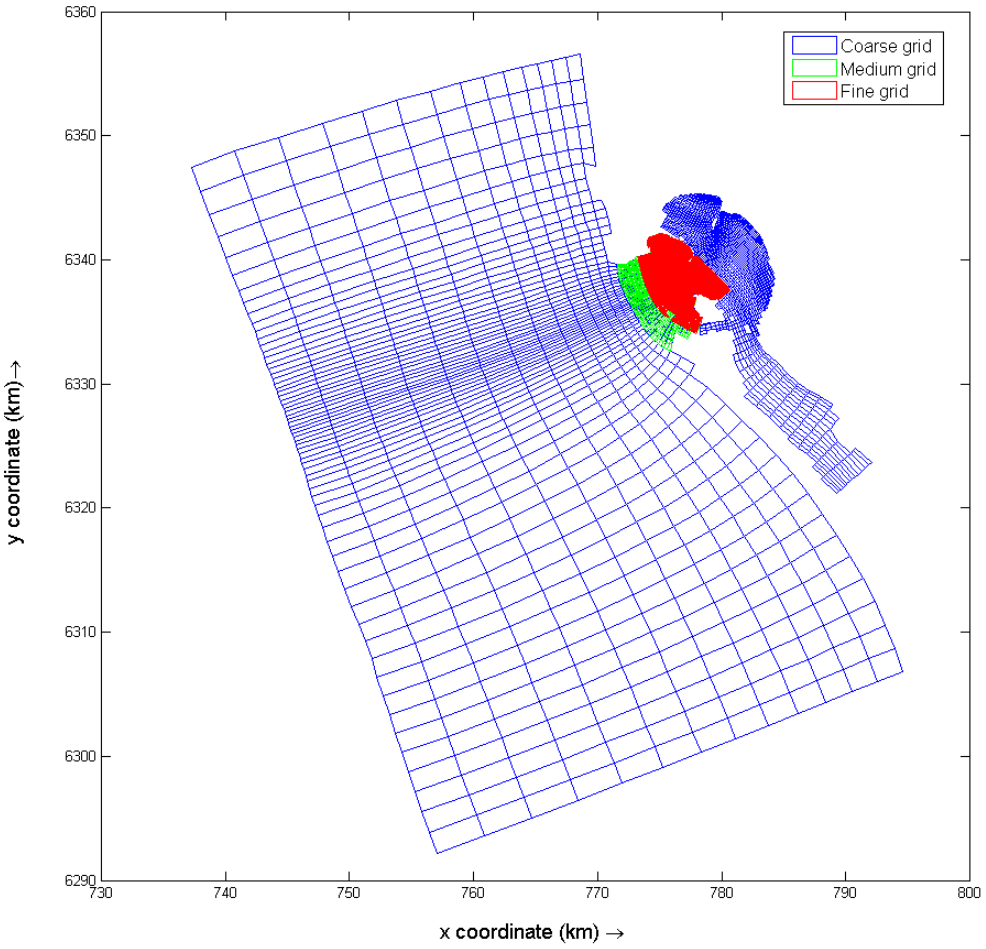

Figure 6.3: Saldanha Bay computational grids.

The fine grid was made specifically for the wave farm in the area of interest. The location of the wave farm is approximately 2.5 km from the shore, at a water depth of 30 m. The number of directions, frequency bins, and model grid resolution are listed in Table 6.2.

Table 6.2: Grid resolution for the computational grids.

Computational domain	Coarse	Medium	Fine
grid resolution	940 m × 3000 m	85 m × 304 m	32 m × 82 m
number of frequency bins	36	36	36
number of directions	72	72	72

6.5.2 Input boundary conditions

The yearly percentage occurrence of wave parameters from the offshore NCEP wave data was considered in this study and are given in Tables 6.3 and 6.4. The colours in the tables represent low (blue), average (green) and energetic (red) wave heights percentage occurrence, respectively. The boundary conditions are necessary for SWAN simulations. They provide deep water wave parameters obtained from the NCEP WaveWatchIII global wave model. The NCEP output extraction point is located approximately 42.02 km from the Saldanha Bay station.

Table 6.3: NCEP wave data, precentage occurrence of significant wave height against peak wave period. The colours represent low, average and energetic wave heights, respectively.

Hmo (m)	0-2	2-4	4-6	6-8	8-10	10-12	12-14	14-16	16-18	18-20	20-22	22-24	24-26	26-28	28-30	30-32	Total
0.0 - 0.5		0.00	0.01	0.02	0.03	0.09	0.09	0.02	0.00								0.27
0.5 - 1.0	0.00	0.03	0.01	0.05	0.08	0.17	0.07	0.00	0.02								0.44
1.0 - **1.5**		0.03	0.12	0.23	1.29	**3.01**	1.08	0.19	0.05								6.00
1.5 - 2.0			0.45	0.57	2.6	8.31	3	0.62	0.14	0.01							15.69
2.0- 2.5			0.49	1.15	**2.63**	**11.18**	5.42	0.99	0.19	0.02							22.06
2.5 - 3.0			0.18	1.93	1.81	9.16	6.91	1.23	0.17	0.02	0.00						21.40
3.0 - 3.5			0.01	1.31	0.65	5.39	**5.92**	1.05	0.1	0.02							14.46
3.5 - 4.0				0.33	0.31	2.7	3.79	0.96	0.11								8.20
4.0 - **4.5**				0.09	0.13	1.38	**2.35**	0.71	0.08	0.00							4.73
4.5 - **5.0**				0.01	0.12	0.62	1.52	**0.69**	0.05								3.02
5.0 - 5.5					0.02	0.25	0.85	0.46	0.07								1.64
5.5 - **6.0**					0.01	0.09	0.46	**0.31**	0.06	0.00							0.94
6.0 - 6.5						0.05	0.22	0.21	0.04								0.51
6.5 - 7.0						0.02	0.12	0.14	0.01								0.29
7.0 - **7.5**						0.00	**0.09**	0.07									0.16
7.5 - 8.0						0.00	0.01	0.05									0.07
8.0 - 8.5							0.00	0.03	0.00								0.03
8.5 - **9.0**							0.01	**0.03**	0.00								0.05
9.0 - 9.5							0.00	0.02									0.02
9.5 - 10.0							0.00	0.01									0.01
Total	0.00	0.06	1.26	5.7	9.67	42.41	31.95	7.78	1.1	0.07	0	0	0	0	0	0	100

Table 6.4: NCEP wave data, percentage occurrence of significant wave height against wave direction. The colours represent low, average and energetic wave heights, respectively.

Hmo (m)	N	NNE	NE	ENE	E	ESE	SE	SSE	S	SSW	SW	WSW	W	WNW	NW	NNW	Total
0.0 - 0.5	0.01				0.00	0.00	0.04	0.01	0.01	0.03	0.13	0.04	0.00				0.27
0.5 - 1.0	0.01						0.02	0.01	0.01	0.04	0.24	0.06	0.01	0.00	0.02	0.00	0.44
1.0 - **1.5**		0.01					0.02	0.1	0.25	0.86	3.3	1.27	0.1	0.02	0.06	0.01	6.00
1.5 - 2.0	0.00	0.02	0.00				0.05	0.38	0.81	2.14	9.26	**2.71**	0.19	0.05	0.03	0.03	15.69
2.0 - 2.5	0.00		0.00				0.03	0.57	1.19	3.1	**13.6**	3.33	0.11	0.03	0.05	0.05	22.06
2.5 - 3.0	0.01	0.00	0.00				0.00	0.72	1.57	**3.82**	11.86	3.16	0.11	0.03	0.06	0.05	21.40
3.0 - 3.5								0.48	0.98	2.47	8.11	2.23	0.11	0.04	0.03	0.00	14.46
3.5 - 4.0								0.11	0.31	1.56	4.87	1.22	0.08	0.03	0.02	0.00	8.20
4.0 - **4.5**								0.01	0.07	**0.95**	2.61	0.97	0.05	0.04	0.02	0.01	4.73
4.5 - **5.0**								0.02	0.07	0.46	1.69	**0.73**	0.03	0.02	0.00		3.02
5.0 - 5.5									0.00	0.22	0.99	0.4	0.03				1.64
5.5 - **6.0**										0.12	0.6	**0.21**	0.01				0.94
6.0 - 6.5										0.08	0.3	0.12	0.00				0.51
6.5 - 7.0										0.05	0.16	0.08	0.00				0.29
7.0 - **7.5**										0.01	**0.12**	0.03					0.16
7.5 - 8.0											0.04	0.02					0.07
8.0 - 8.5										0.00	0.03	0.00					0.03
8.5 - **9.0**										0.00	**0.04**	0.00					0.05
9.0 - 9.5											0.02	0					0.02
9.5 - 10.0											0.01	0.01					0.01
Total	0.04	0.03	0.01	0.00	0.00	0.00	0.17	2.41	5.28	15.91	57.97	16.59	0.84	0.27	0.3	0.17	100

The selected conditions listed in Table 6.5, are based on the highest percentage occurrence of the significant wave height, peak period and wave direction. Using Tables 6.3 and 6.4, the conditions were consistently selected based on significant wave height ranges (H_{mo} vs T_p and H_{mo} vs θ). The conditions listed in Table 6.5 are representative of a wave climate with a dominant wave direction of 225° as shown in Figure B.1. These conditions will be used as input boundary conditions for the SWAN wave model.

Table 6.5: Selected model boundary wave condition from the offshore NCEP data.

Condition	H_{mo} (m)	T_p (s)	θ (degrees)	γ	spreading (degrees)
1	1.5	10	247.5	2.2	24.9
2	2.0	11	202.5	2.2	24.9
3	2.5	12	202.5	2.2	24.9
4	3.0	12	225.0	2.2	24.9
5	4.5	14	225.0	2.2	24.9
6	5.0	14	202.5	2.2	24.9
7	6.0	15	247.5	2.2	24.9
8	7.5	16	247.5	2.2	24.9
9	9.0	16	225.0	2.2	24.9

Configurations used for the Saldanha Bay are listed in Table 6.6. The γ values were obtained in Chapter 4 based on the measured data for various locations along the South African coast. Saldanha Bay γ value listed in Table 4.2, was used. The parameters listed in Table 6.6 are based on the study conducted by Van Ballegooyen *et al.* (2002) and have been used as the default values in this study. Although the frequency range is larger than required, it was decided to keep this configuration as this was the range specified by Van Ballegooyen *et al.* (2002).

Table 6.6: Wave model setups.

Physical parameters	**Schemes**
White-capping	Active (Komen *et al.*, 1984)
Bottom friction	JONSWAP type (Hasselmann *et al.*, 1973)
Depth-induced breaking	Bore-based model (Battjes and Janssen, 1978)
Spectral shape	JONSWAP spectrum (Hasselmann *et al.*, 1973)
Directional spreading	Cosine power
Peak enhancement factor	2.2
Spreading value (cosine power)	4
Frequency range	0.036 - 1 (Hz)

It must be noted that the diffraction is not accounted for in SWAN, it was therefore, assumed that diffraction does not affect the model results.

6.6 Modelling the WECs

6.6.1 Transmission and reflection coefficients

In SWAN, users can insert obstacles into a computational grid where physical obstacles occur. An obstacle in SWAN is modelled as a sub-grid structure. Examples of such obstacles could be breakwaters or, in this study, hypothetical WECs. The location of the obstacles in SWAN is defined by a polygon. The propagation of wave energy is interrupted from one grid point to another by the presence of the obstacles in the computational domain. The height of the waves may be reduced as it propagates over or through the obstacles and a percentage of the waves are be reflected or absorbed (Diaconu and Rusu, 2013).

In this study, obstacles were defined to represent the hypothetical WECs in a wave farm. In SWAN, there are two types of obstacles that can be used to model the wave farms. These include sheet and dam types. The dam type depends on the wave height and the incident wave conditions at the obstacles. The sheet type allows the transmission coefficient to be constant along the obstacles. The dam type only allows the reflection coefficient to be active not the transmission coefficient. In this study, the sheet is considered since it allows both coefficients to be included in the model. Also, SWAN models two types of reflection for obstacles: specular and diffuse reflections. The diffuse type is when the wave energy is reflecting in all directions. The specular type is when the angle of incidence equals the angle of reflection. In this study, specular reflection was applied.

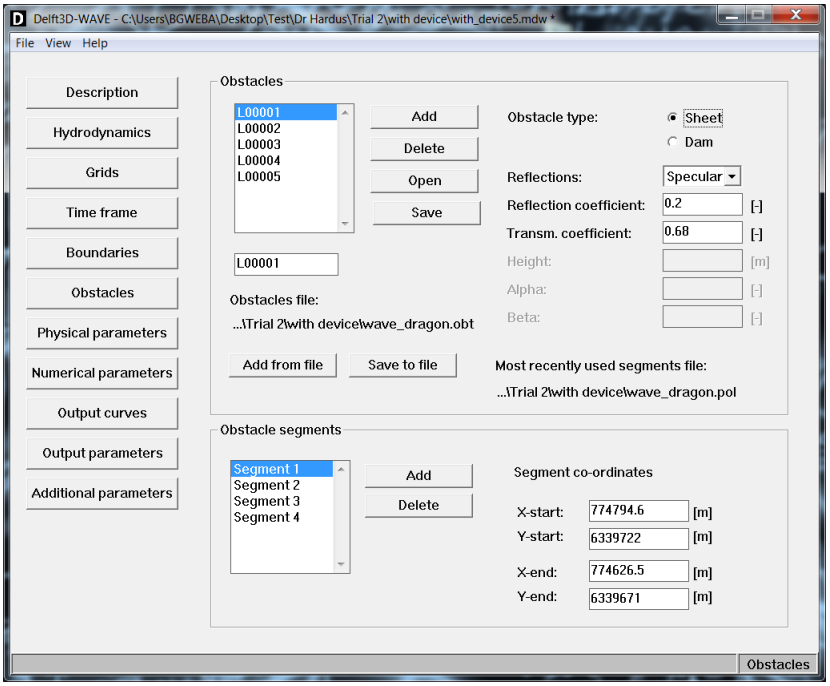

Figure 6.4: An example of the wave farm defined by the obstacle command in SWAN.

According to a study by Diaconu and Rusu (2013) and Veigas and Iglesias (2014) on the modelling of the wave field changes induced by a Wave Dragon array in which a practical guide for the design and construction of the floating structures was applied, the reflection, and transmission coefficients were set to 0.2 and 0.68, respectively. The information as to how these values were obtained is not explained and therefore it can be assumed that these values were based on the physical model tests in a laboratory basin. These values will be used in this study. The reflection coefficient is defined as the reflected significant wave height divided by the incident significant wave height. The transmission coefficient is defined as the transmitted wave height divided by the incident wave height.

The output locations are listed in Table 6.7. These locations were positioned in the computational domain to provide the wave field variability from offshore to the area of interest.

Table 6.7: The model output locations arranged from offshore to nearshore of Saldanha Bay.

Output location number	Depth	Description
L1	194.3 m	Offshore, 43 km away from the entrance area.
L2	78.1 m	Offshore ≈ 20 km from the area of interest.
L3	53.5 m	9.8 km away from Marcus Island.
L4	48.8 m	Nearshore output location, in front of Jutten Island.
L5	41.1 m	Adjacent to Malgas Island and behind L7.
L6	30.5 m	Nearshore output location, north of Jutten Island.
L7	35.5 m	Nearshore location in front of the wave farm.
L8	23.0 m	Nearshore location close to the shore, behind the wave farm.
L9	25.5 m	Nearshore location, ≈ 1.2 km from the coastline of Marcus Island.
L10	17.3 m	Nearshore location on the Big Bay, about 3.6 km from Mykonos Resort in Langebaan.
L11	14.8 m	3 km from the Port of Saldanha Bay.

Figure 6.5 shows the Saldanha Bay coastal embayment which consists of Small Bay, Big Bay, and Outer Bay. The description in Table 6.7 is based on the information represented by Figures 6.5 and 6.6. The output locations, L5, L6, L7, L8 and L9 will be used to analyse the wave field parameters induced by wave farm as the locations are located in the medium grid.

Figure 6.5: The coastal embayment of Saldanha Bay area (Van Ballegooyen *et al.*, 2002).

Figure 6.6, shows the bathymetry of the coarse grid with output locations from offshore to nearshore.

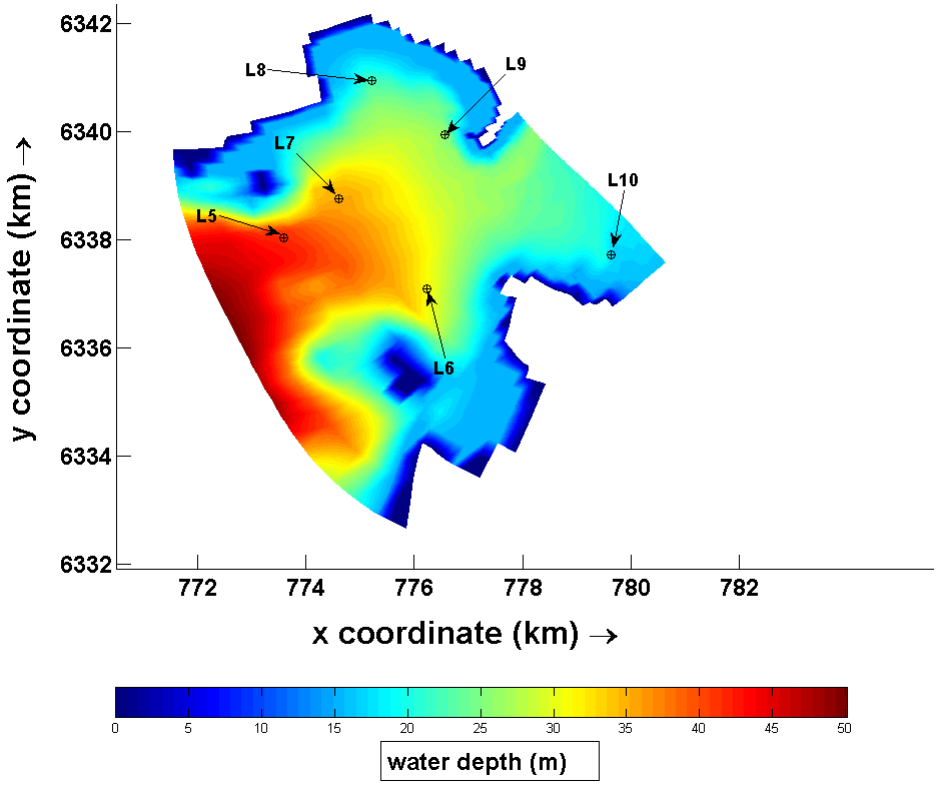

Figure 6.6: The bathymetry of the medium grid (water depth in in meters below chart datum), showing the positions of the output locations.

The results of the Saldanha Bay wave model runs will be shown in the next sections. The results include the energy spectra with and without the wave farm. Nearshore wave field parameters with and without the wave farm will be analysed at specific locations. Also, the significant wave height difference with and without the wave farm will be presented. This will show a difference of the significant wave height between two simulations to clearly see the net effect induced by the wave farm on the individual wave parameters. The equation for significant wave height difference is given as

$$\Delta Hs = H_{s_{wif}} - H_{s_{nof}}, \tag{6.6.1}$$

where $H_{s_{nof}}$ and $H_{s_{wif}}$ represent the significant wave height without the wave farm and with the wave farm, respectively.

The next section is an analysis of the nearshore wave field parameters with and without the wave farm for all 9 wave condition listed in Table 6.5.

6.7 Assessment of the wave field changes induced by the wave farm

The wave data used in this study covered a database of 10 years. The data includes seasonal and yearly wave conditions. In this study, 9 conditions for the yearly wave data were considered. Significant wave height and peak period starting from the lowest to highest were selected to quantify the change in the downfield wave conditions, induced by the wave farm. With regards to wave direction input conditions, the selection was based on the geometry of the area of interest.

This section will deal with the results obtained from the Saldanha Bay wave model. For the purpose of the analysis, few conditions were selected. All the simulated conditions for the model are shown in Appendix D. The model was run in the absence and presence of arrays of five Wave Dragons which are shown in Figure 6.1.

6.7.1 Significant wave height change induced by wave farm

The significant wave height with and without the wave farm for conditions 3, 5 and 8 are shown in Figures 6.7, 6.8 and 6.9, respectively. These conditions correspond to low, average and energetic wave conditions, respectively. For these selected conditions, it can be seen that the significant wave height of the model changes as the wave approaches the shore.

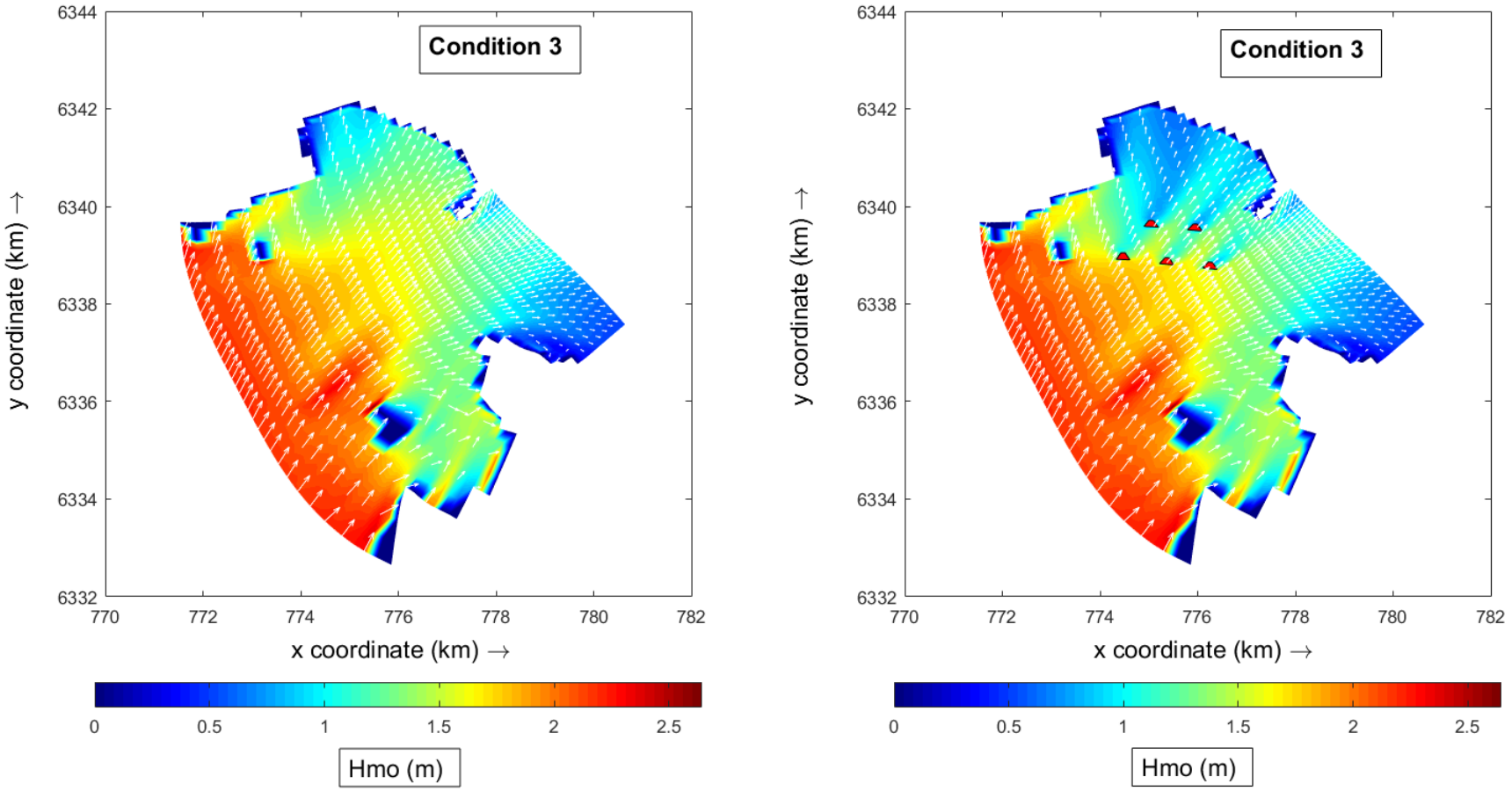

Figure 6.7: The significant wave height without (left) and with (right) the wave farm, $H_{mo} = 2.5$ m, $T_p = 12$ s and $\theta = 202.5°$.

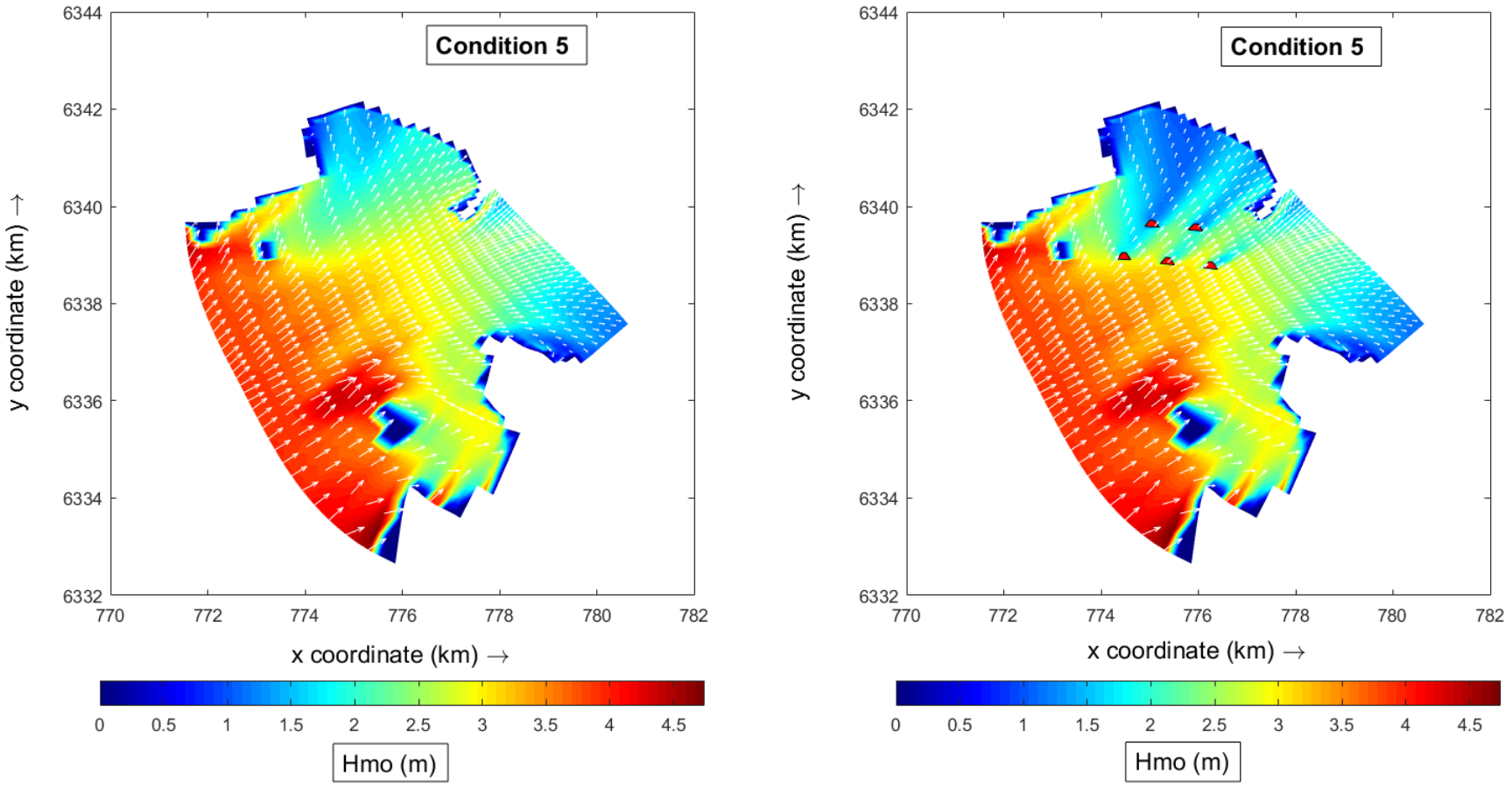

Figure 6.8: The significant wave height without (left) and with (right) the wave farm, $H_{mo} = 4.5$ m, $T_p = 14$ s and $\theta = 225.0°$.

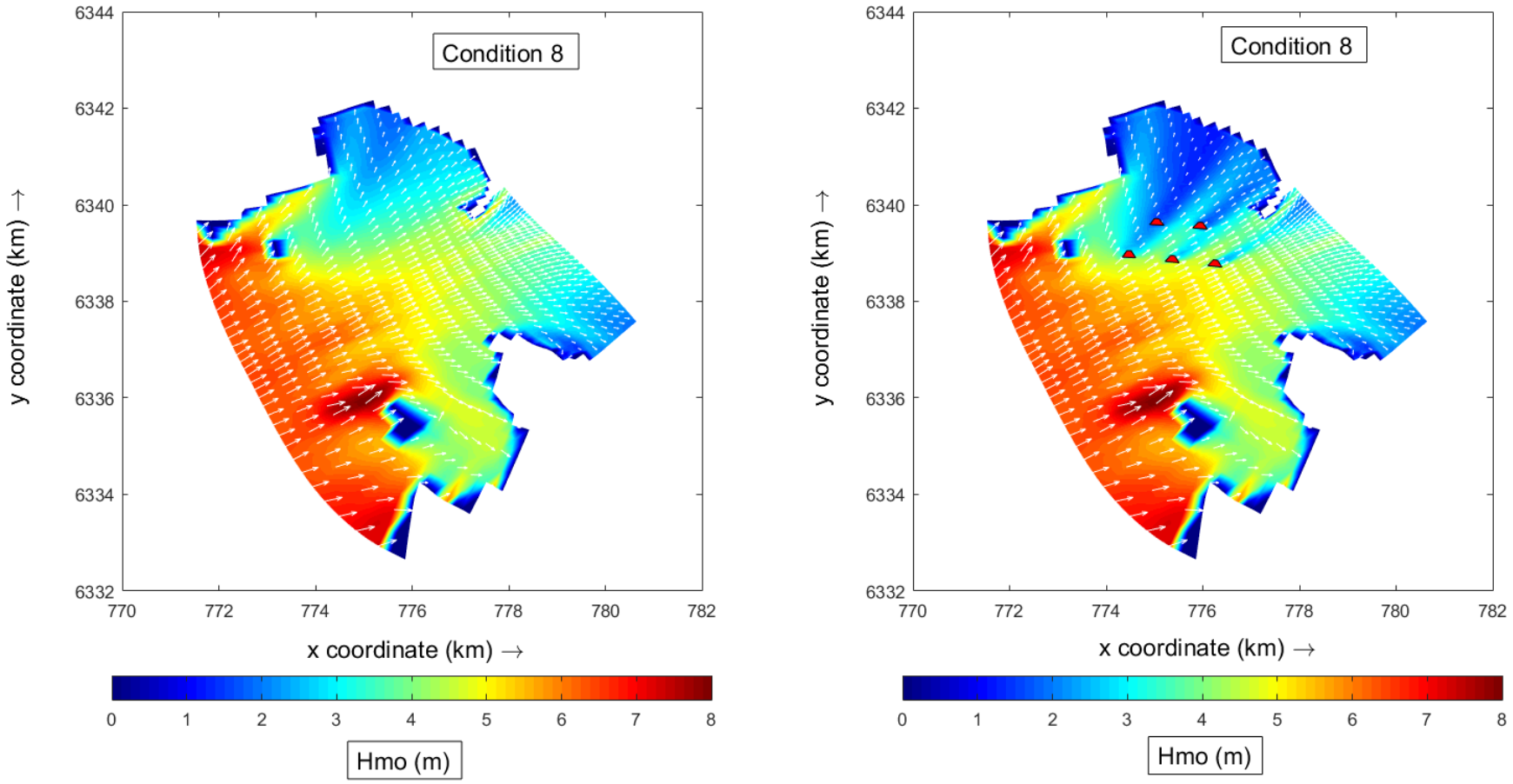

Figure 6.9: The significant wave height without (left) and with (right) the wave farm, $H_{mo} = 7.5$ m, $T_p = 16$ s and $\theta = 247.5°$.

The difference in significant wave height for conditions 3, 5 and 8 as computed by Equation (6.6.1) is shown in Figure 6.10. The colour bar in Figure 6.10 indicates the amount of significant wave height change, with the negative value showing the reduction in significant wave height induced by the wave farm. The differences in significant wave height for other conditions are shown in Figures D.10 and D.12 in Appendix D.

The nearshore wave field changes are also given at the selected output locations in Tables 6.8, 6.9 and 6.10. They show changes in the locations with and without the wave farm in the medium grid, as shown in Figure 6.6. The red values in the tables show the wave height reduction behind the wave farm of L8 and L9. The amount of wave height reduction depends on the input wave conditions. The wave height reduction behind the first row of the array is affecting the second row as shown by Figures 6.7, 6.8 and 6.9. This has an effect on the wave energy extraction by the second-row of devices. The results indicate that the presence of the wave farm in the nearshore region has an effect on the wave field conditions. Seaward change may be attributed to reflection due to wave farm.

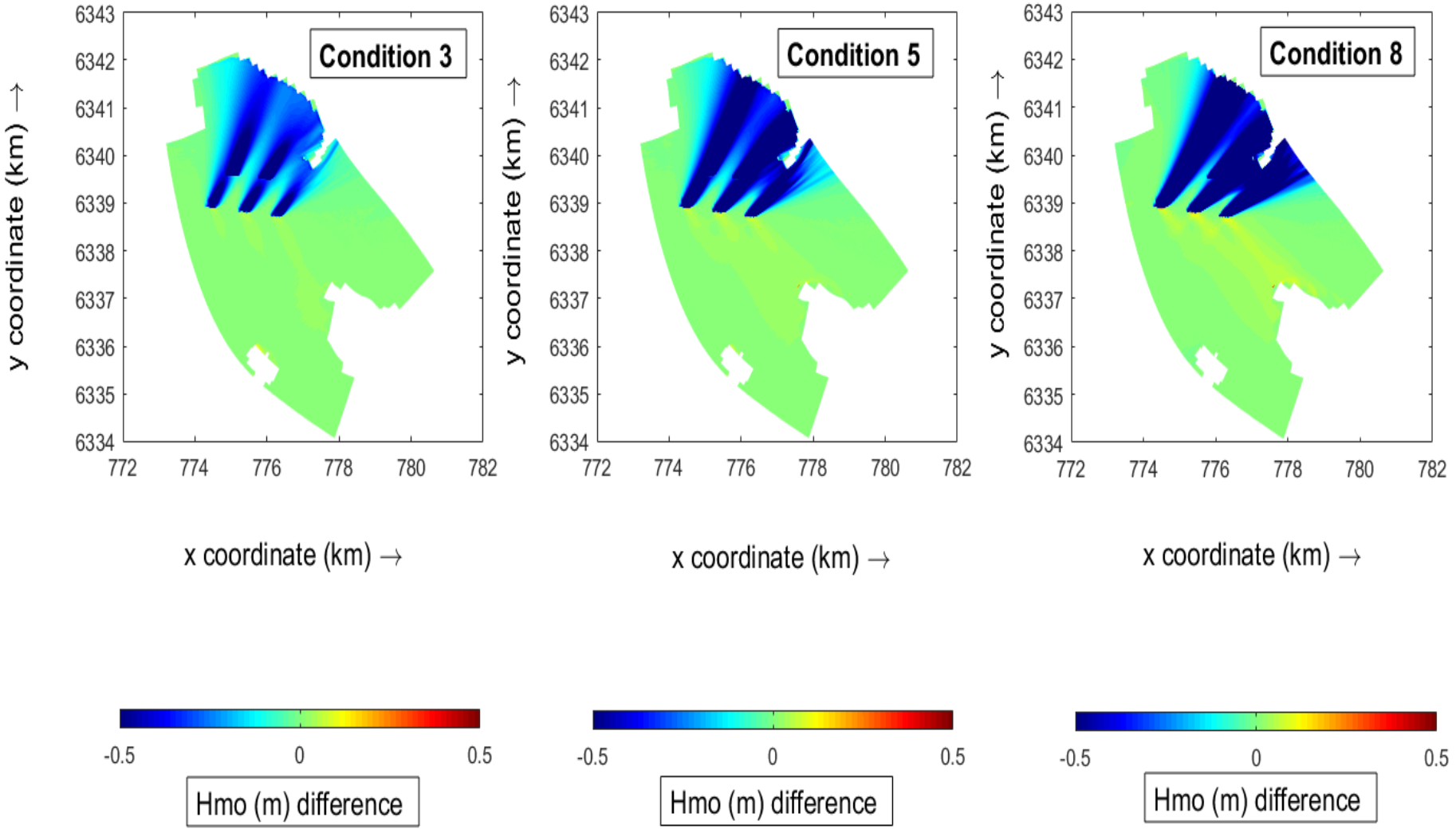

Figure 6.10: The difference in significant wave height induced by the wave farm for conditions 3, 5 and 8.

Table 6.8: Wave model output with and without the wave farm in the medium grid showing the wave field changes of condition 3.

OL	Depth (m)	$H_{s_{nof}}$ (m)	$H_{s_{wif}}$ (m)	ΔHs (m)	$\%\Delta H_s$	θ_{nof} (°)	θ_{wif} (°)
L5	41.48	1.97	1.98	0.01	0.50	212.60	212.52
L6	31.22	1.52	1.53	0.01	0.65	241.97	242.99
L7	35.32	1.74	1.76	0.02	1.14	214.22	215.25
L8	21.92	1.10	0.77	-0.33	30	196.94	199.50
L9	25.75	1.49	1.07	-0.42	28	221.52	218.19

Table 6.9: Wave model output with and without the wave farm in the medium grid showing the wave field changes of condition 5.

OL	Depth (m)	$H_{s_{nof}}$ (m)	$H_{s_{wif}}$ (m)	ΔHs (m)	$\%\Delta H_s$	θ_{nof} (°)	θ_{wif} (°)
L5	41.48	3.58	3.59	0.01	0.27	227.08	227.01
L6	31.22	3.07	3.09	0.02	0.65	249.84	250.43
L7	35.32	3.03	3.06	0.03	0.99	223.87	224.98
L8	21.92	1.62	1.23	-0.39	24	199.76	201.98
L9	25.75	2.58	1.62	-0.96	37	227.88	276.34

Table 6.10: Wave model output with and without the wave farm in the medium grid showing the wave field changes of condition 8.

OL	Depth (m)	$H_{s_{nof}}$ (m)	$H_{s_{wif}}$ (m)	ΔHs (m)	$\%\Delta H_s$	θ_{nof} (°)	θ_{wif} (°)
L5	41.48	5.87	5.88	0.01	0.17	239.62	239.61
L6	31.22	4.86	4.88	0.02	0.41	258.80	259.09
L7	35.32	4.51	4.56	0.05	1.10	231.51	232.61
L8	21.92	2.11	1.78	-0.33	16	201.08	201.64
L9	25.75	3.57	1.96	-1.61	45	233.01	229.64

The impact induced by a wave farm can be noticed in L8 and L9 which are the output locations behind the wave farm. The percentage difference of significant wave height expressed as

$$\%\Delta H_s = 100 * \left[\frac{\left| H_{s_{wif}} - H_{s_{nof}} \right|}{H_{s_{nof}}} \right], \tag{6.7.1}$$

has been used to compute the percentage differences for the selected conditions and are listed in Tables 6.8, 6.9 and 6.10, respectively.

6.7.2 Wave direction changes induced by the wave farm

Wave direction is an important parameter with regards to energy extraction of the WECs. For WECs to harness optimal wave energy, they must be installed in such a way that they face the dominant wave direction. Various wave directions in the wave model have been considered as shown in Table 6.5. The choice of these directions is based on the location of the area of interest.

Wave direction changes are listed in Tables 6.8, 6.9 and 6.10 and they show a direction changes induced by wave farm at the selected output locations. This is due to the reflected wave field around the device; as a result there is a wave direction change. The results indicate that the wave direction change induced by the wave farm is minimal. It is possible that if there were more WECs considered, the direction change will be larger. Furthermore, factors such as refraction and wave-wave interactions around the wave farm can influence the wave direction as the waves approach the shore.

6.7.3 Wave peak period changes induced by wave farm

The model results show a constant peak period for all selected conditions. It can be concluded that this parameter was not affected by the presence of the wave farm. The significance of this parameter in the spectrum will be discussed in the next section, where energy density of the output locations will be presented to show the changes of the wave spectrum induced by the wave farm.

6.8 Transformation of wave energy with and without the wave farm

The aim of this section is to describe the wave energy variability at the output locations with and without the wave farm. The output locations in Figure 6.6 have been positioned for the purpose of identifying wave field conditions around the wave farm. Due to the position of these output locations, it is expected that the wave energy will vary. The energy spectra at certain locations have been plotted to quantify the change in the spectra as shown in Figure 6.11.

Two locations L8 and L9 in the spectrum were identified as places where change is taking place. This is due to the wave farm extracting the energy from the waves. The amount of energy extracted at these locations is shown in Figure 6.12. The net amount of wave energy in the absence of a wave farm for L8 and L9 is 14 600 and 35 400 in $J/m^2/Hz$, respectively. In the presence of a wave farm, the energy is reduced to 5 860 for L8 and 17 400 $J/m^2/Hz$ for L9. The net reduction for these locations is 8 740 for L8 and 18 000 $J/m^2/Hz$ for L9. From these results, it is clear that the wave energy from offshore to nearshore and behind the wave farm is changing.

Figure 6.13 shows the amount of energy differences for L8 and L9. For all the selected conditions in this analysis, L8 and L9 wave energy is changing. This is illustrated by figures in Appendix D.3. It can be concluded that the amount of energy available at the output location depends on the area where they are positioned and the wave conditions associated with an area of interest.

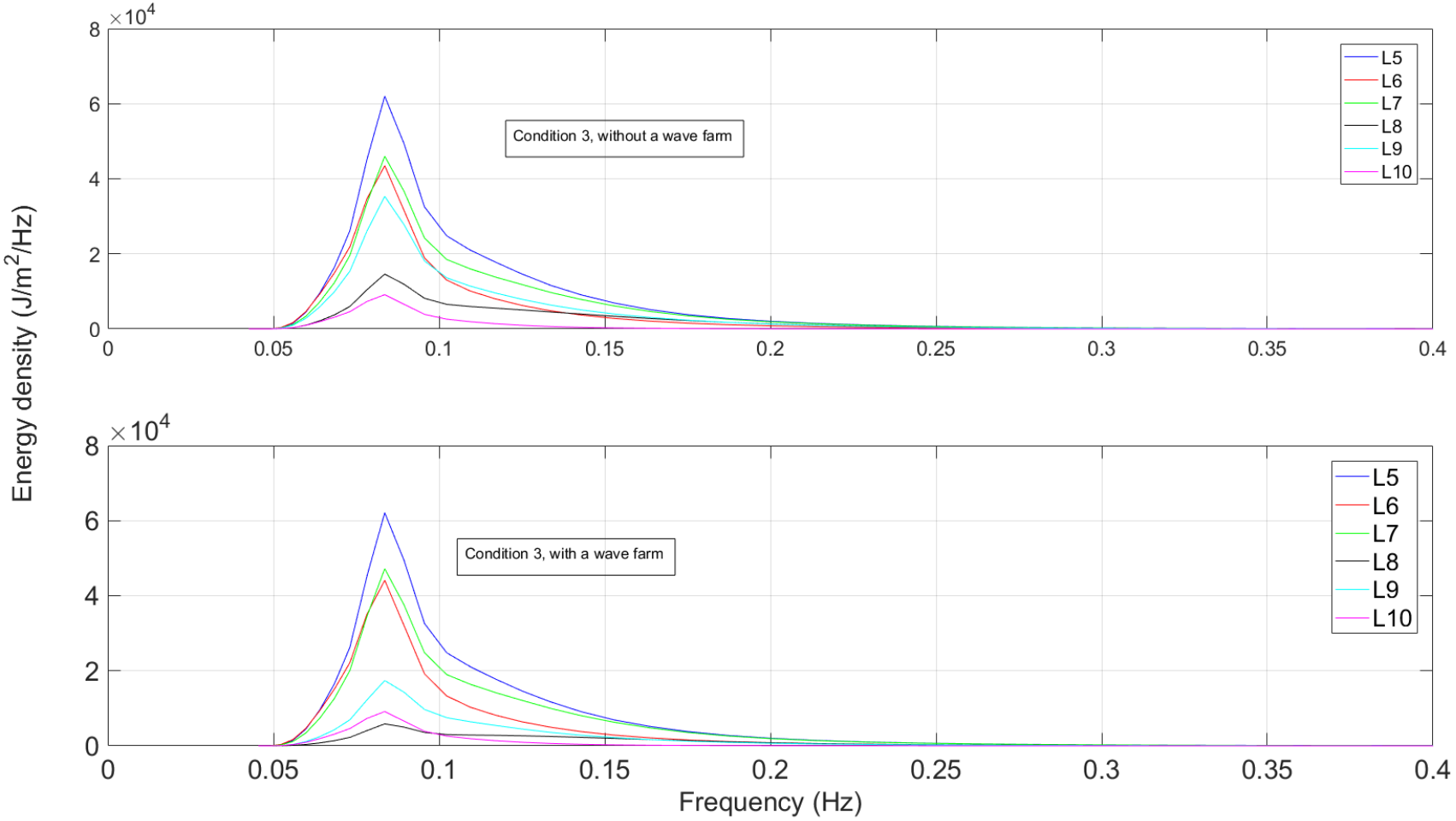

Figure 6.11: Wave energy spectrum with and without the wave farm of condition 3.

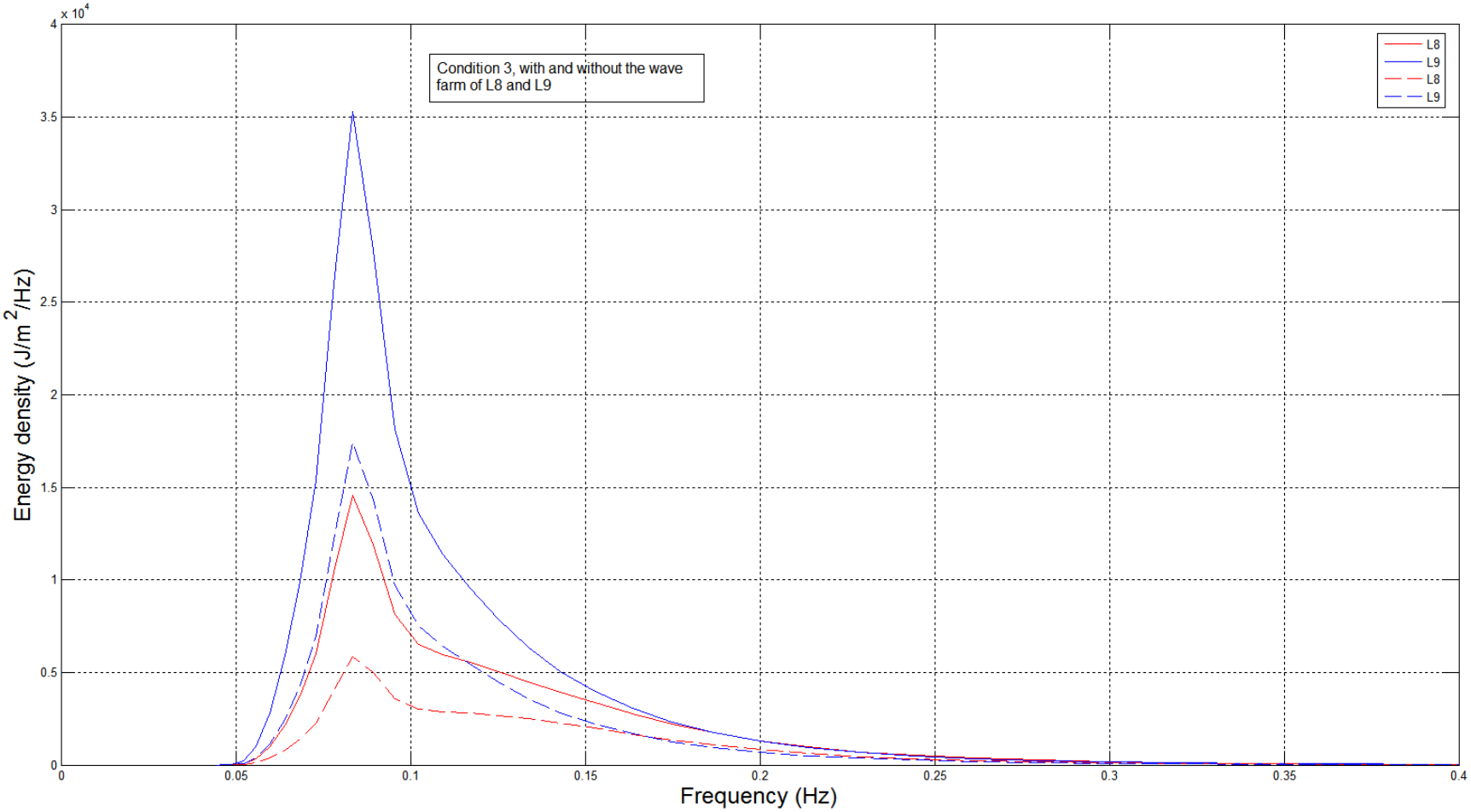

Figure 6.12: Wave energy spectrum of L8 and L9 with and without the wave farm.

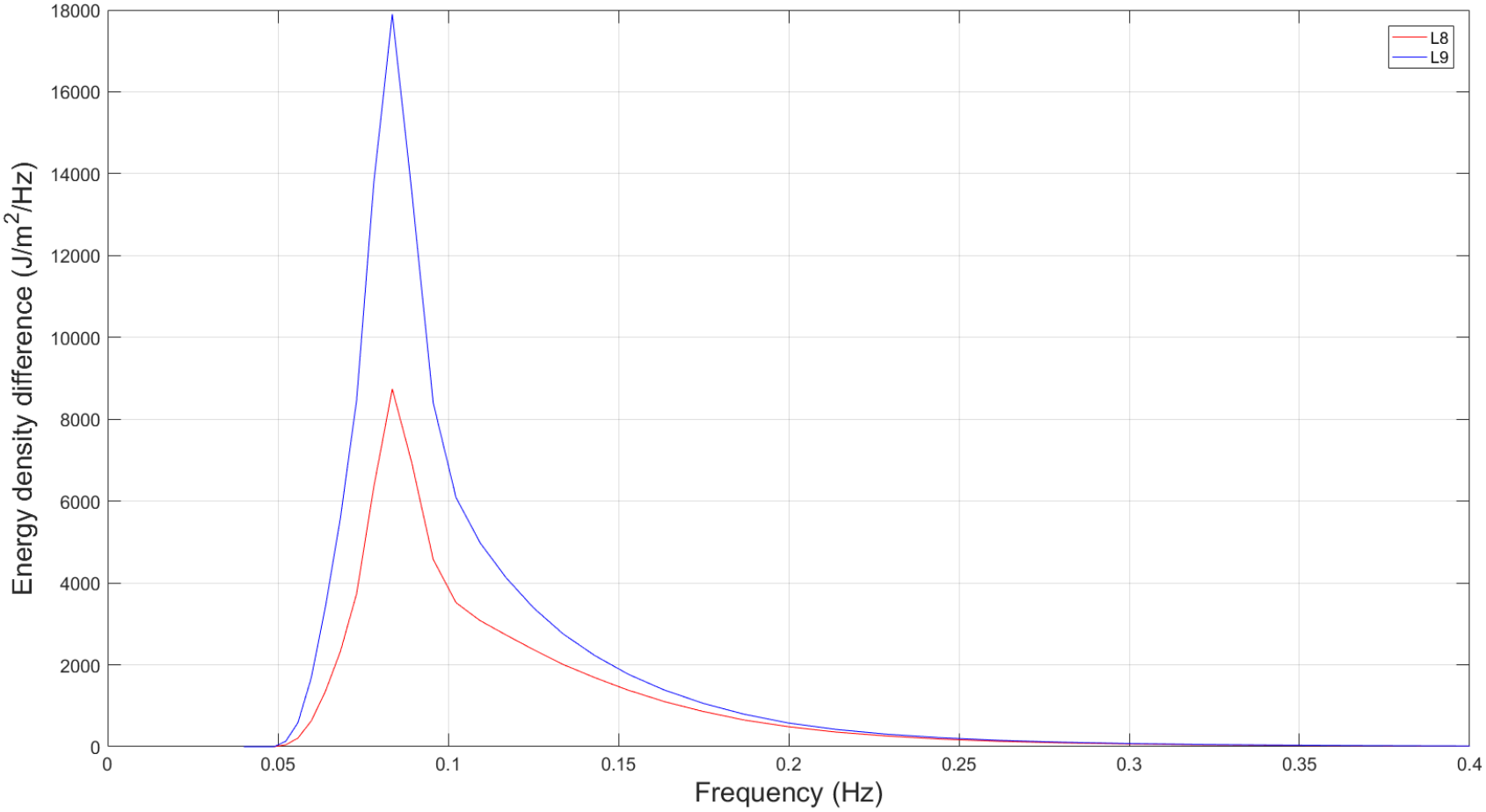

Figure 6.13: The wave energy difference for L8 and L9 of condition 3.

6.9 Sensitivity assessment

Two scenarios for sensitivity assessment were considered in the study. These include adding two extra devices to the original wave farm layout and changing the orientation of the wave farm relative to the dominant wave direction. Similar analysis using conditions 3, 5 and 8 were considered. Based on the results, a reduction in significant wave height for both scenarios was noticed as shown in Figures 6.14, 6.15, 6.16, 6.17, 6.18 and 6.19, respectively.

In analysing the effect of these two scenarios and the original wave farm layout as illustrated in Figure 6.20, the changes in the nearshore wave field were noticed as shown in Tables 6.11 and 6.12. For illustration purposes, condition 3 in Figure 6.20 was used. As expected, at the output locations L8 and L9 changes were noticeable due to their position in the computational domain as illustrated by Figure 6.6. Based on the percentage difference of the significant wave height for both scenarios and the original wave farm layout, it can be concluded that the original wave farm layout (see left panel of Figure 6.20) is not the better layout for this study. The reason is that the orientation of the wave farm as shown in Figure 6.20 is facing the dominant wave direction inside the Outer Bay which is 247.5° as shown by the vector arrows. The dominant wave direction of the offshore NCEP data is 225.0° as shown in Table 6.4, but the waves tend to change direction as they approach the entrance of the Saldanha Bay.

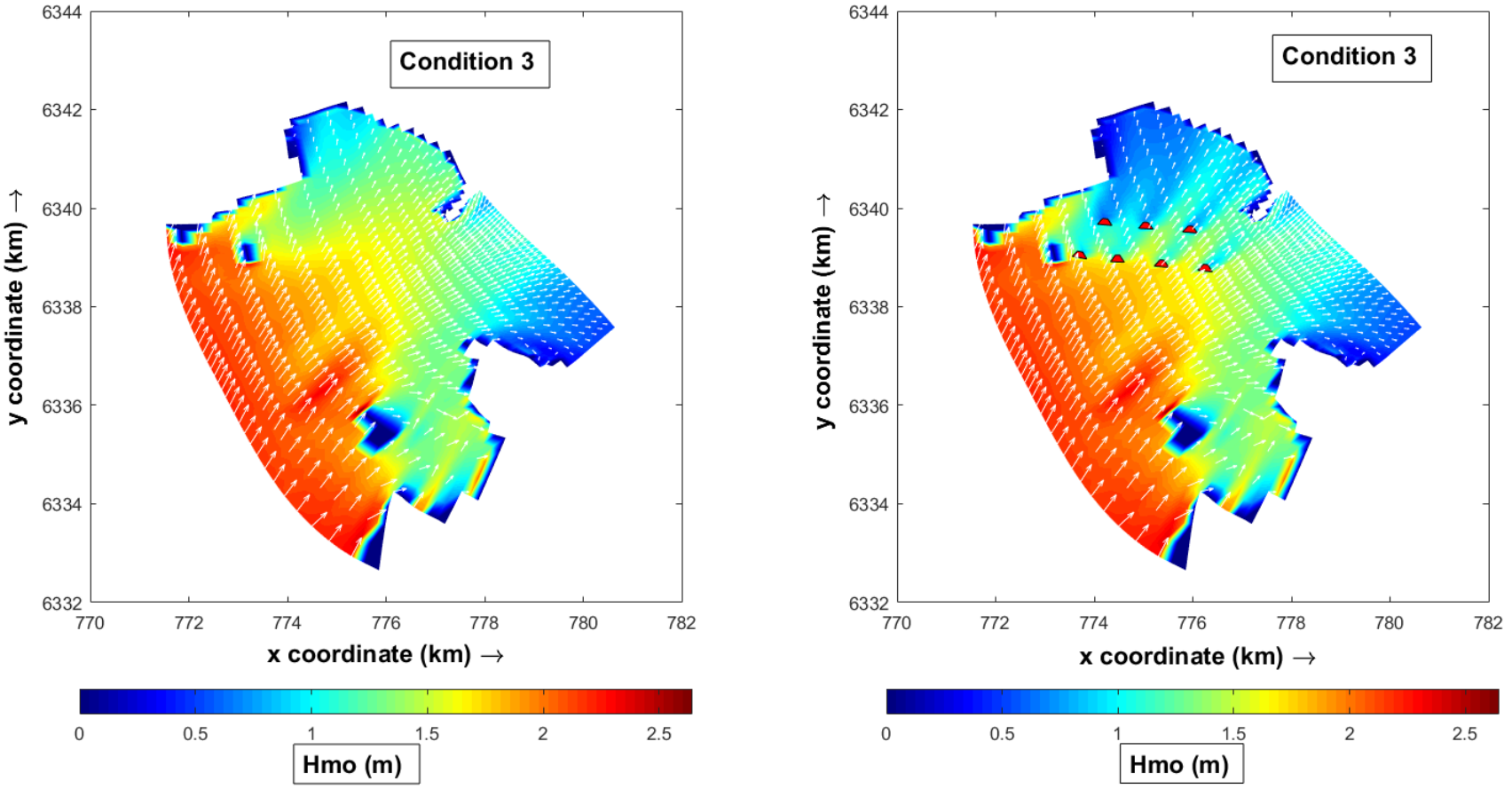

Figure 6.14: The significant wave height without (left) and with (right) the wave farm, $H_{mo} = 2.5$ m, $T_p = 12$ s and $\theta = 202.5°$.

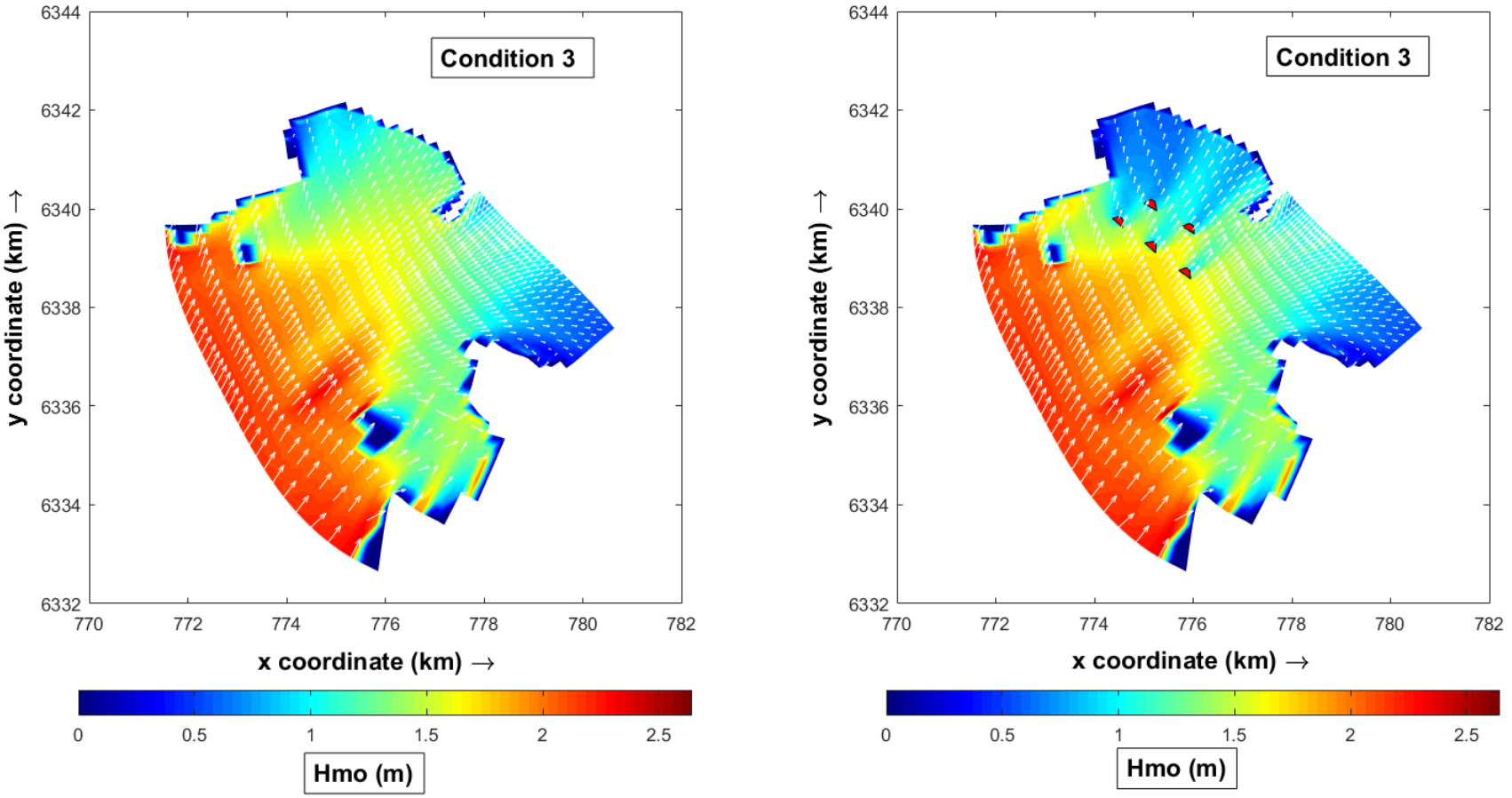

Figure 6.15: The significant wave height without (left) and with (right) the wave farm, $H_{mo} = 2.5$ m, $T_p = 12$ s and $\theta = 202.5°$.

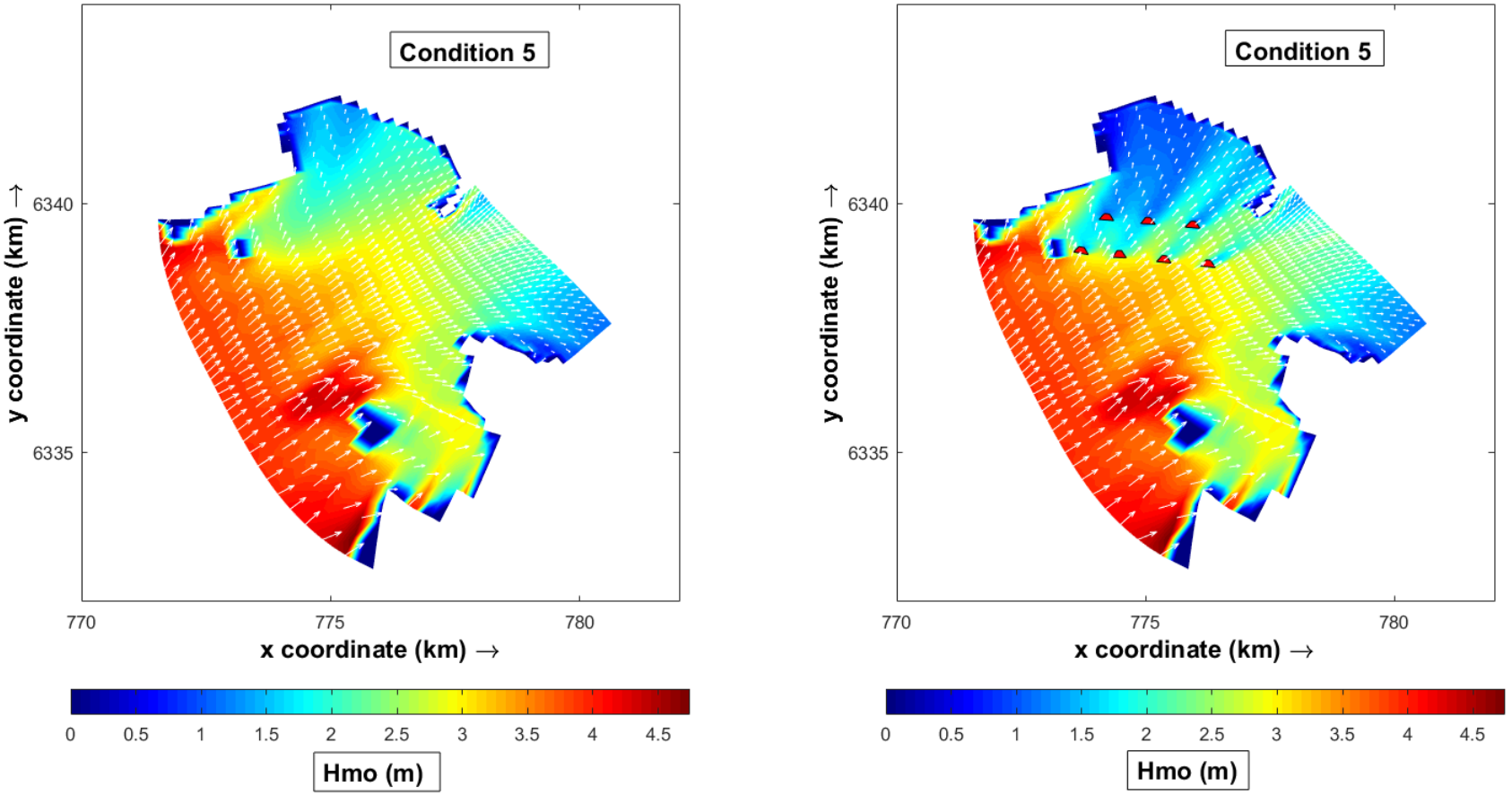

Figure 6.16: The significant wave height without (left) and with (right) the wave farm, $H_{mo} = 4.5$ m, $T_p = 14$ s and $\theta = 225.0°$.

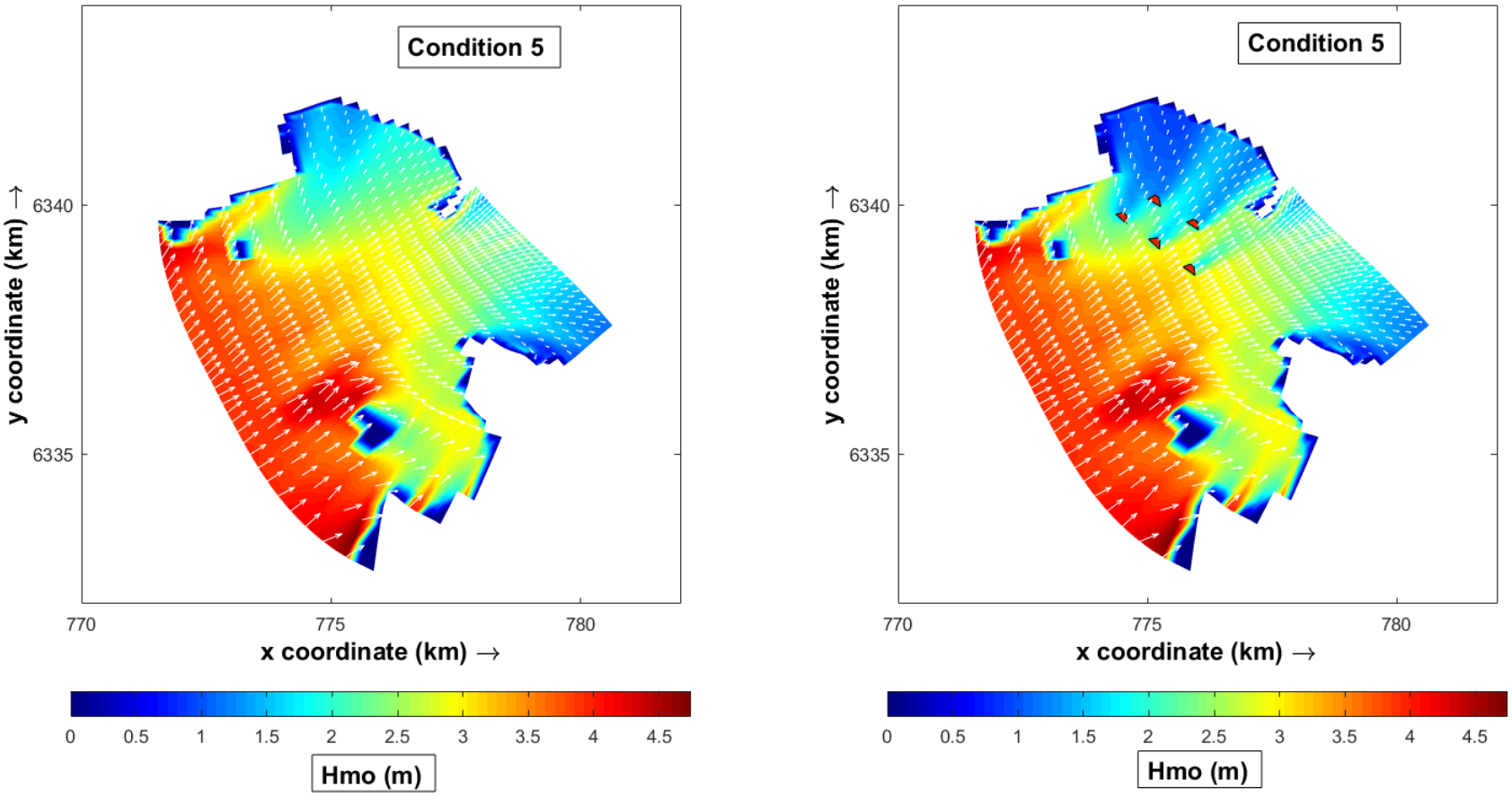

Figure 6.17: The significant wave height without (left) and with (right) the wave farm, $H_{mo} = 4.5$ m, $T_p = 14$ s and $\theta = 225.0°$.

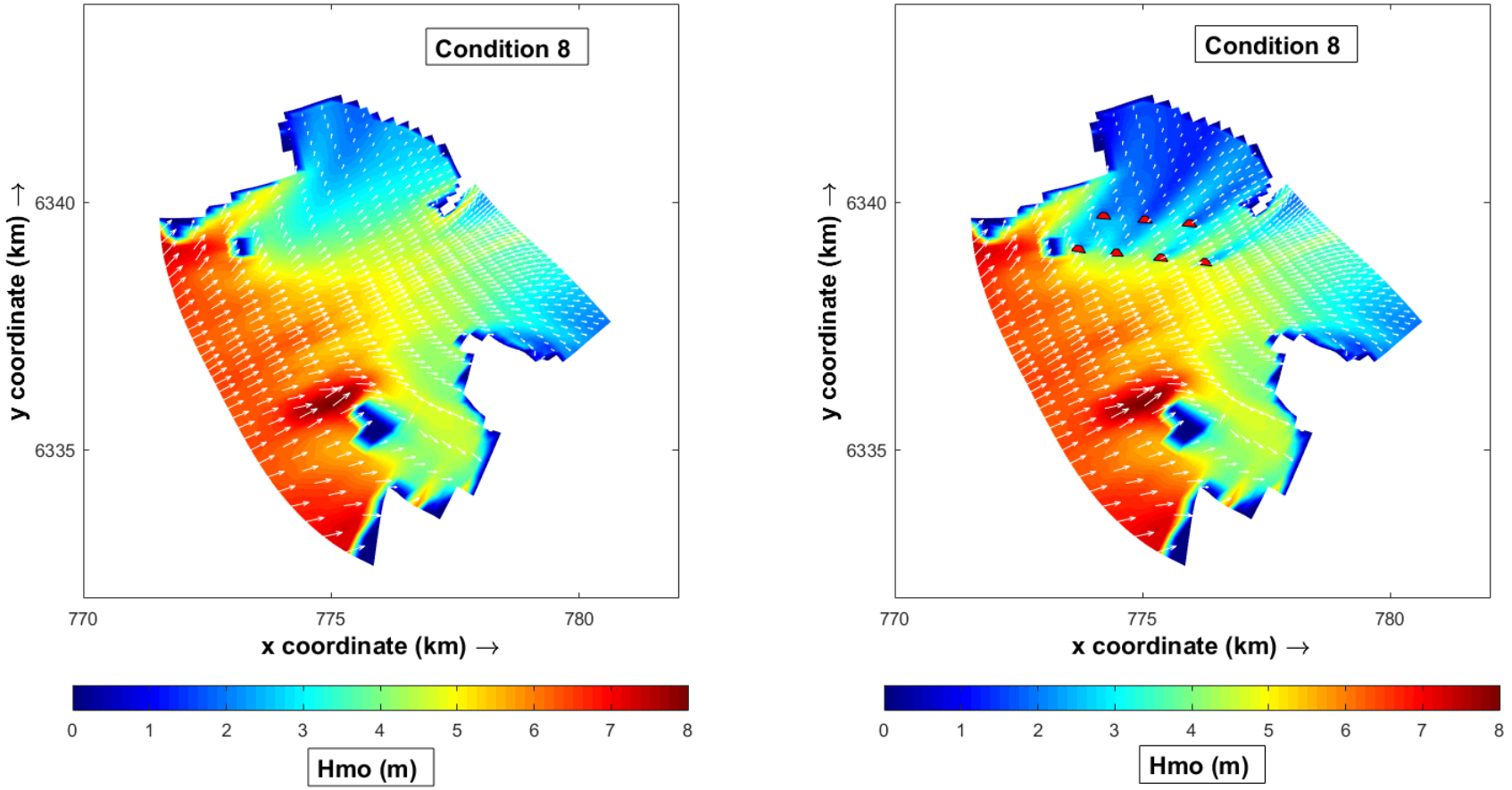

Figure 6.18: The significant wave height without (left) and with (right) the wave farm, $H_{mo} = 7.5$ m, $T_p = 16$ s and $\theta = 247.5°$.

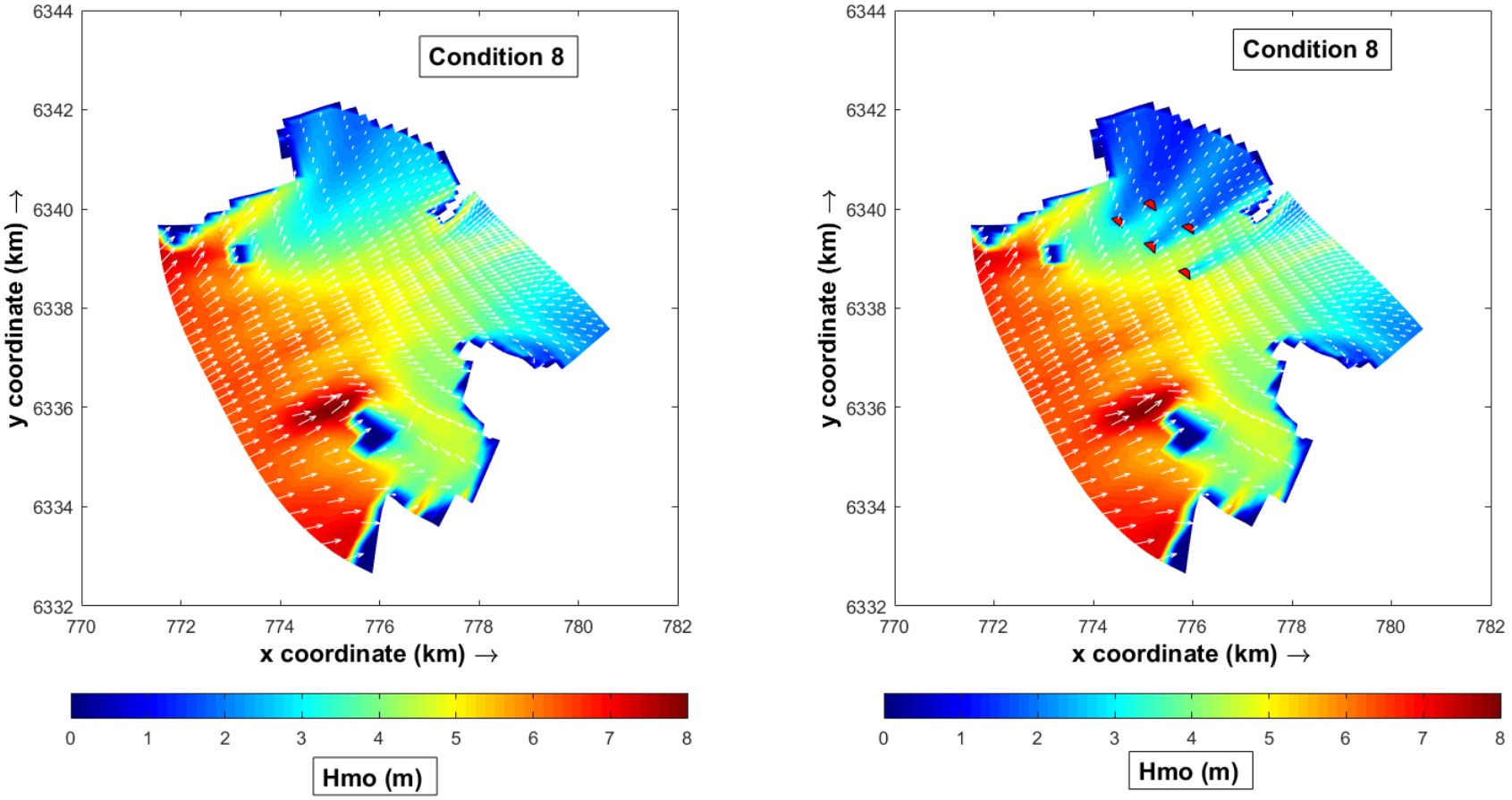

Figure 6.19: The significant wave height without (left) and with (right) the wave farm, $H_{mo} = 7.5$ m, $T_p = 16$ s and $\theta = 247.5°$.

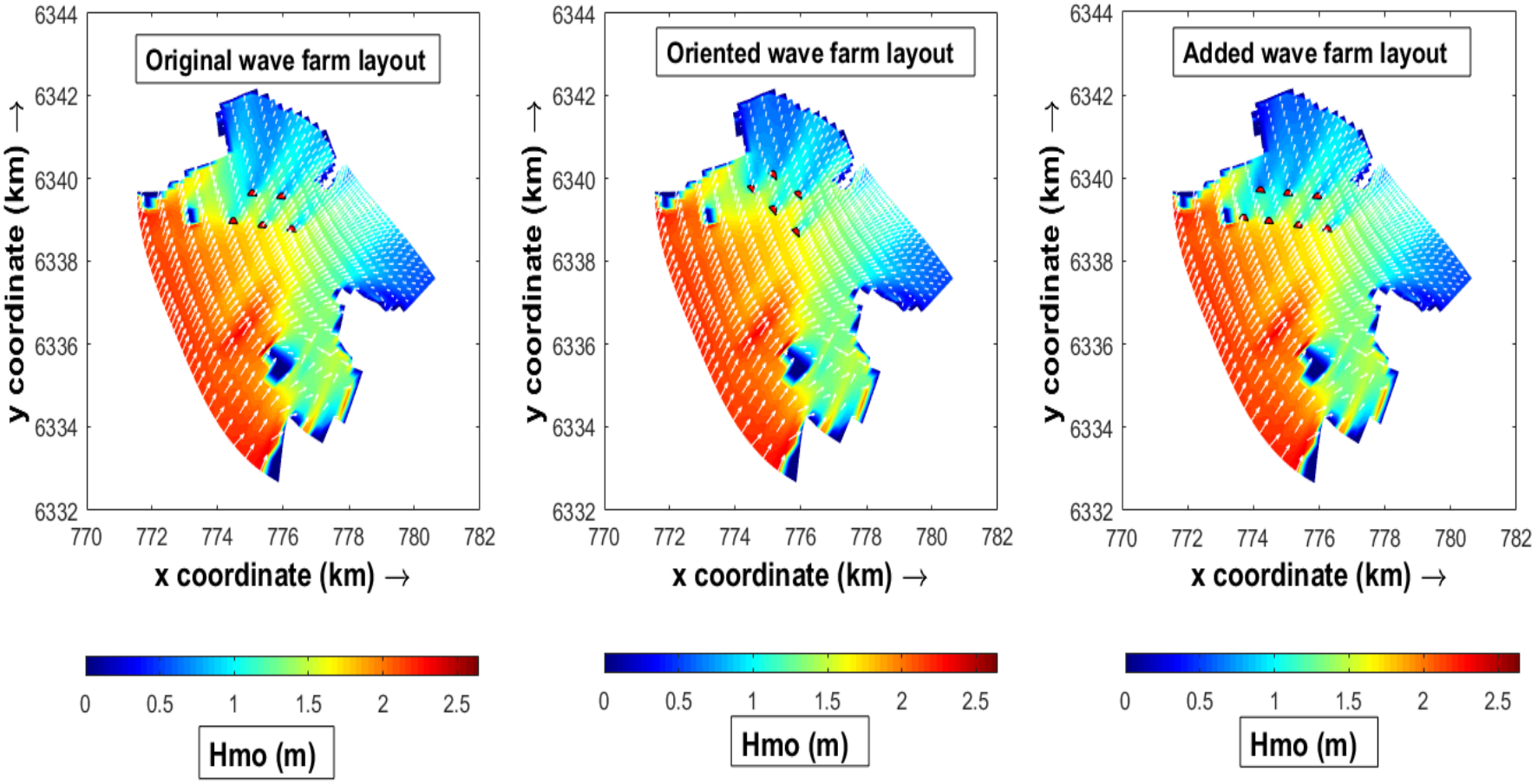

Figure 6.20: The figure shows the original, oriented and the addition of two extra devices in a wave farm.

Table 6.11: Percentage difference of significant wave height for L8 and L9 of the oriented wave farm.

Selected conditions	Percentage differences
Condition 3	L8: 36% L9: 25%
Condition 5	L8: 29% L9: 36%
Condition 8	L8: 35% L9: 36%

Table 6.12: Percentage difference of significant wave height for L8 and L9 for the addition devices in a wave farm.

Selected conditions	Percentage differences
Condition 3	L8: 34% L9: 28%
Condition 5	L8: 30% L9: 37%
Condition 8	L8: 23% L9: 45%

6.9.1 Changing the orientation of the wave farm

To further examine the sensitivity the orientation and addition of two devices to the original wave farm layout, two output locations L8 and L9 are considered for condition 3. The energy density of L8 and L9 for both scenarios against the original wave farm layout was plotted to see the variability in wave energy as illustrated by Figures 6.21 and 6.22. It can be seen in Figure 6.21, that there is a significant energy change in L9 with energy difference of $1\,565 \times 10^4$ J/m^2/Hz were L9 of the oriented wave farm has more energy extracted compared to L9 of the original layout. This implies that wave energy is sensitive to the orientation of the wave farm. The output location L8 of the oriented layout against L8 of the original layout showed a low energy extraction with energy difference of 8662 J/m^2/Hz.

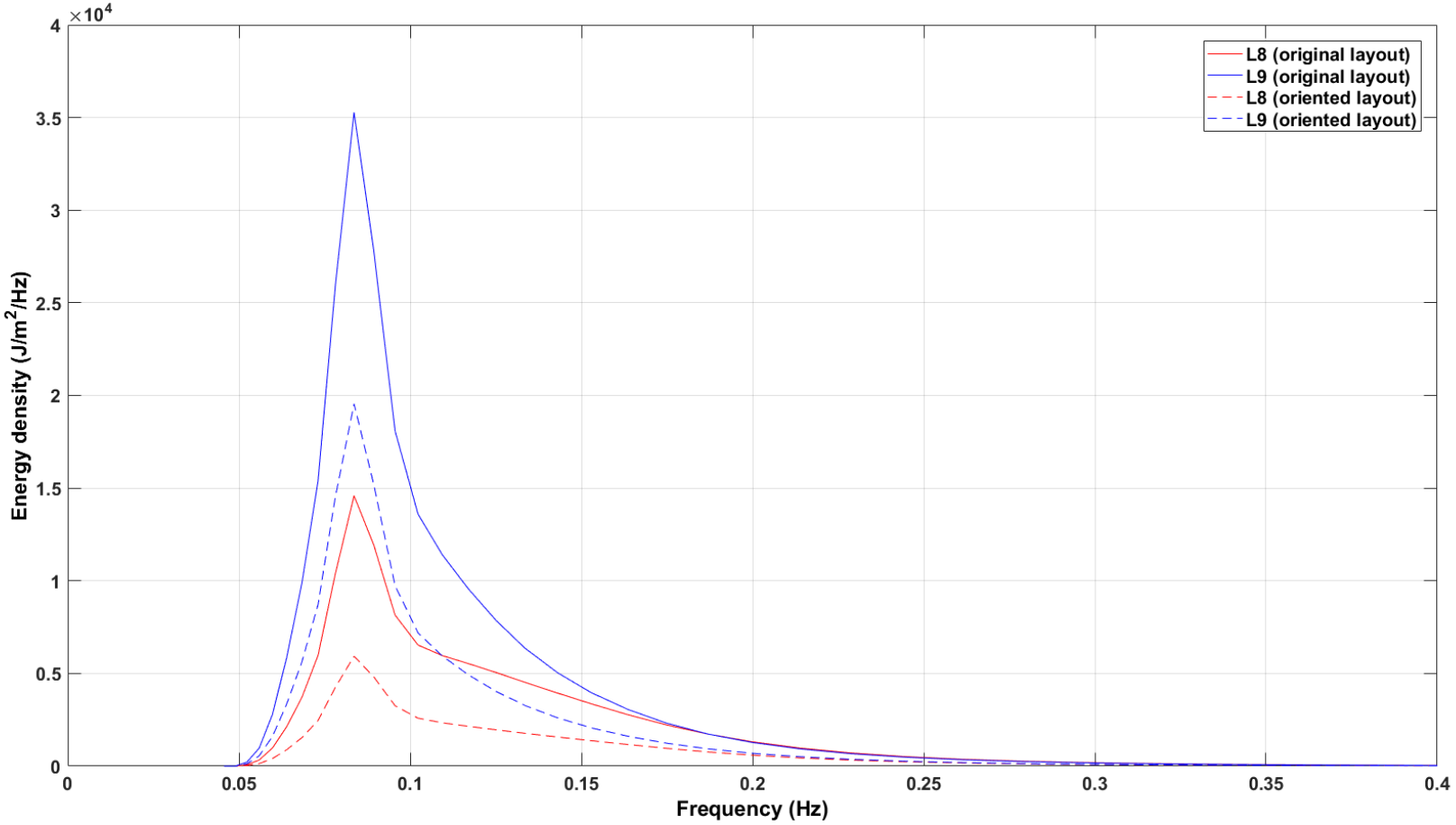

Figure 6.21: The figure shows the original and oriented output location L8 and L9 spectrum of condition 3.

6.9.2 Adding two WECs to the original wave farm

The energy density in Figure 6.22 shows the difference in energy for the original and modified layout for locations L8 and L9. The energy difference between the original and the modified layouts for position L9 is only 10 $J/m^2/Hz$ and is shown more clearly in Figure 6.23(a). Also, the output location L8 shown in box (b) of Figure 6.22 showed a small difference in energy extracted and is clearly shown in Figure 6.23(b) with an difference of 393 $J/m^2/Hz$. In this case, it can be concluded that an addition of two devices to the original layout has little impact on the spectra of L8 and L9 since little difference is noted. This could be, because the added devices were in the shadow of the Malgas Island as shown by the right panel of Figure 6.20. In this scenario, the oriented wave farm showed an increase in wave energy extraction since the wave farm is facing the dominant wave direction 247.5° inside the Outer Bay, implying that the oriented wave farm could be the better layout.

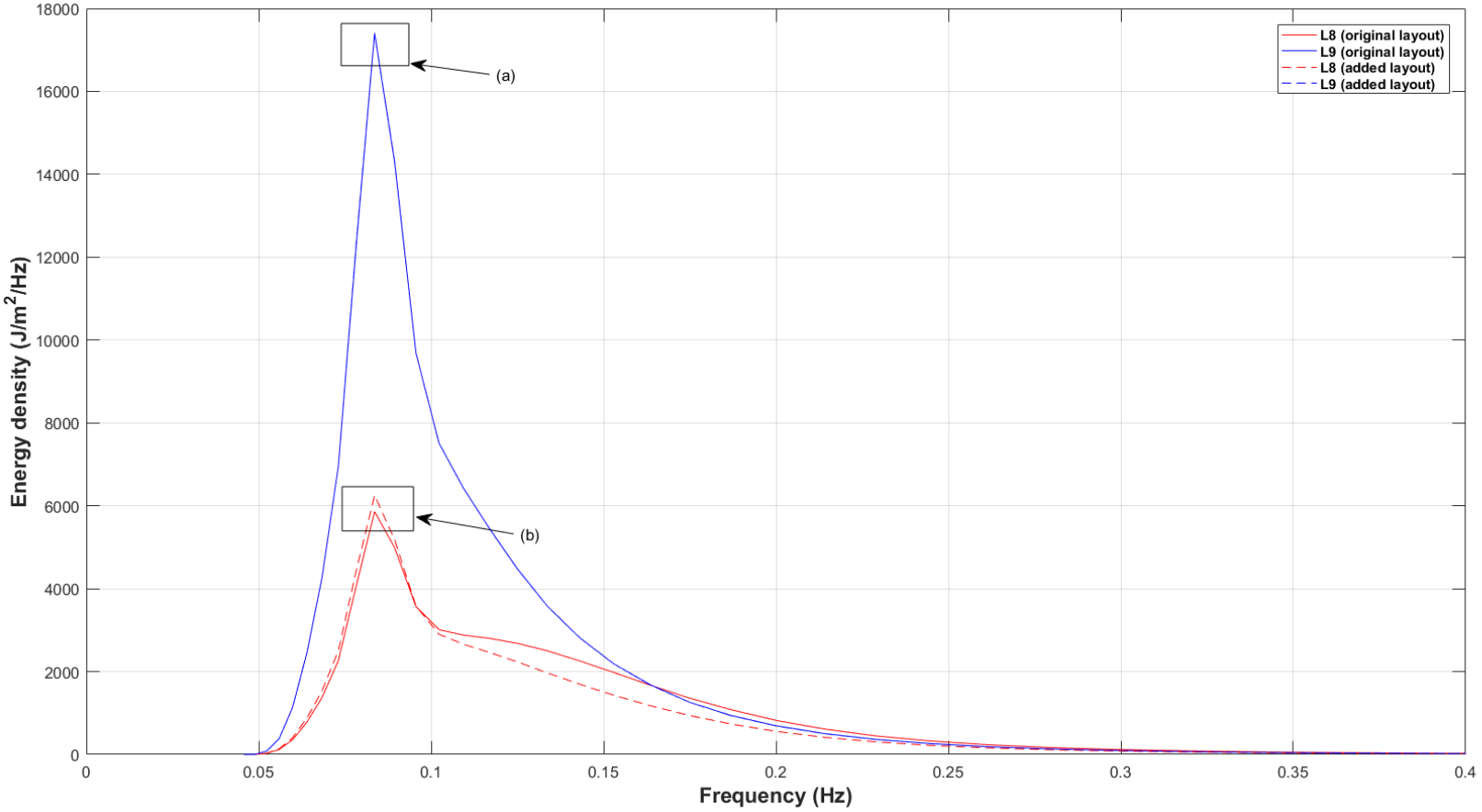

Figure 6.22: The figure shows the original and the addition of two extra devices in a wave farm for L8 and L9 of condition 3.

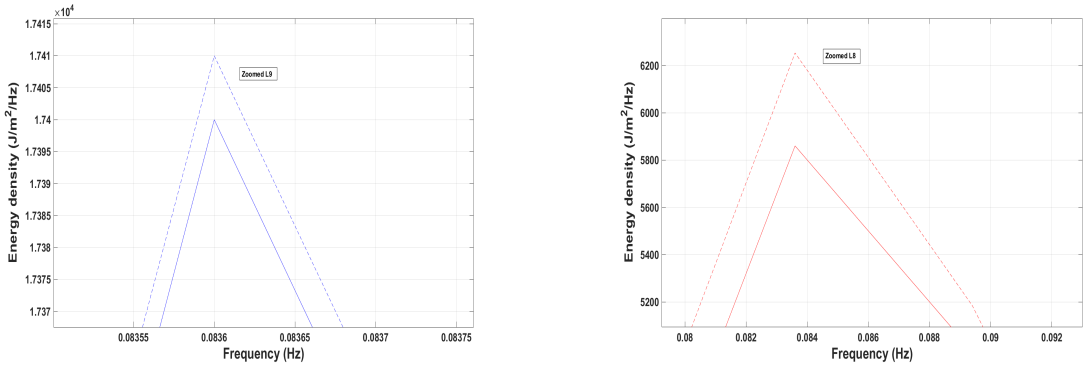

(a) Energy spectrum of L9 added devices **(b)** Energy spectrum of L8 added devices

Figure 6.23: The energy density of L8 and L9 zoomed for an added devices in a wave farm.

6.10 Proposed methodology

The main objective of this study is to develop a methodology for the assessment of wave energy along the South African coast. This study presents a methodology for determining the impact that these WECs may have on the nearshore wave field parameters. Saldanha Bay was selected for the case study, wave conditions were assessed using the numerical wave model SWAN. In order to use the SWAN model, the peak enhancement factor parameter of the model was evaluated using South African wave conditions as discussed in Chapter 4. Offshore boundary wave conditions were obtained from the NCEP. Two wave simulation cases, with and without the wave farm, were considered. In this case, the model obstacles were represented by an array of Wave Dragons. The nearshore wave field parameters were analysed using output locations that were positioned in front and behind the obstacles (wave farm). Based on the findings of this study, the proposed methodology for assessing wave energy along the South African coast for wave farm implementation are summarised as follows:

1. The JONSWAP spectral model should be fitted to a set of measured data at the location of interest to obtain the peak enhancement factor (γ) which is used as an input parameter for the numerical wave model SWAN. Other parameters such as peak frequency, f_p, and proportionality constant, α_{PM}, are kept constant. It must be noted that other fitting techniques such as multi-parameter, non-linear least squares curve fitting can be used to obtain γ.

2. Obtain the input boundary conditions from offshore NCEP data if measurements are not available. The boundary conditions are necessary for SWAN simulations and are characterised by deep water wave parameters.

3. Steps 1 and 2 are used as the input information to run the numerical wave model SWAN. To model the impacts of WECs, two cases must be considered and they

include a case with no WECs and a case with WECs in the model. Transmission and reflection coefficients are required to model the WECs impact in SWAN. Depending on the type of WEC chosen, various coefficients are used which are computed by device developers. In this study, a practical guide for the design and construction of floating structures as explained by Diaconu and Rusu (2013) was used for transmission and reflection coefficients of a Wave Dragon.

4. Analyse the nearshore wave field parameters using the output locations included in Step 3. The parameters in this case are analysed separately, where the percentage difference in significant wave height is evaluated in the presence and absence of a wave farm. The analysis is carried out using the output locations.

5. Once the above steps have been implemented, an assessment of wave energy using selected output locations is carried out. This is assessed through wave energy spectra at the output locations behind the wave farm. This step will indicate how much energy has been extracted by the addition of extra devices or the orientation of the original wave farm layout.

6. A sensitivity analysis should be done to determine the impact of additional converters as well as the impact of a wave farm orientation change.

6.11 Summary

The objective of this chapter was to analyse the nearshore effects induced by a wave farm. Small to large numbers of WECs will be deployed into the ocean for electricity generation. These WECs will cause nearshore wave changes which in turn can modify the coastline. Therefore, studies concerning the nearshore wave field changes induced by WECs are very important in the assessment of wave energy resource. Other changes that can occur are the sediment transport along the coastline caused by the presence of wave farm. It is, therefore, necessary to analyse these wave field changes induced by the wave farm to predict changes in the coastline morphology as mentioned in Section 1.3. In addition the modelling procedure implemented here may be used to determine optimal wave farm parameters.

The SWAN wave model was used in this study. An array of five Wave Dragons was included in the model as obstacles. Transmission and reflection coefficients of 0.68 and 0.2 respectively were used. The values were obtained from a practical guide for the design and construction of the floating structures as given by Diaconu and Rusu (2013). It can be assumed that the values were determined through physical model tests specifically for wave dragon device. In this thesis, the particular device was chosen based on its ability to use two long wave reflectors to direct the waves toward the ramp. In general, WECs are designed to extract wave energy in different ways at different wave conditions. Wave Dragon is a unique device since it has only one moving part, the Wells turbines. This makes it easy to maintain the device in the nearshore region. Due to extreme conditions in the offshore region, it might be difficult to maintain or repair devices.

The investigation of nearshore wave field changes induced by a wave farm has been done by using a set of 9 wave conditions selected from offshore NCEP wave data. Three conditions out of 9 were selected for the purpose of the analysis. These include conditions 3, 5 and 8. Each wave field parameter change induced by the wave farm was analysed. As expected, it was noticed that wave height has decreased behind the wave farm. The difference in significant wave height is shown in Figure 6.10 where the colour blue indicates a reduction in wave height. To further examine this, output locations in the medium grid were analysed. It was noticed that at locations L8 and L9, the wave height decreased significantly compared to other locations in that grid. These results were expected since both L8 and L9 are behind the wave farm.

Wave direction and peak period changes induced by wave farm were minimal. Wave transformation processes such as refraction and wave-wave interactions contributed to the direction change. The wave farm has no influence on the peak period since there

was no change in this parameter. The output location results for selected conditions have shown the constant peak period throughout the computational domain implying that the wave farm has no effect on the parameter.

The wave energy spectra at the output locations were plotted to see the variability in wave energy. This is an important concept in this study because it shows how much energy can potentially be extracted by the wave farm. The general shape of the spectra was the same as its shape in the absence of the wave farm, only L8 and L9 changed in the presence of the wave farm. Therefore, these two output locations were analysed separately to see the net energy removed by the wave farm. The energy difference is shown in Figure 6.13 for L8 and L9. The energy difference between these output locations is not the same due to their position in the computational domain. In conclusion, the wave farm has an effect on the wave energy according to the results of the SWAN wave model.

A sensitivity assessment in this chapter has been included to analyse the changes on the nearshore wave field due to the addition of two extra devices in the original wave farm layout and the orientation of the wave farm relative to the dominant wave direction. It was analysed using the wave energy spectra at the selected output locations that are behind the wave farm. Based on the results of the spectra, the oriented wave farm showed more wave energy extraction compared to the original wave farm layout, due to this reason, it was concluded that it is the best layout in this study. The spectra for the original and the addition of two devices showed small energy changes and therefore, it cannot be considered as the best layout in this study. The devices were added in the left position to avoid blocking the ship navigation in and out of the bay.

The proposed methodology for the assessment of wave energy along the South African coast has been outlined in Section 6.10 and it includes several steps to be followed when assessing wave energy at the specific area of interest.

Chapter 7

Summary and Conclusions

7.1 Summary

Ocean wave energy appears to be one of the most promising and sustainable renewable resources for South Africa due to our long coastline and energetic wave conditions. To harness this energy resource, an array of WECs must be installed for sufficient generation of electricity. These WECs might have an impact on the nearshore region which can possibly lead to coastal morphology changes. However, WECs can also be used for coastal protection, as mentioned in Section 1.4. In this study, a numerical wave model to analyse the nearshore wave field changes induced by the presence of a wave farm has been presented.

The measured wave spectrum at various locations has been assessed to see the variability of the energy along the South African coast. The JONSWAP spectral model, which is used to describe the wave energy, was fitted onto the measured data at various locations to obtain the peak enhancement factor values for South African wave conditions. The model was suitable for single peaked spectra but not for double and multiple peaked spectra. A sample of measured data for chosen locations is presented in Appendix B.2.

Due to the models inability to fit the double and multi-peaked spectra, a method for separating spectra into two components, sea and swell, was implemented. Based on literature, the JONSWAP model was fitted onto the swell components and for wind sea, the Pierson-Moskowitz model was used to obtain the peak enhancement factor values. Another factor that led to the use of a separation algorithm, was to understand the energy contributions of wind sea and swell on the entire spectra along the coast.

Literature on various WECs for extracting wave energy resources has been presented. These devices have been classified according to their position in the ocean and conversion types. Based on the different designs and working principles, wave energy is extracted

in various ways. For example, Wave Dragon which is chosen as a hypothetical device for this study, has the ability to use two long wave reflectors to direct wave energy onto the ramp. An array of Wave Dragon devices was included in the wave model SWAN as obstacles. The modelling of WECs in SWAN requires transmission and reflection coefficients. The transmission and reflection coefficients for Wave Dragon were based on the practical guide for the design and construction of the floating structures as mentioned by Diaconu and Rusu (2013). There is no information as to how these values were obtained, it was therefore assumed that they were based on the physical model tests in a laboratory basin.

Furthermore, a set of 9 wave conditions for the nested wave model was selected from the offshore NCEP data of 10 years. Two model simulations with and without the wave farm were conducted in the nested fine grid model. The results showed a change in the nearshore wave field parameters in the presence of the wave farm. The results were assessed at selected output locations in the medium and fine grid. A reduction in wave height was noticed behind the wave farm. Based on the selected output locations at different water depths and input conditions, the reduction in wave height varied throughout the model domain. As a result, the difference in wave height was plotted. Output locations L8 and L9 showed a reduction in wave height in the presence of a wave farm. In summary, the model results showed a change in the nearshore wave field during the presence of a wave farm. The changes in local wave climate can lead to changes in sediment transport patterns which can result in shoreline changes.

A sensitivity assessment was conducted to analyse the nearshore wave field parameters induced by an addition of two hypothetical devices and a change in orientation of a wave farm. These two scenarios were analysed individually using wave energy spectra at selected output locations. Based on the spectra of L8 and L9, a rotated wave farm showed an increase in the energy extracted compared to the original and the addition of two devices since this orientation faced the dominant wave direction (247.5°) and therefore extracted more wave energy.

Based on the findings of this thesis, a proposed methodology for the assessment of wave energy along the South African coast was outlined. The proposed methodology could be used as vital information to further studies in assessing the nearshore wave field changes induced by the presence of wave farms.

7.2 Conclusions

Wave energy along the coast was assessed by fitting the JONSWAP model onto measured data to obtain the peak enhancement factor values for South African wave conditions.

The results showed higher values for the west coast than the east coast. Based on a previous studies, the west coast has more energy resource for the installation of WECs than the east coast along the South African coast. Saldanha Bay was therefore chosen as the potential site for the installation of WECs.

In assessing the changes in the dominant wave parameters induced by WECs, the SWAN wave model was used. The input boundary conditions for the model were obtained from offshore NCEP wave data. Boundary conditions were selected based on the highest percentage of occurrence of wave parameters. Two cases, with and without the WECs in the model were simulated. Analysis was conducted using the selected output locations. The results showed changes in dominant wave parameters in the presence of wave farm.

A sensitivity assessment was carried out. Two scenarios which include change in orientation of a wave farm and an addition of two devices in the original layout were investigated. The change in orientation of a wave farm showed more energy extraction than for the addition of devices on the original layout. Based on the findings of this study, the main conclusions that can be drawn from this study include are:

- The peak enhancement factor values for west coast and higher than the east coast.
- There is a clear reduction in nearshore wave field parameters behind the wave farm.
- The change in the orientation of the wave farm has a significant effect on the nearshore wave field and it appears as though this may also have an influence on the amount of energy harvested by the wave farm.

As a result of the findings of the study, the main objective was achieved which outlines procedures to be followed when assessing wave energy along the coast.

7.3 Future work

Further research in understanding the wave energy resource along the South African coast is needed:

- A further investigation of the spectral decomposition method is needed to account for spectra that have several spectral peaks as was observed in the present study. The decomposition method was not able to separate a multi-peaked spectrum.
- Literature studies concerning the wave farm assessment have been presented in Section 1.4. In the present study, a similar procedure using the spectral wave model has been conducted. Power transfer function which is explained in Section

5.6 was not included in the study due to time constraints. Further study is needed to understand the amount of energy extracted by devices at each frequency in the area of interest.

- A physical model study would be valuable in further research of the impact on the nearshore wave field. Careful consideration should be given to scaling of the motions and forces of the WECs.

Appendix A

Mathematical description of ocean waves

A.1 Linear wave theory

Linear wave theory also known as *Airy wave theory* is commonly used to describe the propagation of surface gravity waves (Benassai, 2006). According to Benassai (2006), there are assumptions that are considered in developing the Airy wave theory and they include that the fluid is homogeneous and irrotational and that the Coriolis effects may be neglected. The irrotational fluid is represented by the potential function, ϕ. The Airy wave theory derivation starts by the introduction of the Laplace equation for irrotational flow which is given as

$$\nabla^2\phi = 0, \tag{A.1.1}$$

or

$$\frac{\partial^2\phi}{\partial x^2} + \frac{\partial^2\phi}{\partial z^2} = 0. \tag{A.1.2}$$

Using the three linearized boundary conditions at the bottom and at the free surface,

$$\left.\frac{\partial\phi}{\partial z}\right|_{z=-d} = 0. \tag{A.1.3}$$

$$\frac{\partial\eta}{\partial t} = \left.\frac{\partial\phi}{\partial z}\right|_{z=0}. \tag{A.1.4}$$

$$\left.\frac{\partial\phi}{\partial t}\right|_{z=0} = -g\eta. \tag{A.1.5}$$

We assume that the sea surface elevation in this case is given as

$$\eta(x,t) = a\cos(kx - \omega t). \tag{A.1.6}$$

The Laplace Equation (A.1.2) is considered as the elliptic partial differential equation and its solution can be determined by applying the method of separation of variables to yield

$$\phi = \frac{a\omega}{k}\frac{\cosh(k(d+z))}{\sinh(kd)}\sin(kx-\omega t). \tag{A.1.7}$$

The velocity components of the irrotational fluid are given as

$$u = \frac{\partial\phi}{\partial x} = a\omega\frac{\cosh(k(d+z))}{\sinh(kd)}\cos(kx-\omega t), \tag{A.1.8}$$

and

$$w = \frac{\partial\phi}{\partial z} = a\omega\frac{\sinh(k(d+z))}{\sinh(kd)}\cos(kx-\omega t). \tag{A.1.9}$$

To obtain the dispersion relationship, Equations (A.1.6) and (A.1.7) are substituted into Equation (A.1.5) to yield

$$\omega^2 = gk\tanh(kd). \tag{A.1.10}$$

In the derivation of dispersion relationship in Equation (A.1.10), Benassai (2006) was used. The next sections will be the derivation of phase and group speeds.

A.1.1 Phase speed

The propagation of an individual wave is called the phase speed or wave celerity and is denoted by C_p. By definition, C_p is given as

$$C_p = \frac{L}{T}, \tag{A.1.11}$$

where $C_p = \frac{\omega}{k}$. The wavelength is expressed as $L = \frac{gT^2}{2\pi}\tanh(\frac{2\pi d}{L})$, the wave number is $k = \frac{2\pi}{L}$, the angular frequency is $\omega = \frac{2\pi}{T}$ and T is the wave period. The angular frequency and the wave number can be related by the dispersion relationship in Equation (A.1.10). Substituting ω the dispersion relationship and the wavelength L in Equation (A.1.11), we have

$$C_p = \frac{\frac{gT^2}{2\pi}\tanh(kd)}{T} \tag{A.1.12}$$

$$= \frac{g}{\omega}\tanh(kd) \tag{A.1.13}$$

$$= \frac{g}{\sqrt{gk\tanh(kd)}}\tanh(kd) \tag{A.1.14}$$

$$C_p = \sqrt{\frac{g}{k}\tanh(kd)}. \tag{A.1.15}$$

Equation (A.1.12), denotes the phase speed. The equation indicates that the phase speed depends on the wave number (Holthuijsen, 2010). In deep water, if $\tanh(kd) \to 1$ for $kd \to \infty$, the phase speed, C_p, reduces to

$$C_{p_0} = \sqrt{\frac{g}{k_0}}. \tag{A.1.16}$$

In shallow water, if $\tanh(kd) \to kd$ for $kd \to 0$, the phase speed, C_p, reduces to

$$C_p = \sqrt{gd}. \tag{A.1.17}$$

The superscript "0" indicates the deep water region.

A.1.2 Group speed

The speed at which a wave group is propagating is called group speed and is denoted by C_g. It is given by $C_g = nC_p$, where C_p is the phase speed and n is the ratio between phase and group speed. From the dispersion relationship Equation (A.1.10), we differentiate with respect to the wave number, which leads to

$$\begin{aligned} C_g &= \frac{\partial \omega}{\partial k} \\ &= \frac{1}{2}(gk\tanh(kd))^{-1/2}\frac{\partial}{\partial k}(gk\tanh(kd)). \end{aligned}$$

Using the Product Rule, we have C_g as

$$C_g = \frac{1}{2}(gk\tanh(kd))^{-1/2} g\left\{\frac{kd + \sinh(kd)\cosh(kd)}{\cosh^2(kd)}\right\}.$$

Using trigonometry and rationalizing, the simplified group speed is

$$C_g = \frac{1}{2}\frac{\omega}{k}\left\{\frac{2kd}{\sinh(2kd)} + 1\right\}. \tag{A.1.18}$$

This may be rewritten as

$$C_g = nC_p, \tag{A.1.19}$$

where $n = \frac{1}{2}\left\{1 + \frac{2kd}{\sinh(2kd)}\right\}$ and $C_p = \frac{\omega}{k}$ which is the phase speed. The group speed has different values at various locations in the ocean. In deep water $\frac{2kd}{\sinh(2kd)}$ is approximately zero which implies that $n = \frac{1}{2}$, thus the group speed is given as

$$C_{g_0} = \frac{1}{2}C_{p_0}. \tag{A.1.20}$$

Therefore it means that the group speed in deep water is half the phase speed. In shallow water, the group speed is

$$C_{g_s} = \sqrt{gd}. \tag{A.1.21}$$

The parameter n in Equation (A.1.19) is therefore the ratio between the phase speed and group speed, $n = \frac{C_g}{C_p}$. The value of the ratio differs between deep water ($n_0 = \frac{1}{2}$) and shallow water ($n = 1$). According to Holthuijsen (2010), the phase speed is always larger or equal to the group speed.

Appendix B

Measured and NCEP wave data

B.1 Wave height and direction

The Figures in the Appendix show 10 years annual and seasonal wave heights and directions at chosen locations along the South African coastline. The locations are given in Figure 3.6.

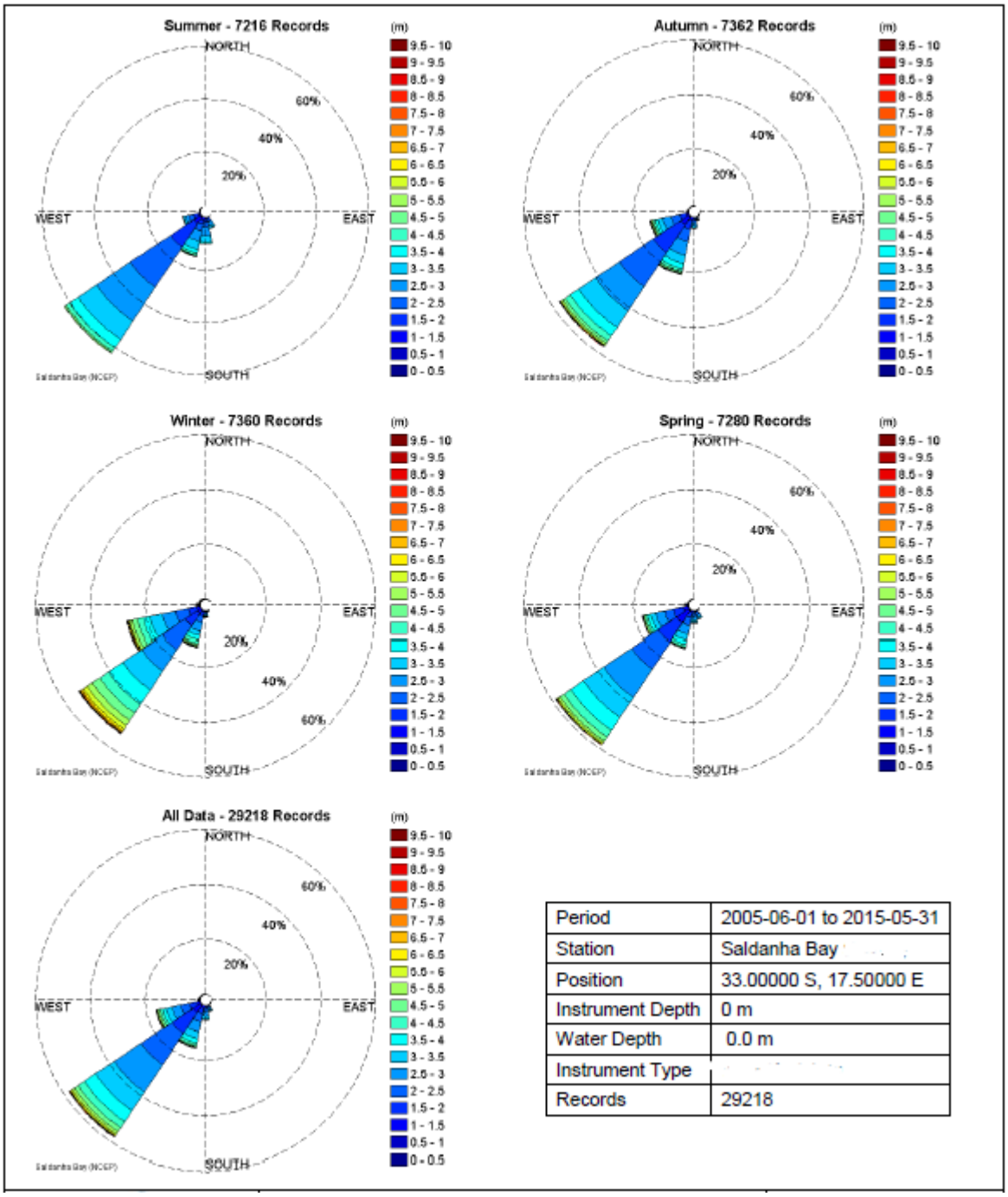

Figure B.1: The NCEP dominant wave directions and heights both seasonal and annually offshore of Saldanha Bay.

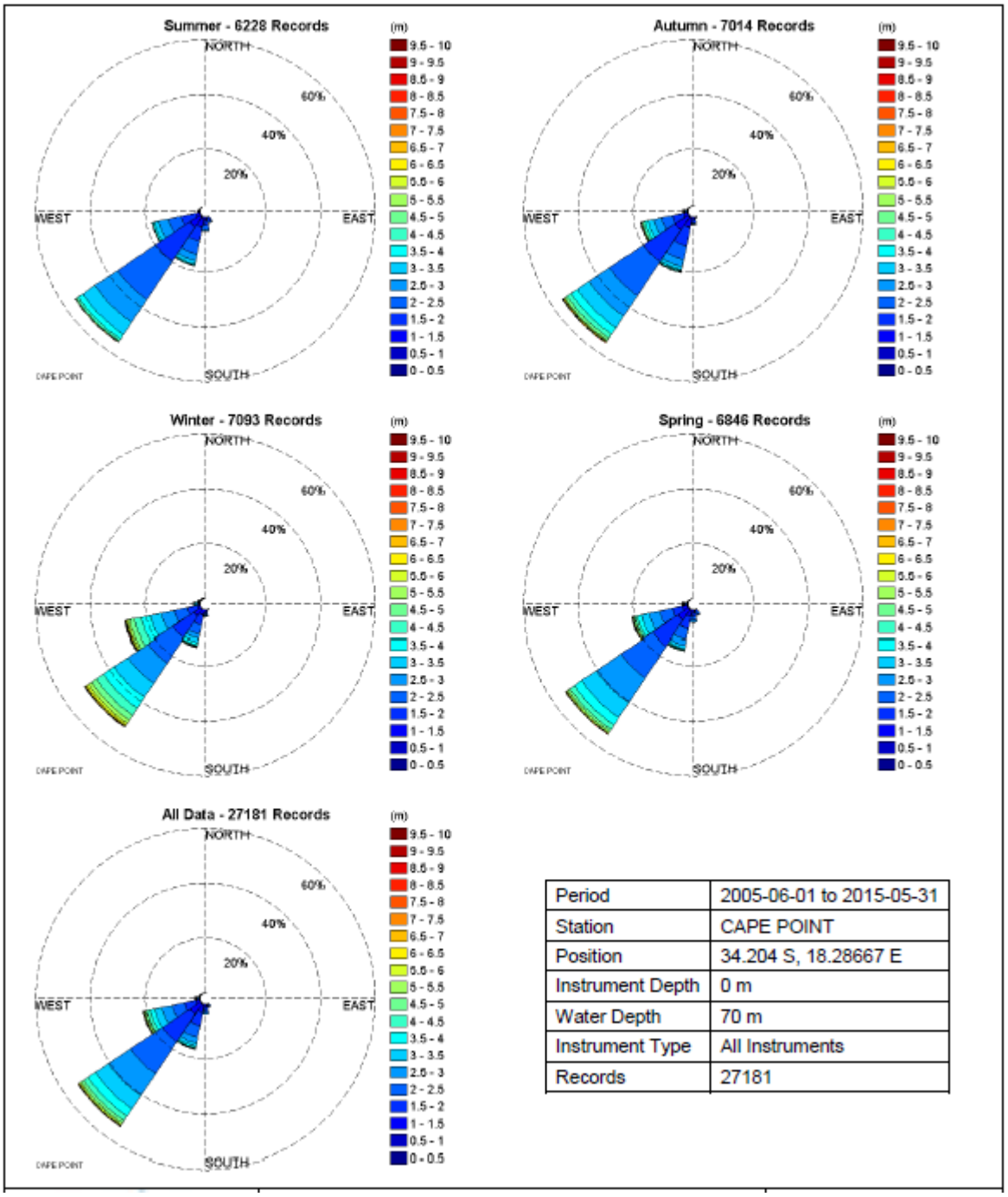

Period	2005-06-01 to 2015-05-31
Station	CAPE POINT
Position	34.204 S, 18.28667 E
Instrument Depth	0 m
Water Depth	70 m
Instrument Type	All Instruments
Records	27181

Figure B.2: The measured dominant wave directions and heights both seasonal and annually at Cape Point.

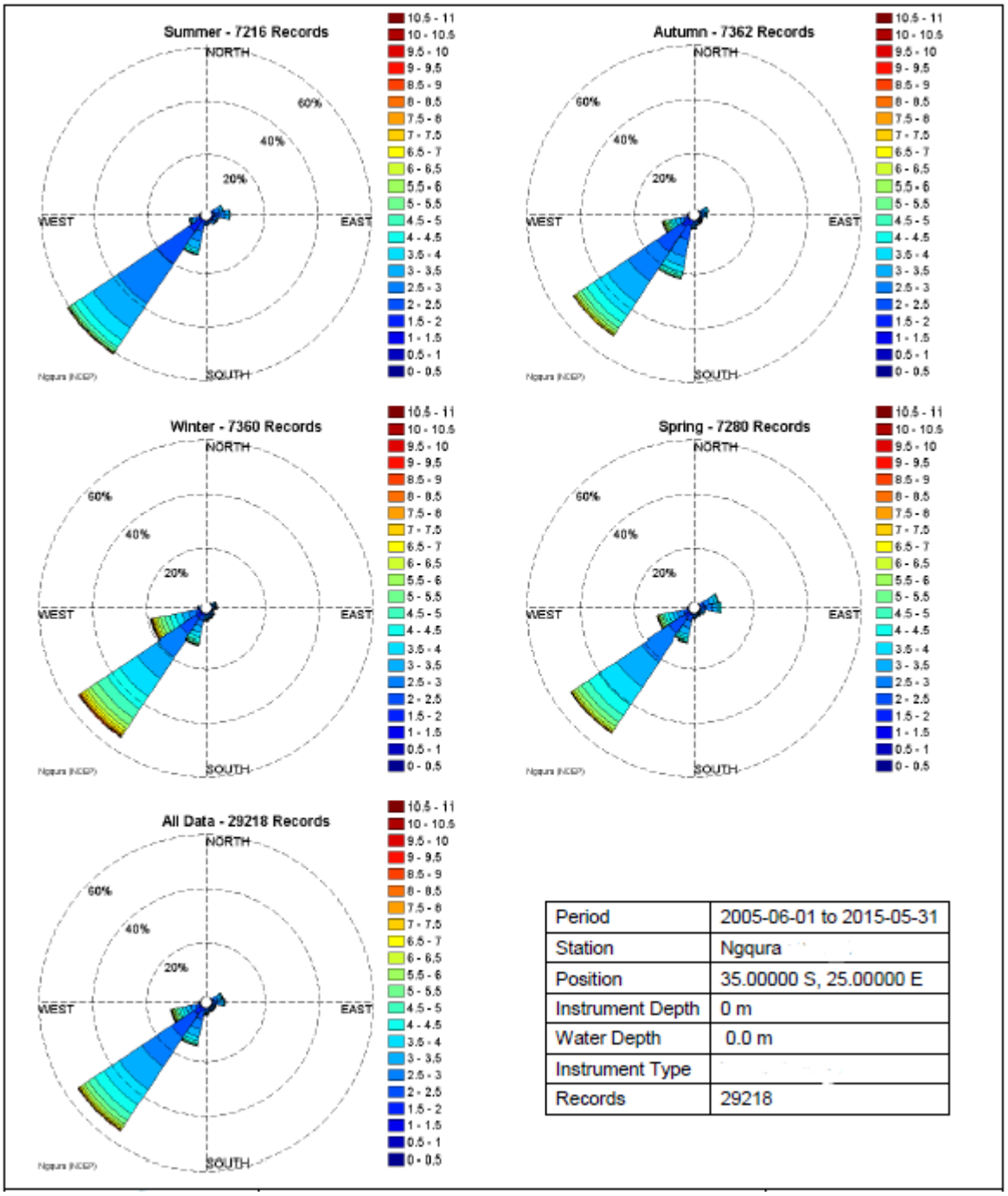

Figure B.3: The NCEP dominant wave directions and heights both seasonal and annually offshore of Nqgura.

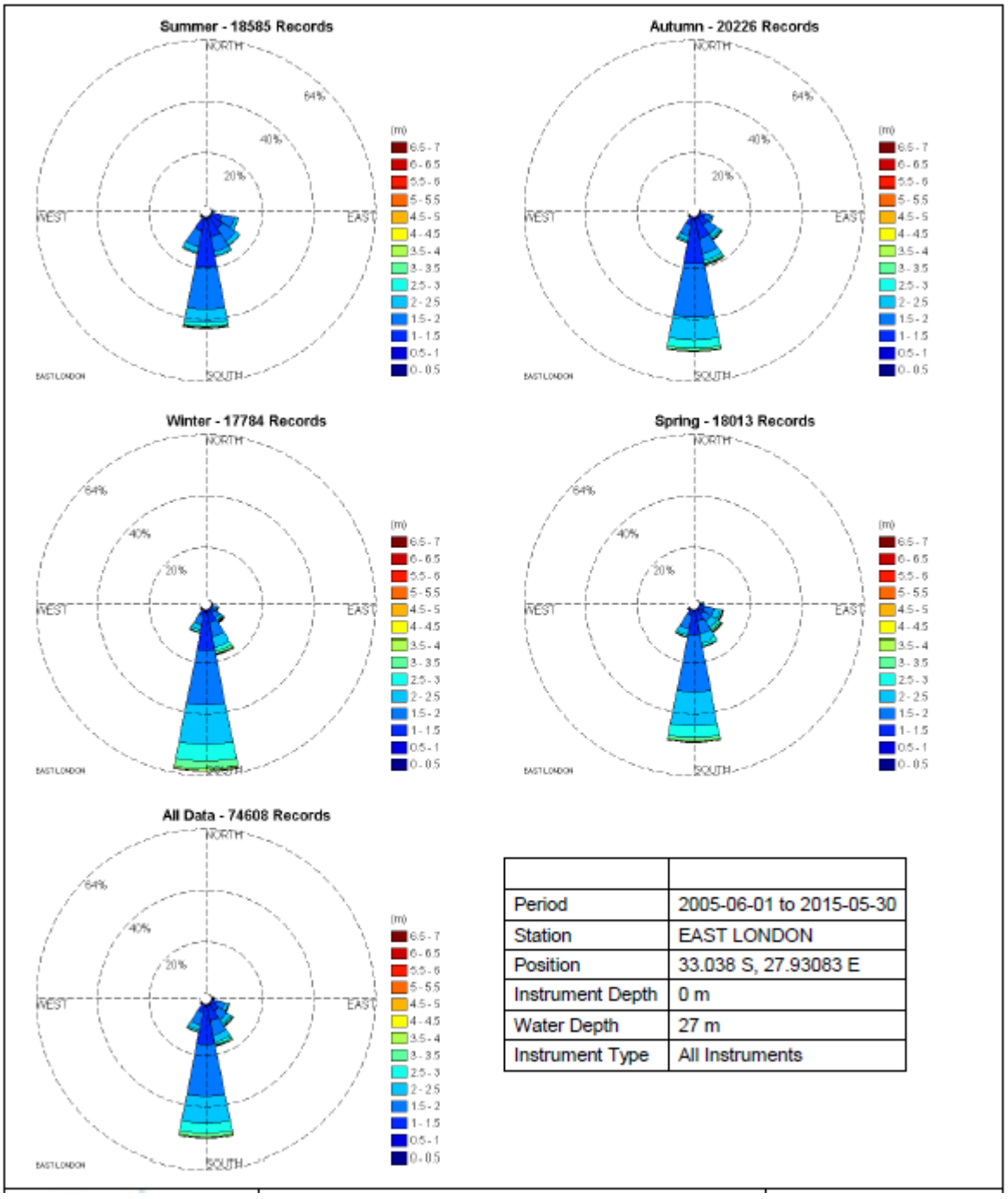

Period	2005-06-01 to 2015-05-30
Station	EAST LONDON
Position	33.038 S, 27.93083 E
Instrument Depth	0 m
Water Depth	27 m
Instrument Type	All Instruments

Figure B.4: The dominant wave directions and heights both seasonal and annually at East London.

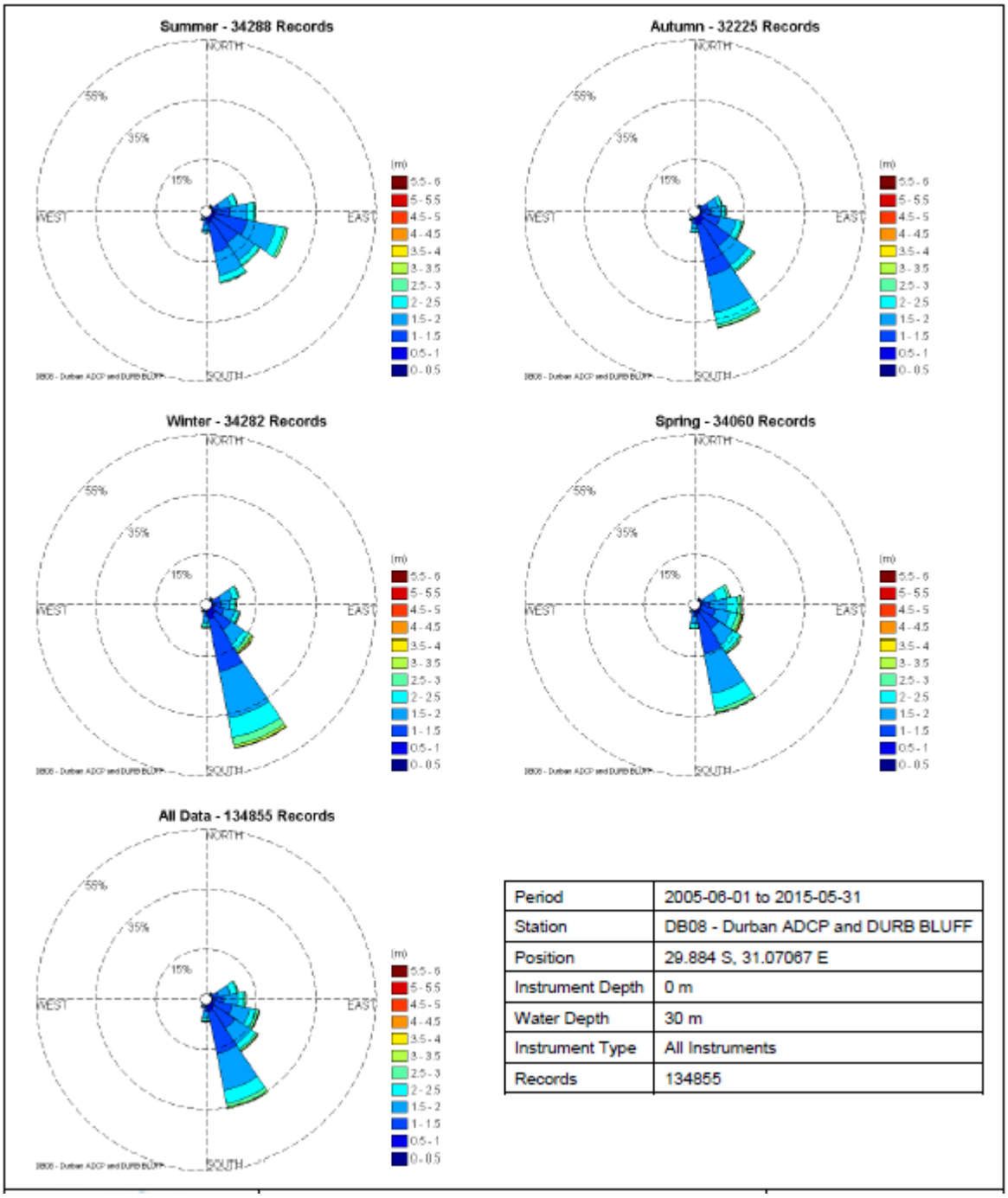

Period	2005-06-01 to 2015-05-31
Station	DB08 - Durban ADCP and DURB BLUFF
Position	29.884 S, 31.07067 E
Instrument Depth	0 m
Water Depth	30 m
Instrument Type	All Instruments
Records	134855

Figure B.5: The measured dominant wave directions and heights both seasonal and annually in Durban.

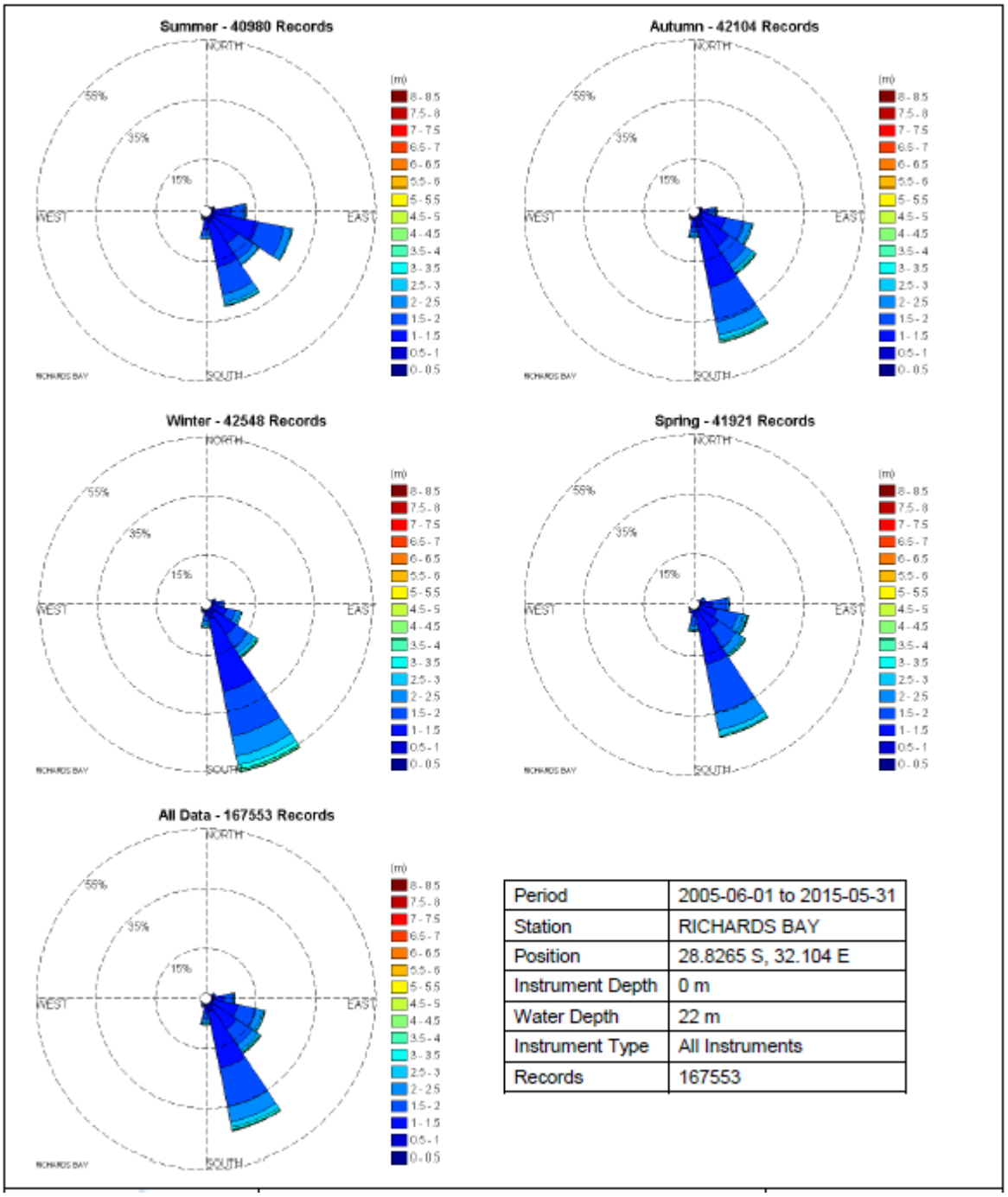

Period	2005-06-01 to 2015-05-31
Station	RICHARDS BAY
Position	28.8265 S, 32.104 E
Instrument Depth	0 m
Water Depth	22 m
Instrument Type	All Instruments
Records	167553

Figure B.6: The measured dominant wave directions and heights both seasonal and annually at Richards Bay.

B.2 Sample measured spectrum data for selected locations

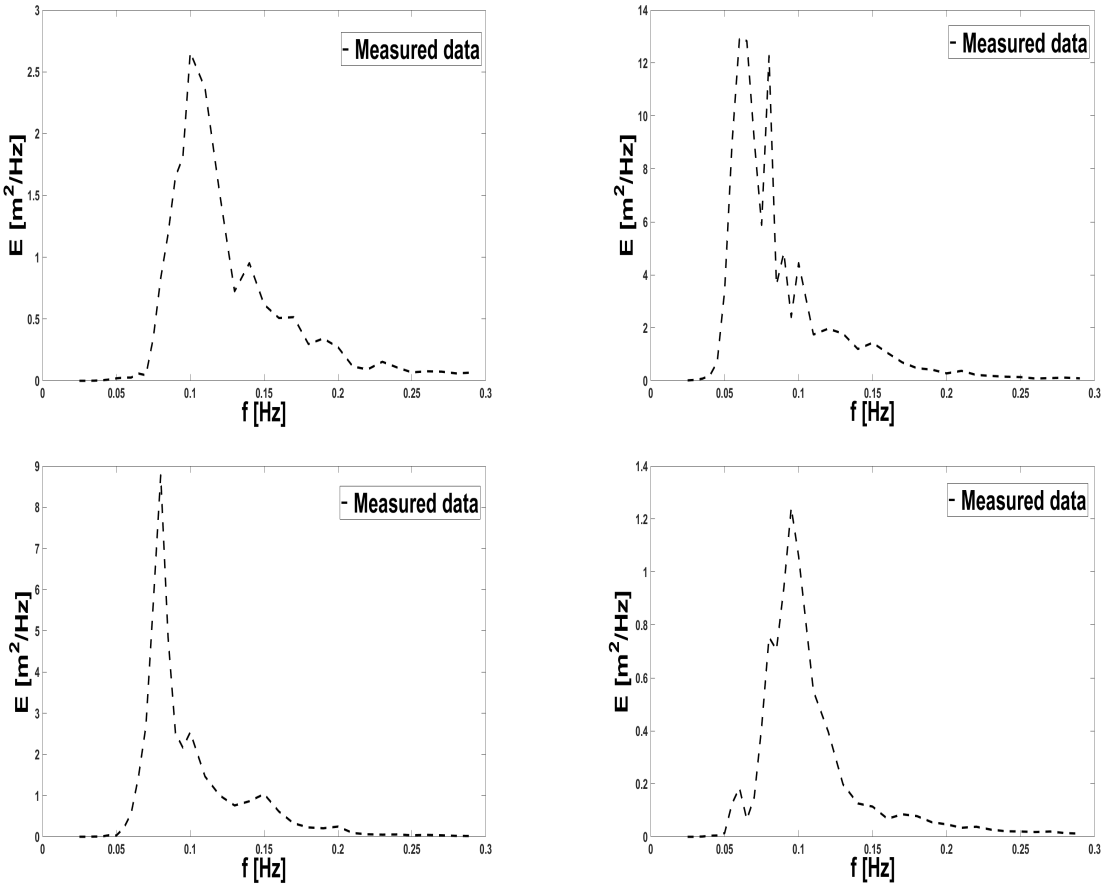

Figure B.7: An example of the measured spectra for Sadanha Bay.

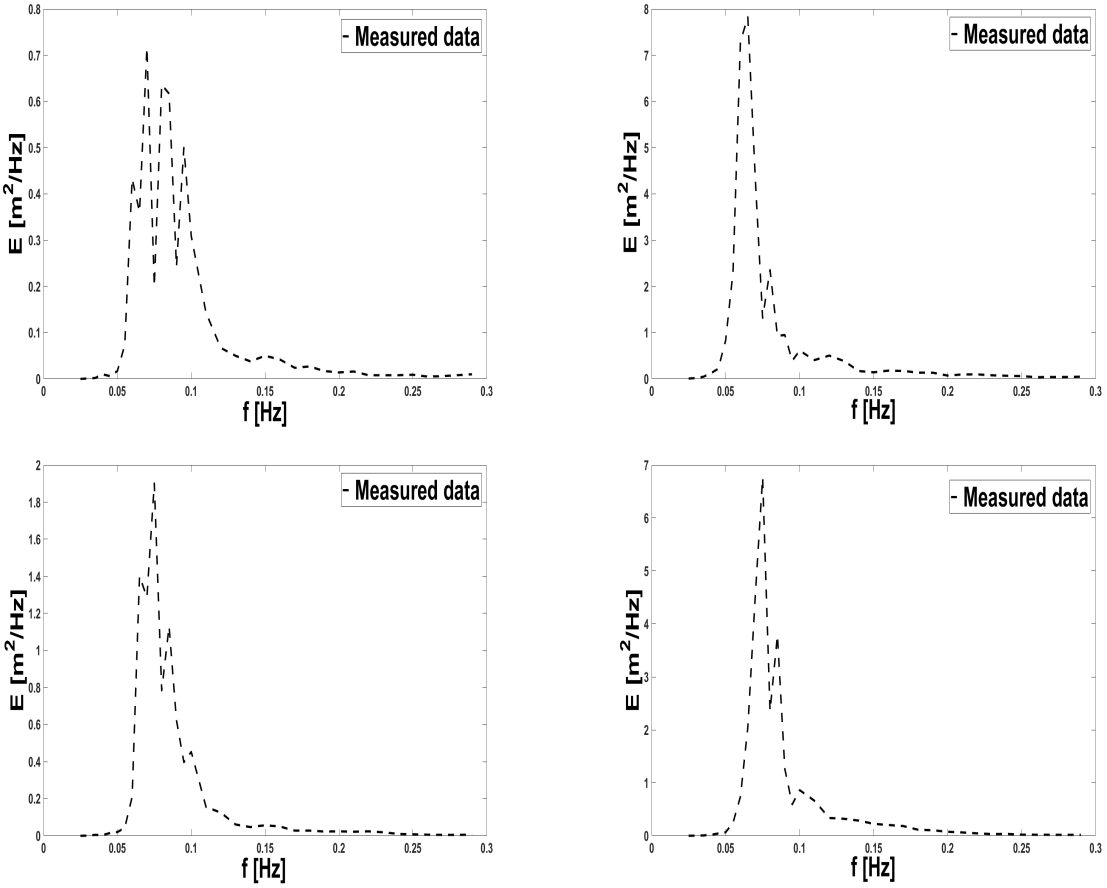

Figure B.8: An example of the measured spectrum for Ngqura.

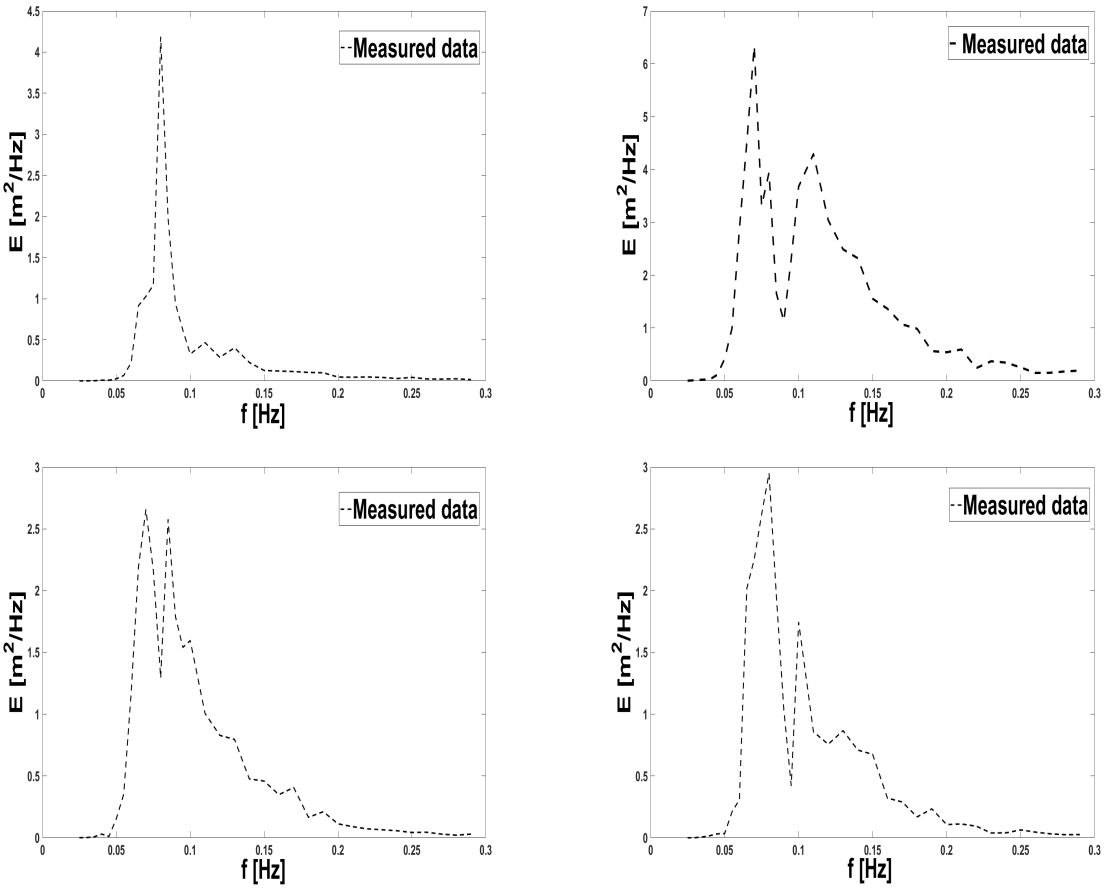

Figure B.9: An example of the measured spectrum for East London.

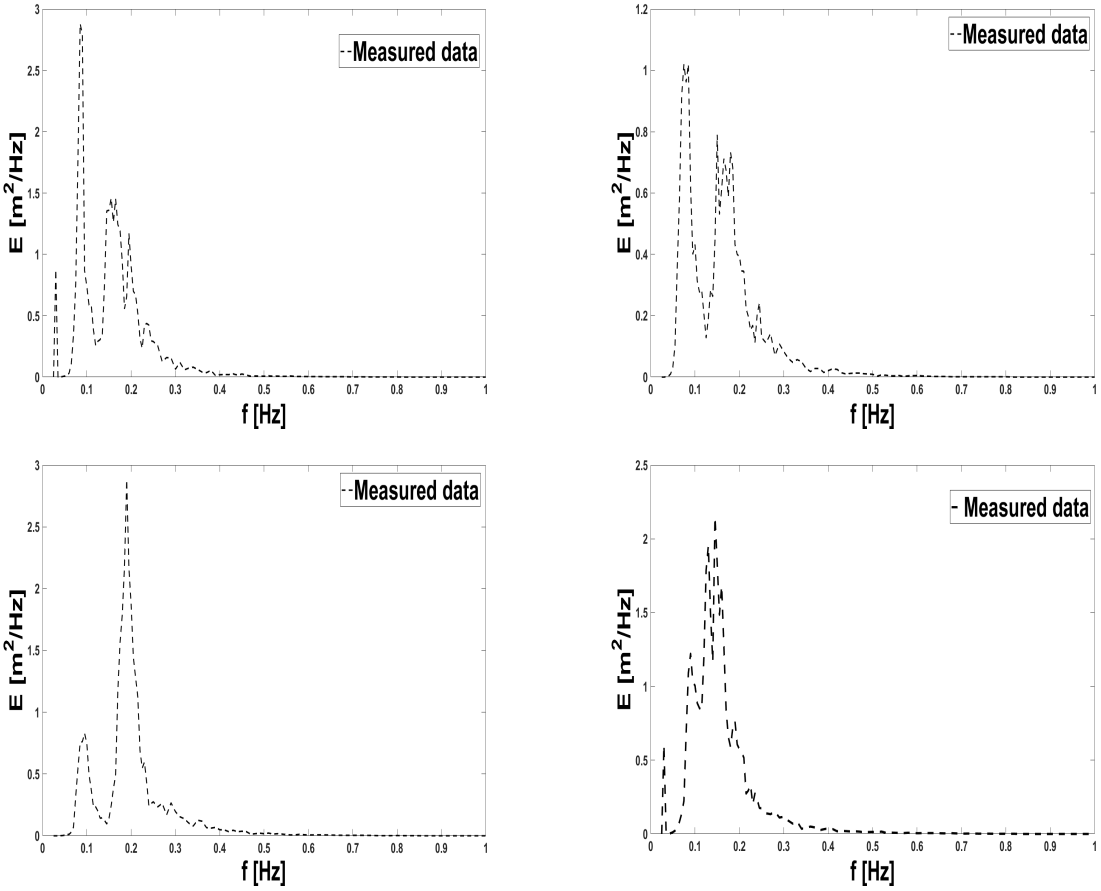

Figure B.10: An example of the measured spectrum for Durban.

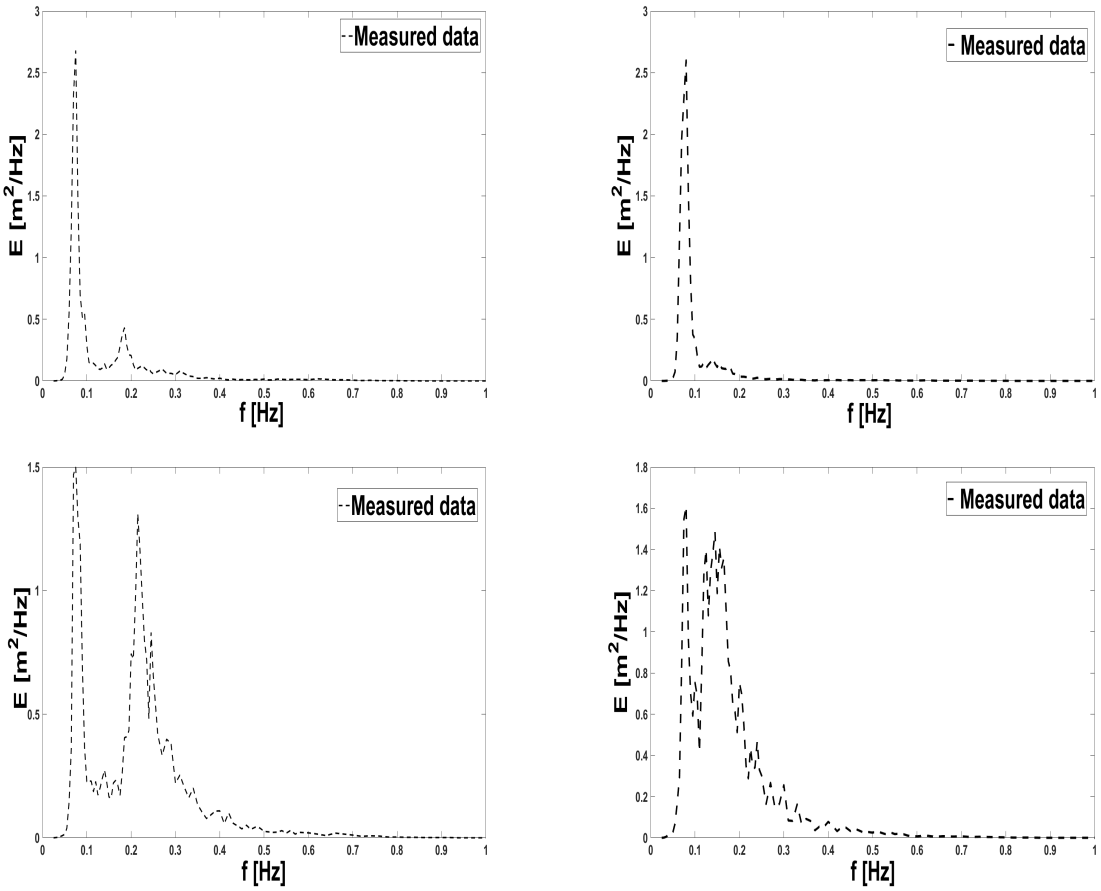

Figure B.11: An example of the measured spectrum for Richards Bay.

Appendix C

The action balance equation source terms and spectral models

C.1 Source terms for the action balance equation

C.1.1 Wave energy dissipation

The steepness dependent coefficient which was estimated by Battjes and Janssen (1978) in fully developed, sea conditions is given as

$$\Gamma_{KJ} = C_{ds}\left((1-\delta)+\delta\frac{k}{\tilde{k}}\right)\left(\frac{\tilde{s}}{\tilde{s}_{PM}}\right)^{P_{ds}}, \tag{C.1.1}$$

where C_{ds}, δ and P_{ds} are tunable coefficients. The parameter $\tilde{s}$ is the overall wave steepness which is defined as $\tilde{s} = \tilde{k}\sqrt{E_{tot}}$ and $\tilde{s}_{PM} = \sqrt{3.0\times10^{-3}}$ is the steepness value of Pierson and Moskowitz (1964). According to Holthuijsen (2010), the value of P_{ds} and C_{ds} was introduced by Komen *et al.* (1984) in idealised deep water conditions.

C.1.2 Depth-induced breaking

The total rate of energy dissipation D_{tot}, is taken from Battjes and Janssen (1978) and is expressed as

$$D_{tot} = -\frac{1}{4}\alpha_{BJ}Q_b\left(\frac{\tilde{\sigma}}{2\pi}\right)H_{max}^2. \tag{C.1.2}$$

The value of $\alpha_{BJ} = 1$ in SWAN, $\tilde{\sigma}$ is the mean frequency and Q_b is the fraction of the wave breaking and is defined by means of the Rayleigh distribution which is given as

$$\frac{1-Q_b}{lnQ_b} = -8\frac{E_{tot}}{H_{max}^2}. \tag{C.1.3}$$

H_{max} is the maximum wave height possible at the given depth and can be determined by $H_{max} = \gamma_{BJ} d$. The coefficient γ_{BJ} is defined as the breaking parameter and d is the total water depth (Battjes and Janssen, 1978).

C.2 Spectral models

C.2.1 Bretschneider spectrum

This spectrum is the two-parameter model which includes the significant wave height Hs and modal or peak frequency ω_m and is expressed as

$$E_B(f) = \frac{1.25}{4}\frac{\omega_m^2}{\omega^5}H_s^2 \exp\left\{-1.25\left(\frac{\omega_m}{\omega}\right)^4\right\}. \tag{C.2.1}$$

Equation (C.2.1) is the modified Pierson-Moskowitz spectrum which is often used to model waves that are narrow banded and follow the Rayleigh distribution. The adjustment coefficients within the model were set by Mitsuyasu and the spectrum is sometimes refereed to as *Bretschneider-Mitsuyasu spectrum* (Goda, 2010).

C.2.2 Ochi-Hubble spectrum

The Ochi-Hubble spectral model was derived to model the mixed sea states, the swell component (low-frequency dominated) and the wind sea component (high-frequency dominated). The model explains which wave system dominates in a specific area of interest. It is a six-parameter formulation which is characterised by the significant wave height, modal (peak) frequency and shape parameter. This model is expressed as

$$E_{OB}(f) = \frac{1}{4}\sum_{j=1}^{2}\frac{\left(\frac{4\lambda_j+1}{4}\omega_{m_j}^4\right)^{\lambda_j}}{\Gamma(\lambda_j)}\frac{H_{s_j}^2}{\omega^{4\lambda_j+1}}\exp\left\{-\frac{4\lambda_j+1}{4}\left(\frac{\omega_{m_j}}{\omega}\right)^4\right\}, \tag{C.2.2}$$

where λ_j is the shape parameter which controls the sharpness of the peak of each wave system. If $\lambda_j = 1$, Equation (C.2.2) is equivalent to Equation (C.2.1) and $\Gamma(\lambda_j)$ is the Gamma function. The parameters H_{s_1}, ω_{m_1} and λ_1 are significant wave height, modal (peak) frequency and shape parameter for the lower frequency, respectively and H_{s_2}, ω_{m_2} and λ_2 are for the higher-frequency component (Ochi and Hubble, 1977).

C.2.3 Torsethaugen spectrum

The Torsethaugen spectrum is similar to the Ochi-Hubble model given by Equation (C.2.2). It is a two-peak spectrum which was developed for one location at Statfjord in the Northern North Sea. The model splits the wave system into two components, swell and wind sea using the modified JONSWAP spectral model for both spectral peaks.

C.2.4 TMA spectrum

The TMA spectral model (TEXEL, MARSEN and ARSLOE experiments) is a modified JONSWAP model that is applied in wind-generated seas of finite water depth (Ochi and

Hubble, 1977). As the waves propagate from deep to shallow water, the spectral form or shape changes and the TMA spectrum was developed to account for the changes during this propagation. It was named after three measured data sets that were used for its development. The model is given as

$$E_{TMA}(f) = S(f)_{JP}\Phi(f,d), \tag{C.2.3}$$

where Φ is the shape parameter and is expressed as

$$\Phi(f,d) = \left\{ \frac{[k(f,\ d)]^{-3}.\frac{\partial k(f,d)}{\partial f}}{[k(f,\infty)]^{-3}.\frac{\partial k(f,\infty)}{\partial f}} \right\}, \tag{C.2.4}$$

where k is the non-dimensional wave number and $E(f)_{JP}$ represents the JONSWAP spectrum. The model in Equation (C.2.3) is the modified JONSWAP spectrum from Equation (4.1.4) that is multiplied by a depth and frequency dependent function. The model is well explained by Young and Verhagen (1996).

Appendix D

The model results

D.1 Significant wave height with and without the wave farm

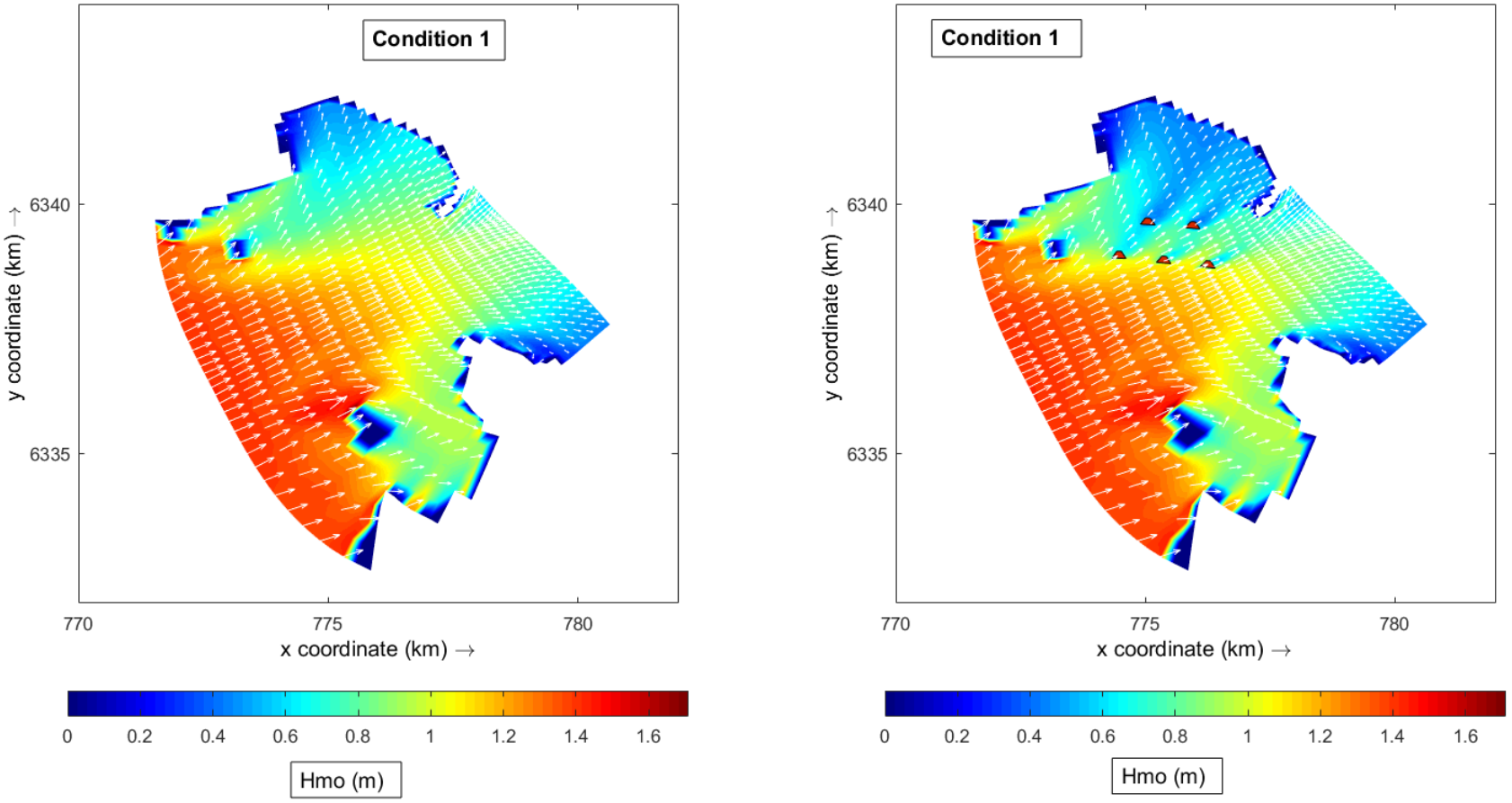

Figure D.1: The significant wave height without (left) and with (right) the wave farm, $H_{mo} = 1.5$ m, $T_p = 10$ s and $\theta = 247.5°$.

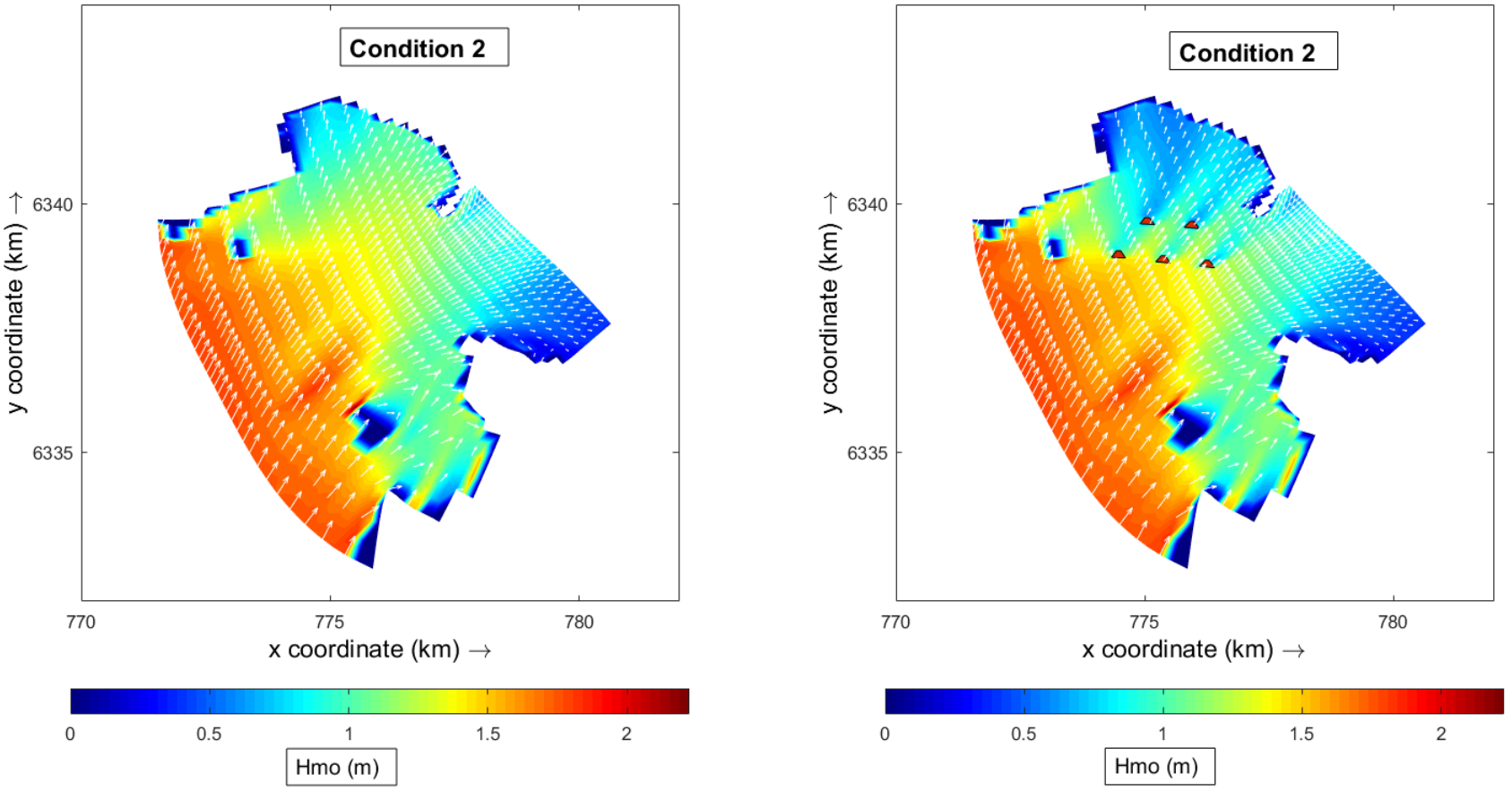

Figure D.2: The significant wave height without (left) and with (right) the wave farm, $H_{mo} = 2.0$ m, $T_p = 11$ s and $\theta = 202.5°$.

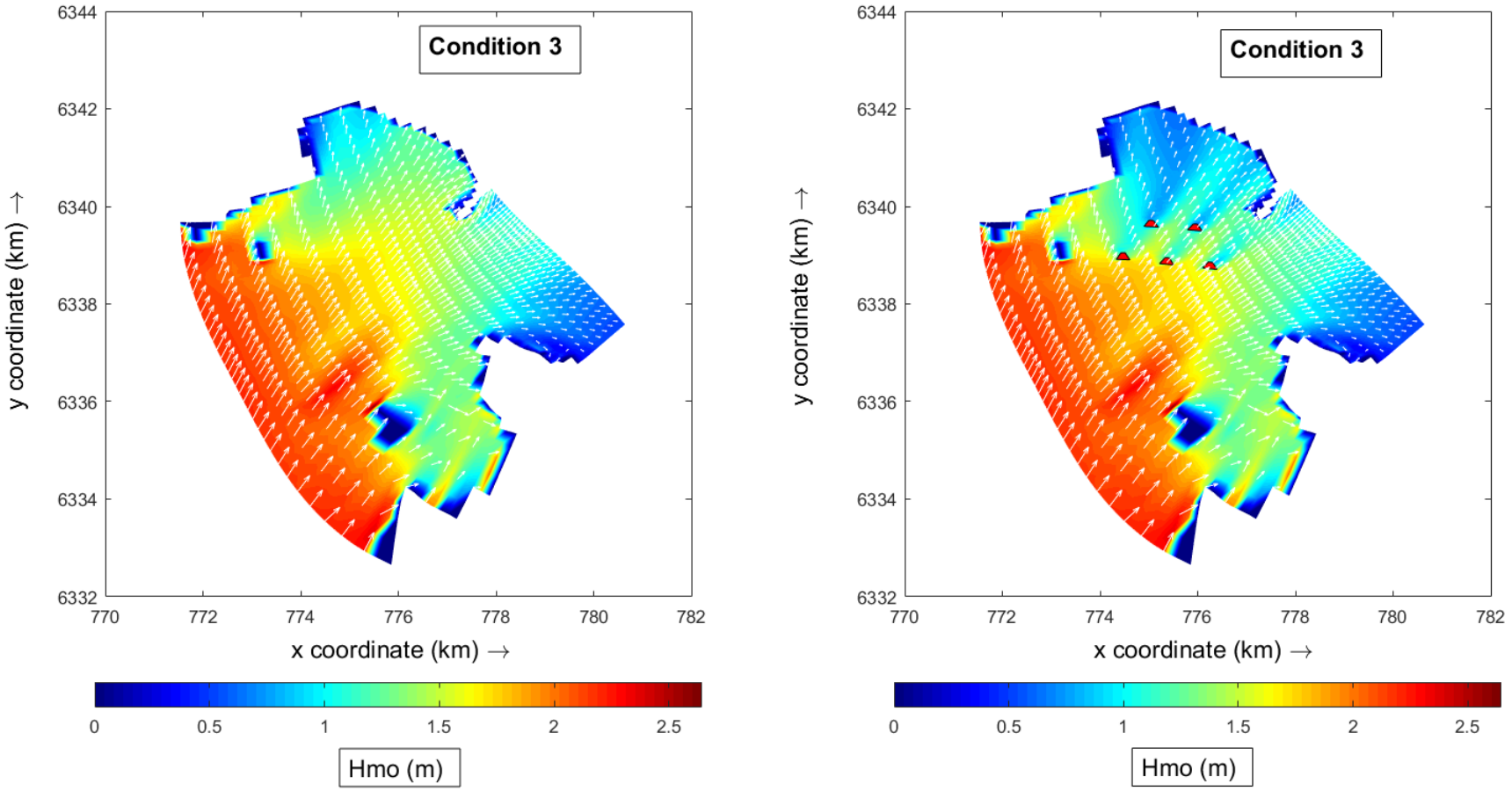

Figure D.3: The significant wave height without (left) and with (right) the wave farm, $H_{mo} = 2.5$ m, $T_p = 12$ s and $\theta = 202.5°$.

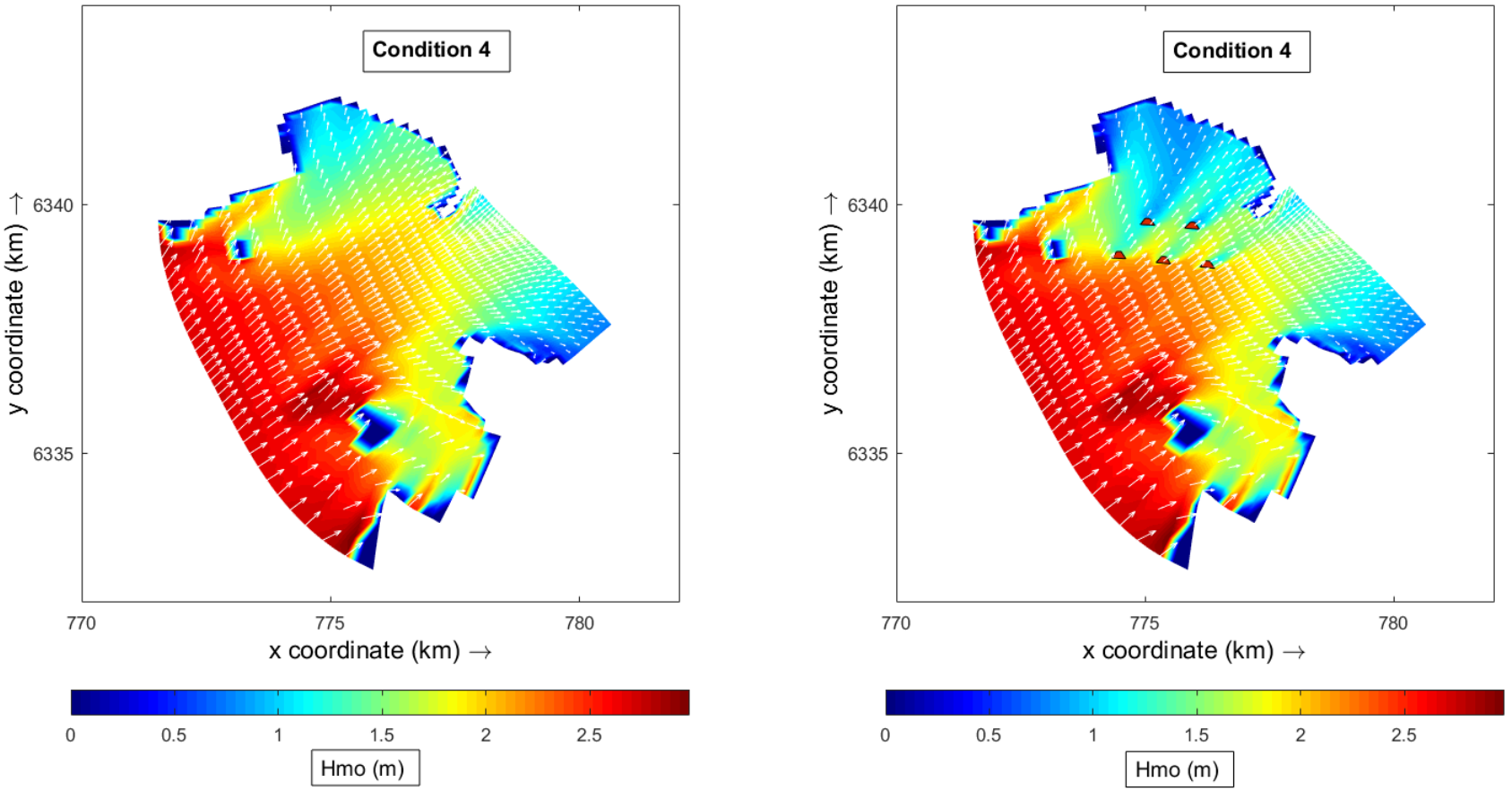

Figure D.4: The significant wave height without (left) and with (right) the wave farm, $H_{mo} = 3.0$ m, $T_p = 12$ s and $\theta = 225.0°$.

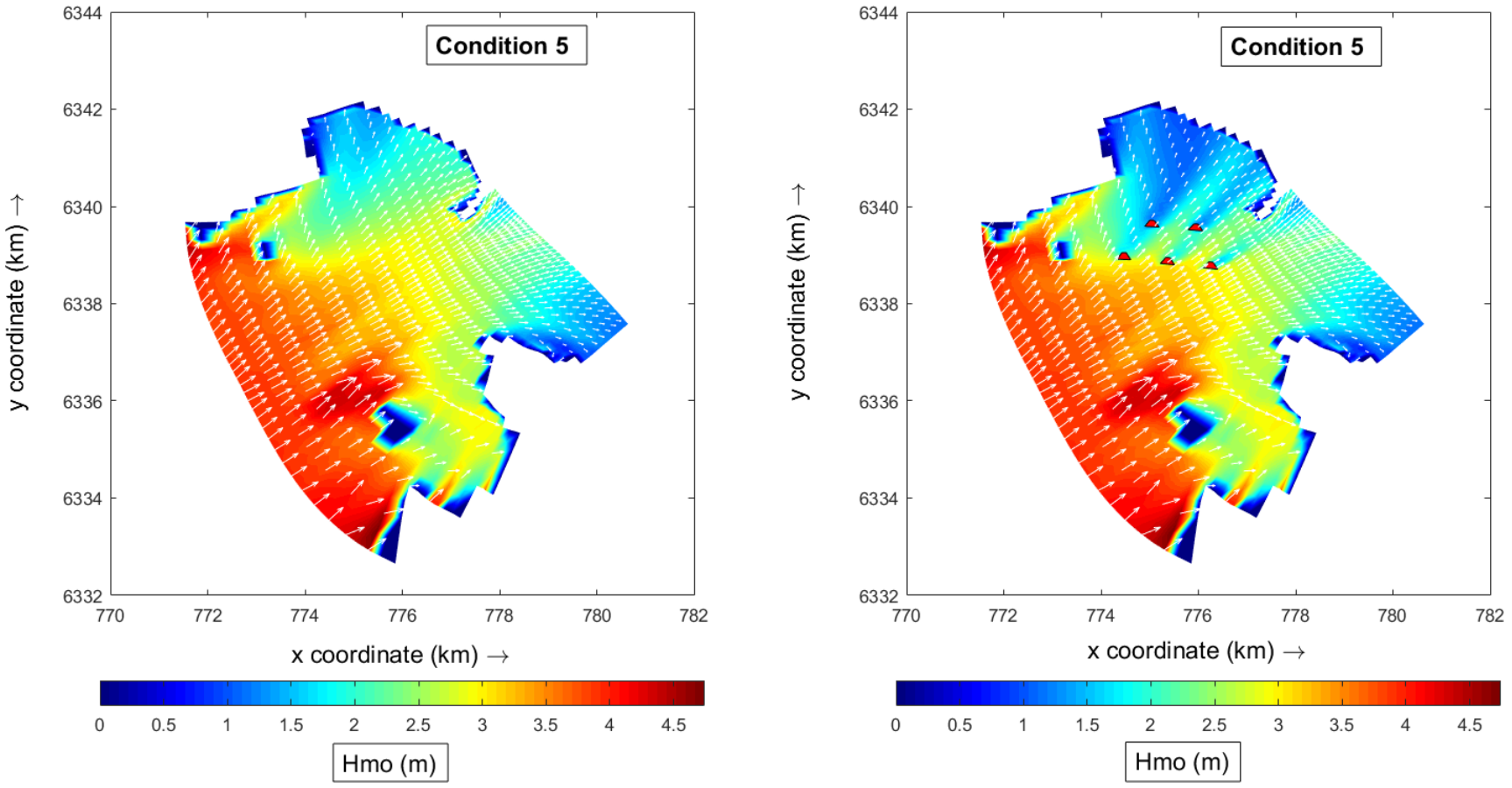

Figure D.5: The significant wave height without (left) and with (right) the wave farm, $H_{mo} = 4.5$ m, $T_p = 14$ s and $\theta = 225.0°$.

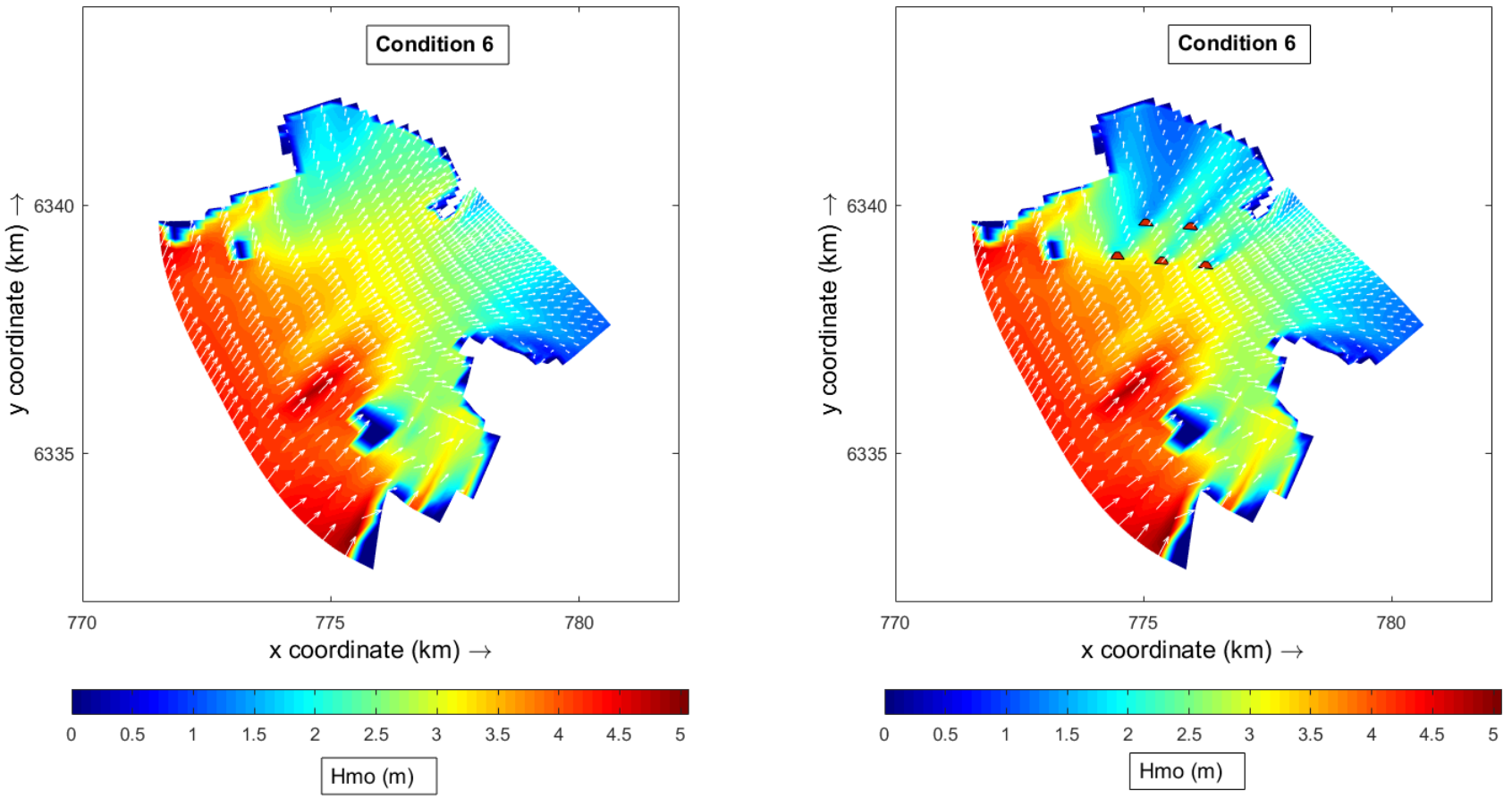

Figure D.6: The significant wave height without (left) and with (right) the wave farm, $H_{mo} = 5.0$ m, $T_p = 14$ s and $\theta = 202.5°$.

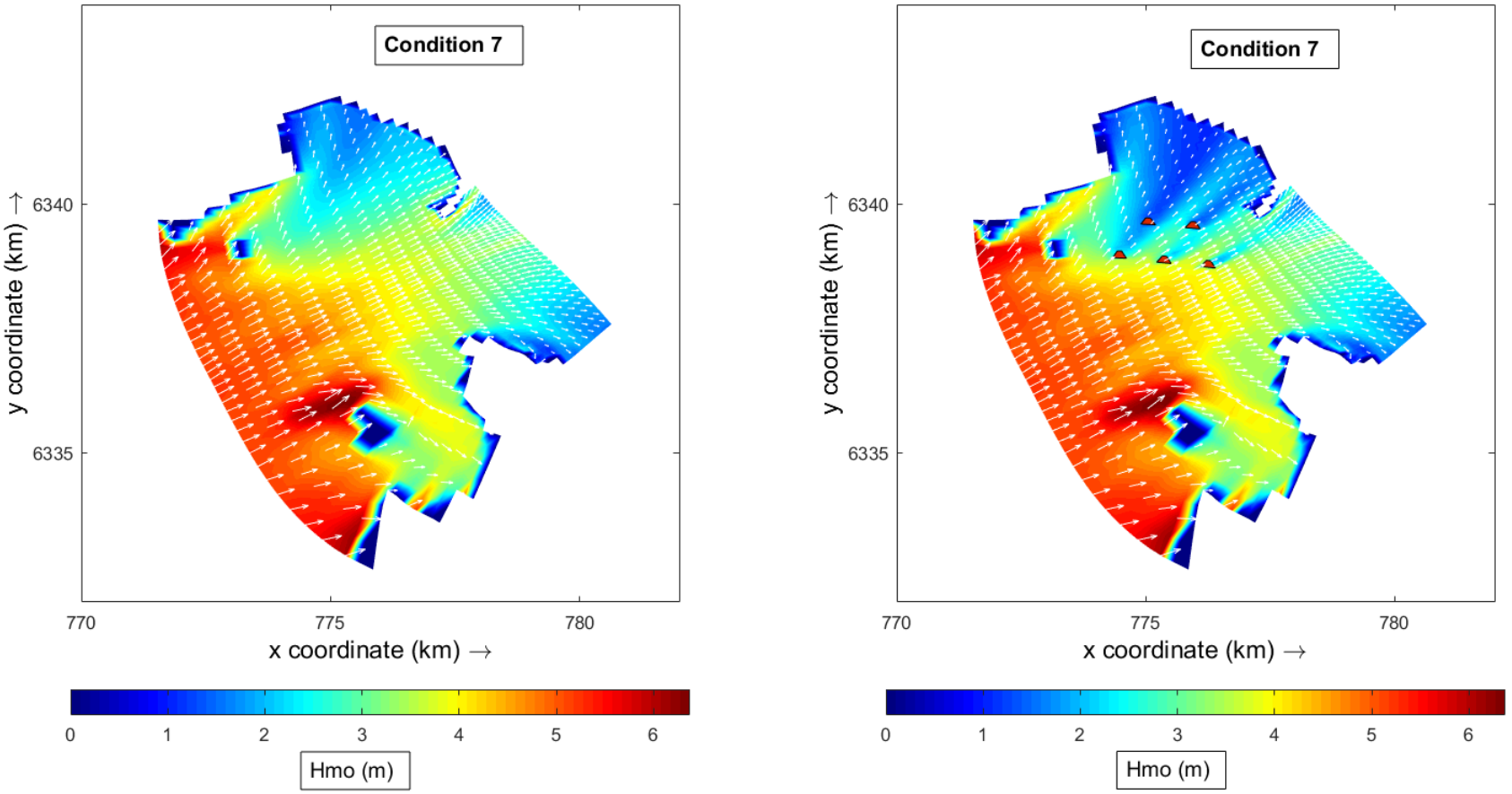

Figure D.7: The significant wave height without (left) and with (right) the wave farm, $H_{mo} = 6.0$ m, $T_p = 15$ s and $\theta = 247.5°$.

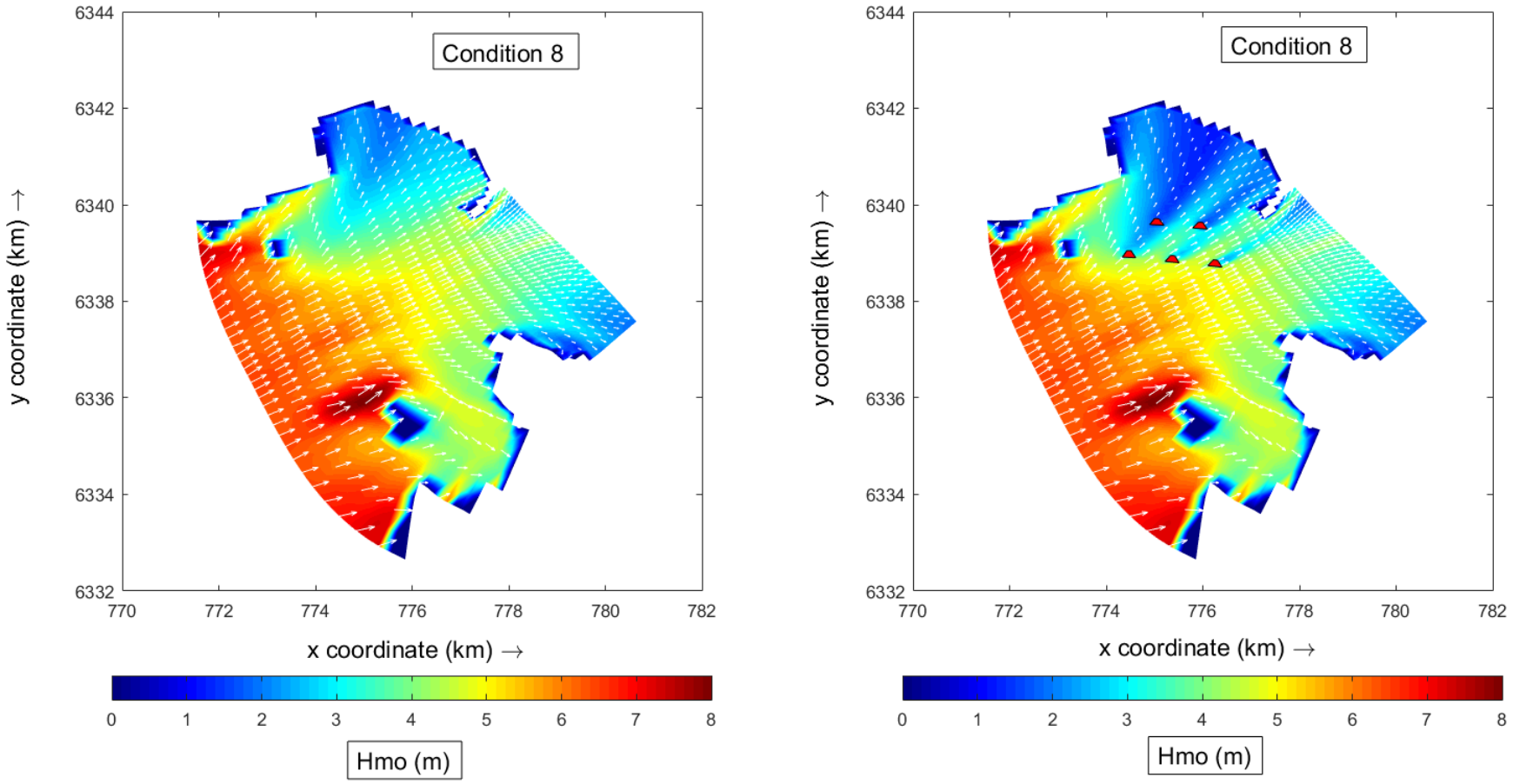

Figure D.8: The significant wave height without (left) and with (right) the wave farm, $H_{mo} = 7.5$ m, $T_p = 16$ s and $\theta = 247.5°$.

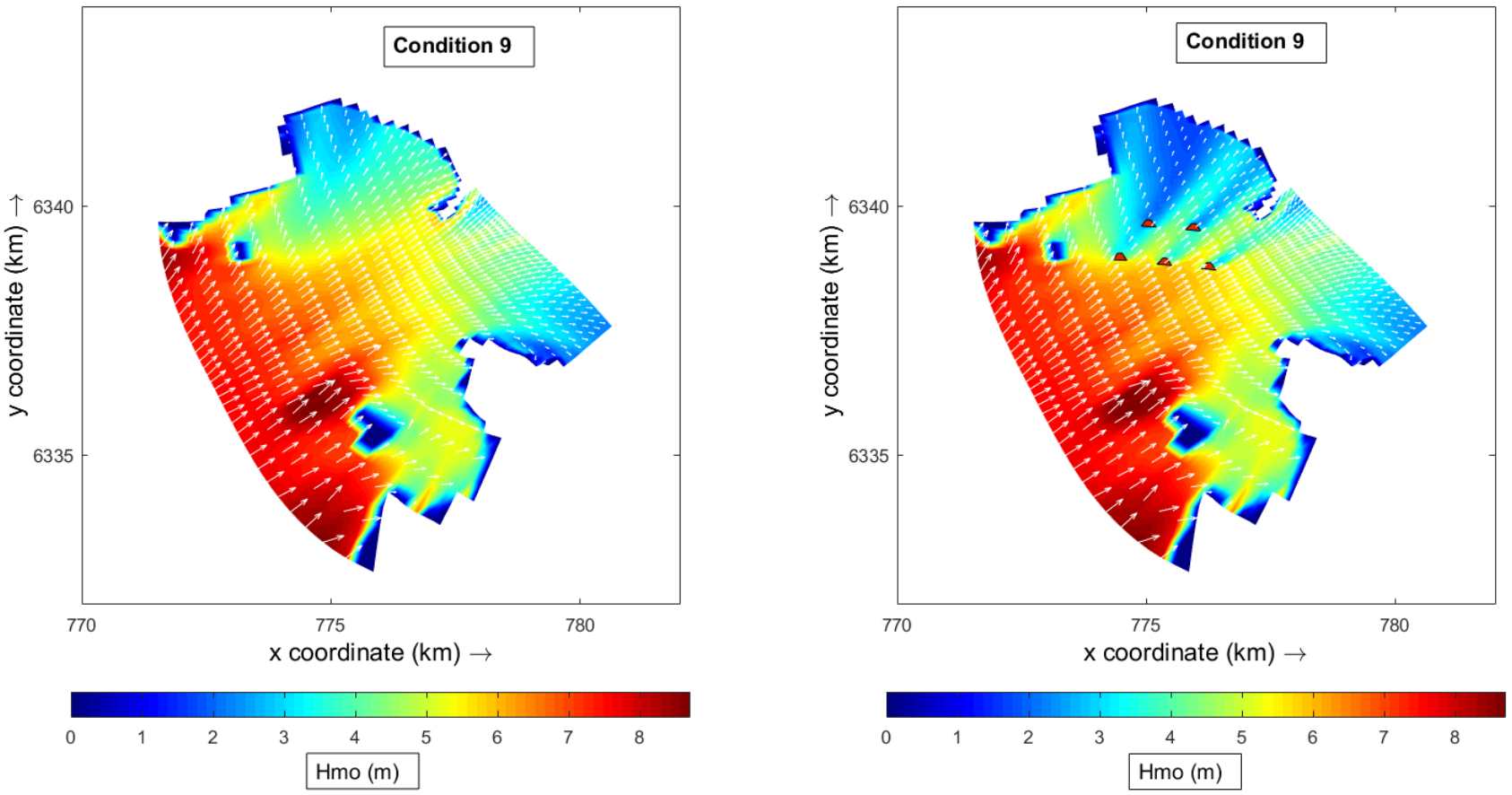

Figure D.9: The significant wave height without (left) and with (right) the wave farm, $H_{mo} = 9.0$ m, $T_p = 16$ s and $\theta = 225.0°$.

D.2 Significant wave height difference for all the conditions

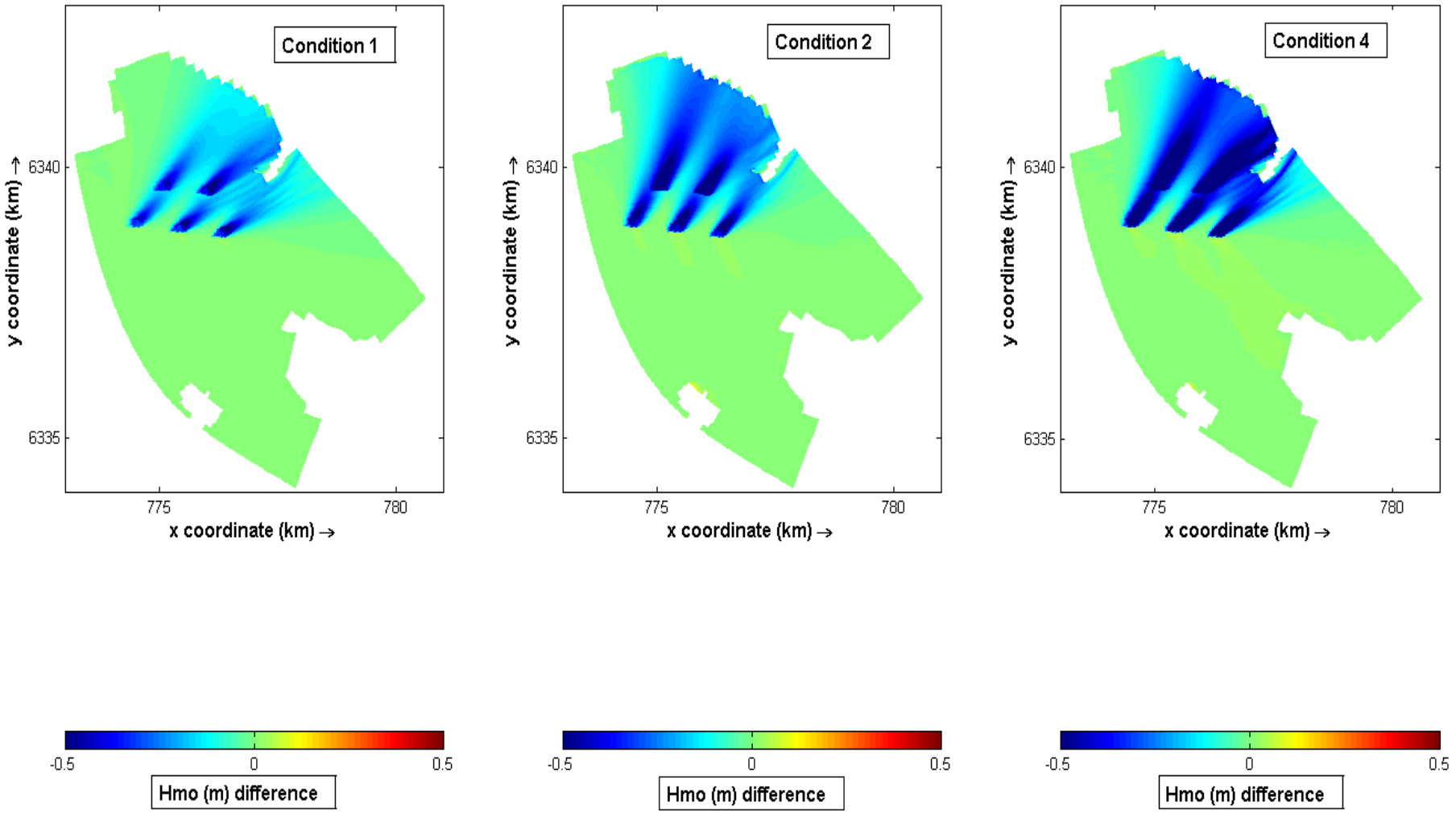

Figure D.10: The difference in significant wave height induced by the wave farm for conditions 1, 2 and 4.

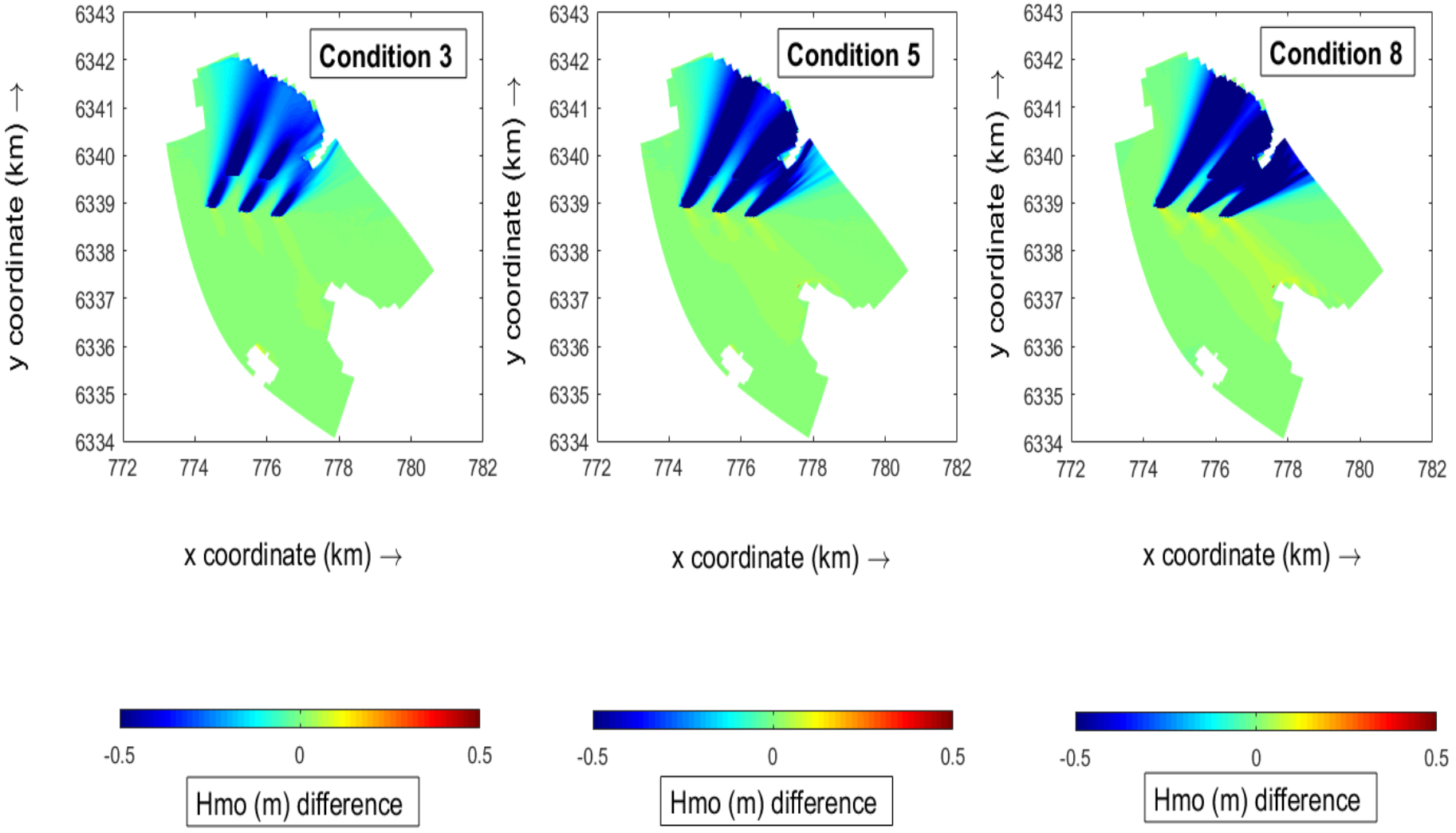

Figure D.11: The difference in significant wave height induced by the wave farm for conditions 3, 5 and 8.

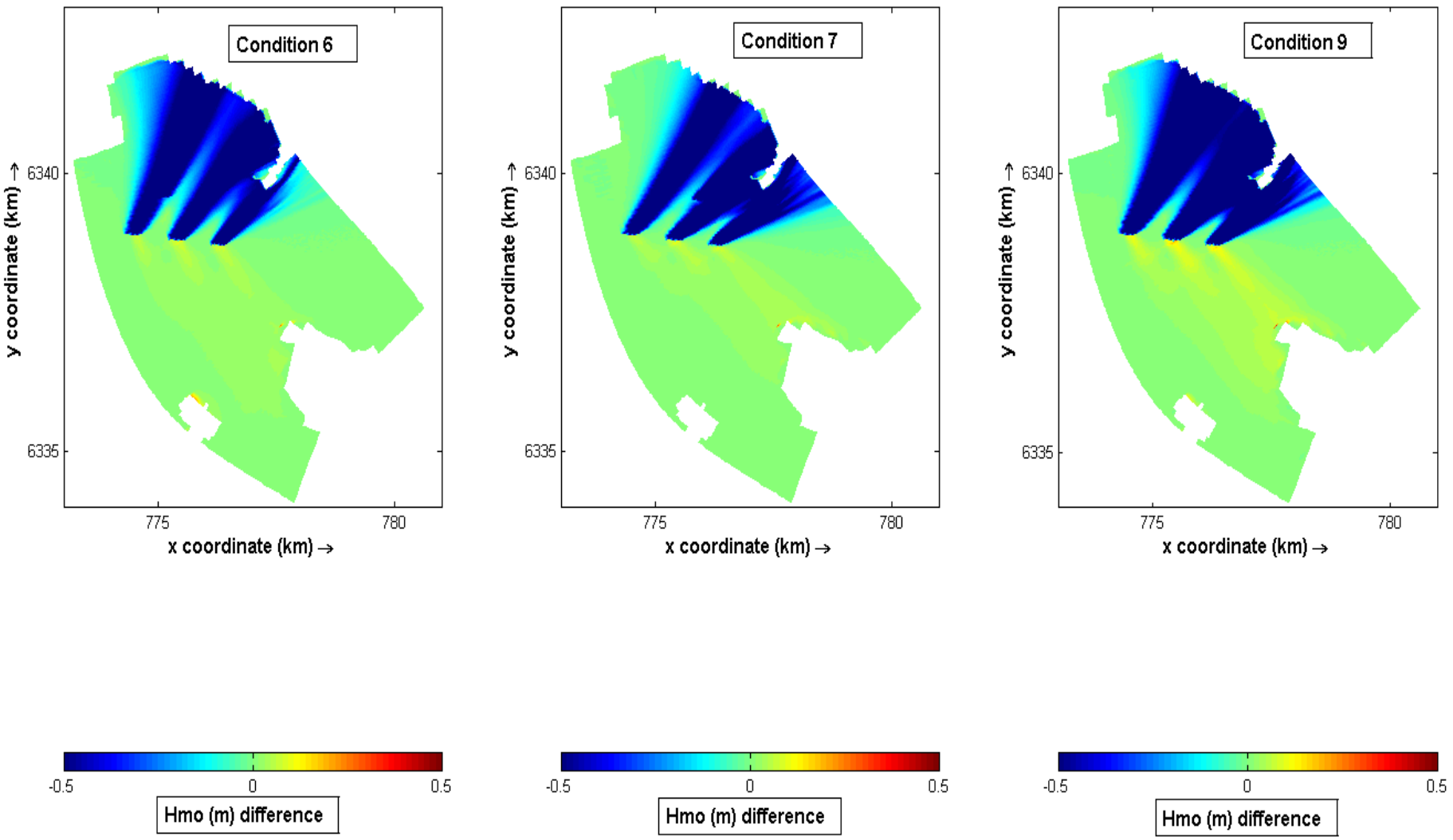

Figure D.12: The difference in significant wave height induced by the wave farm for conditions 6, 7 and 9.

D.3 Wave energy spectra for output location 5 and 8

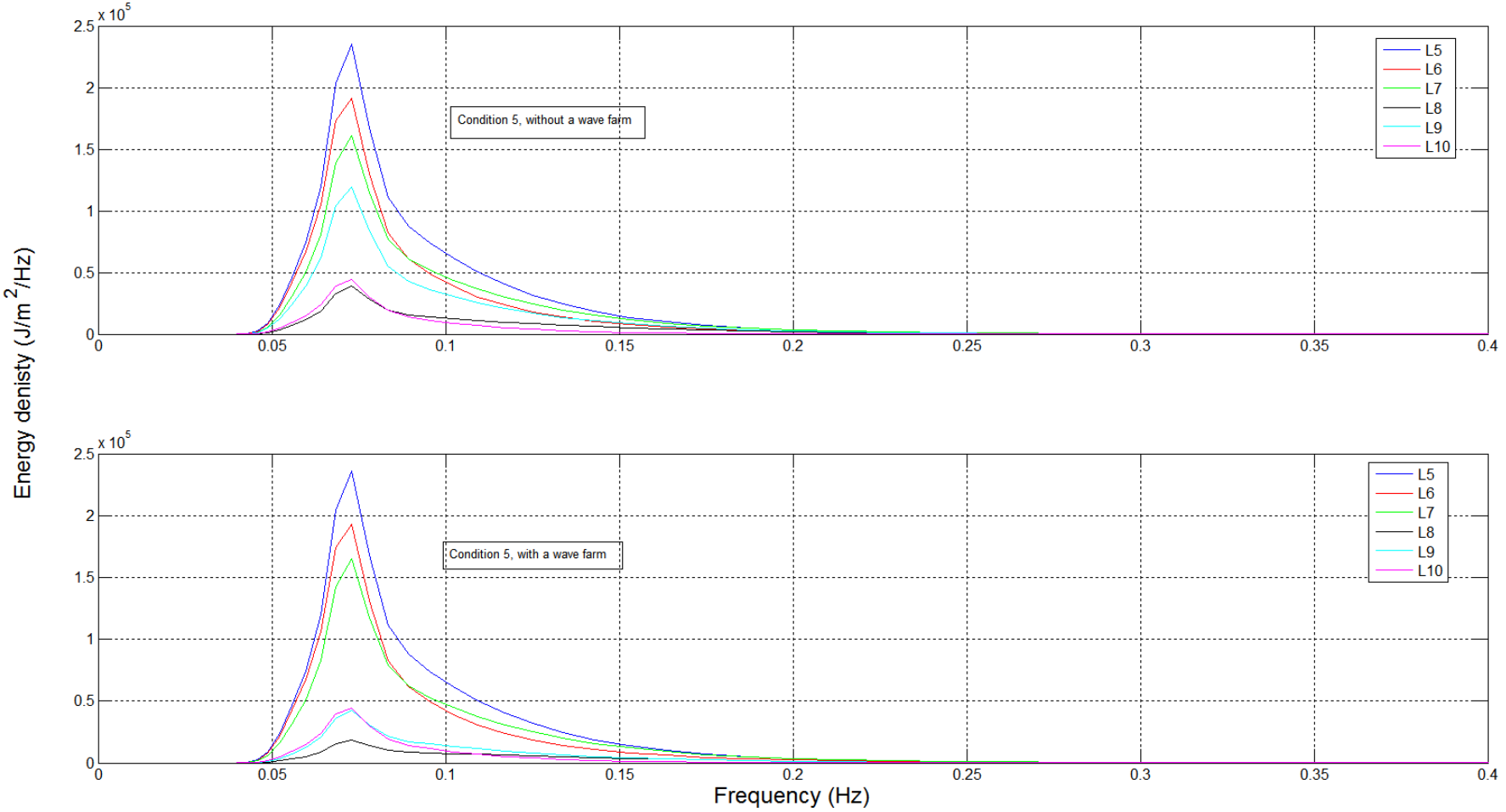

Figure D.13: Wave energy spectrum before and after the wave farm of condition 5.

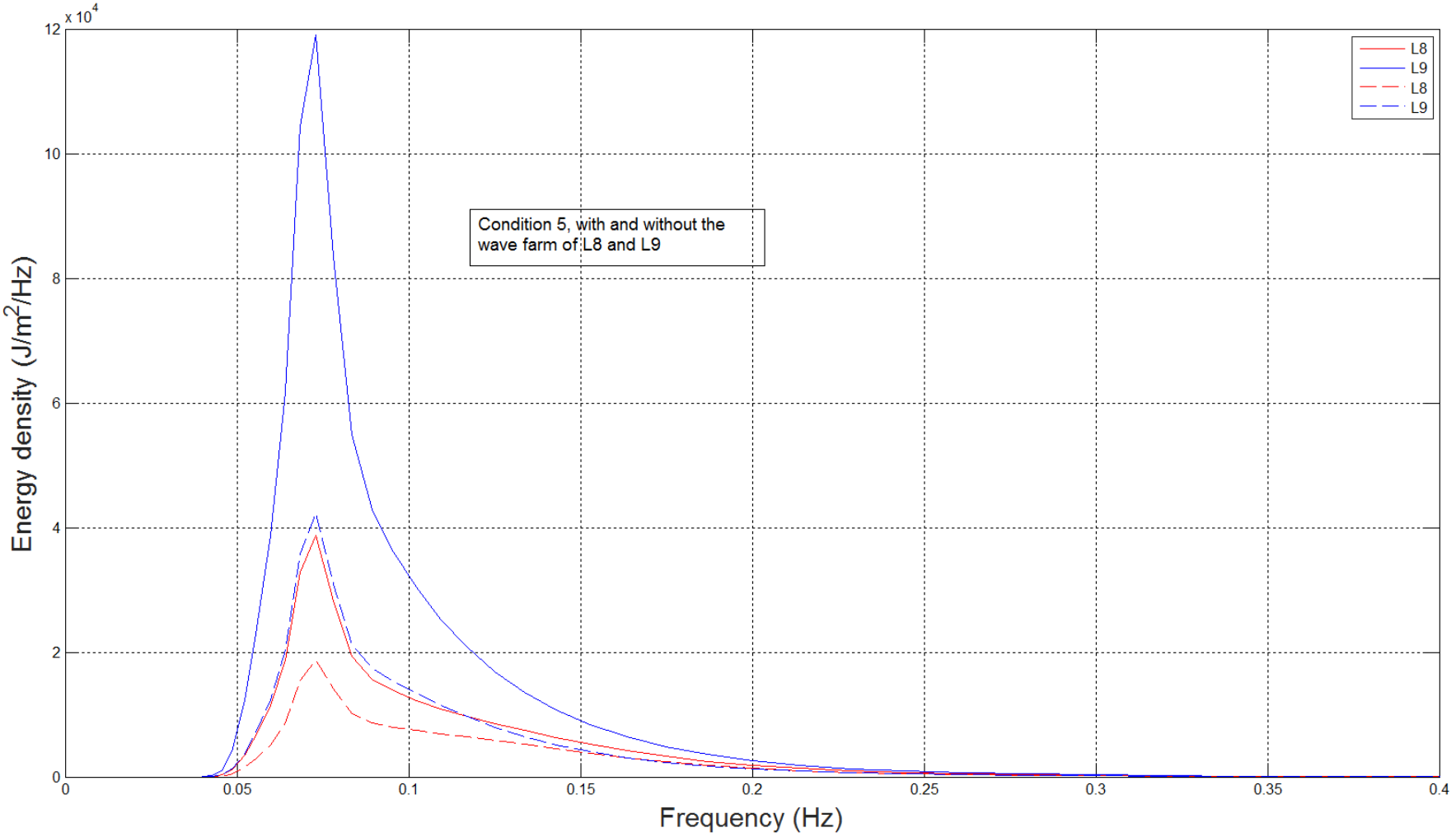

Figure D.14: Wave energy spectrum of L8 and L9 before and after the wave farm of condition 5.

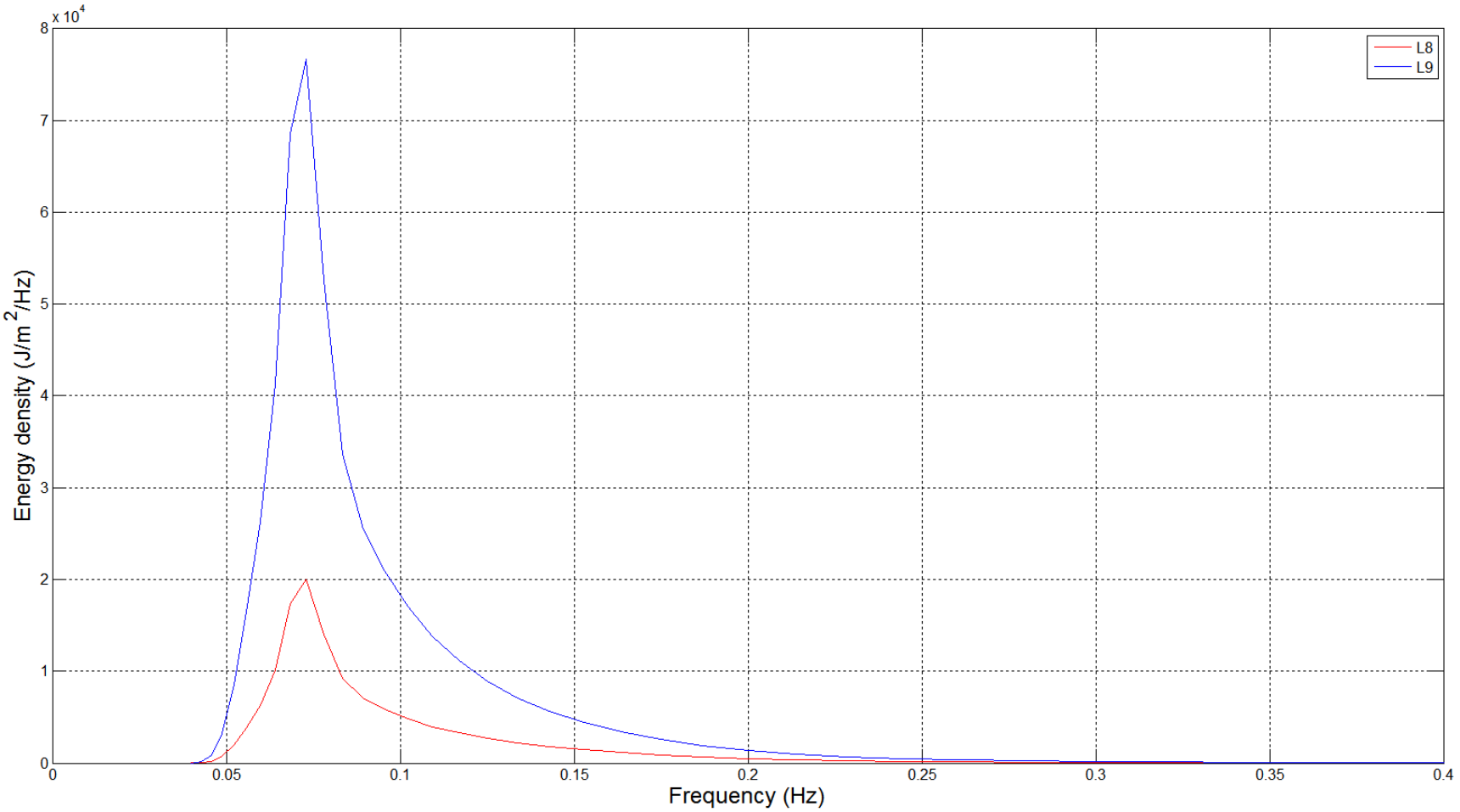

Figure D.15: Wave energy difference for L8 and L9 of condition 5.

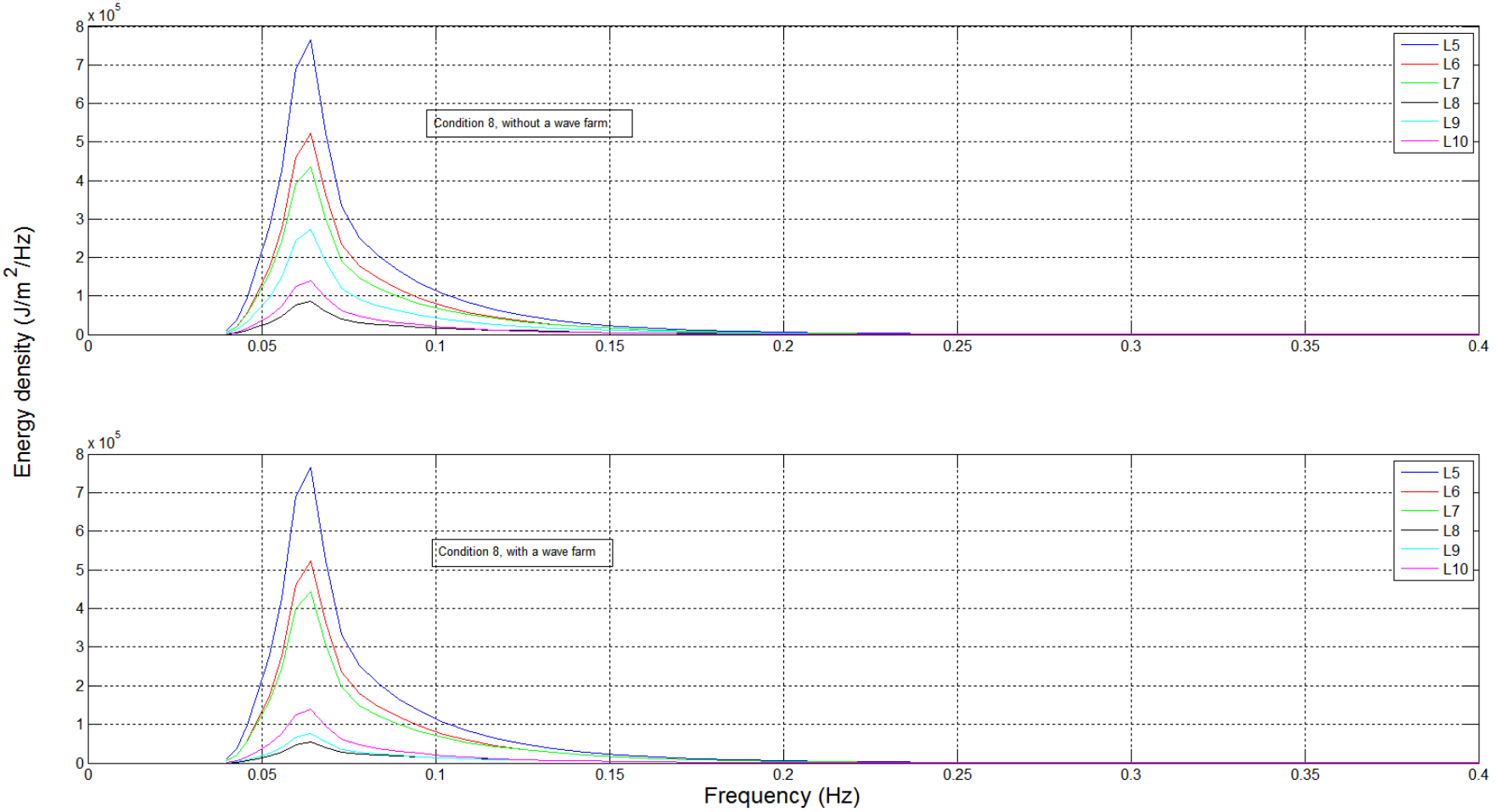

Figure D.16: Wave energy spectrum before and after the wave farm of condition 8.

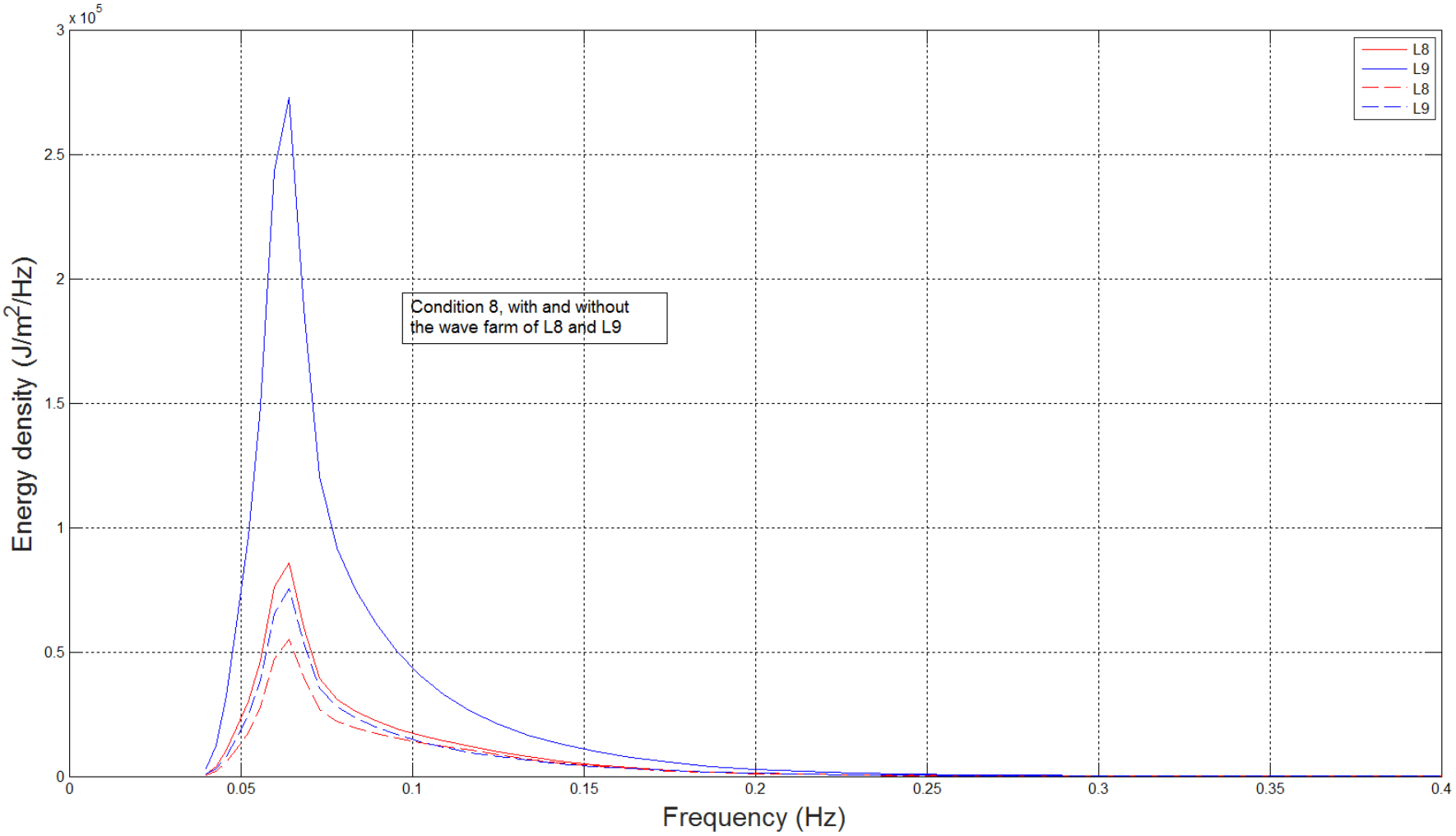

Figure D.17: Wave energy spectrum of L8 and L9 before and after the wave farm of condition 8.

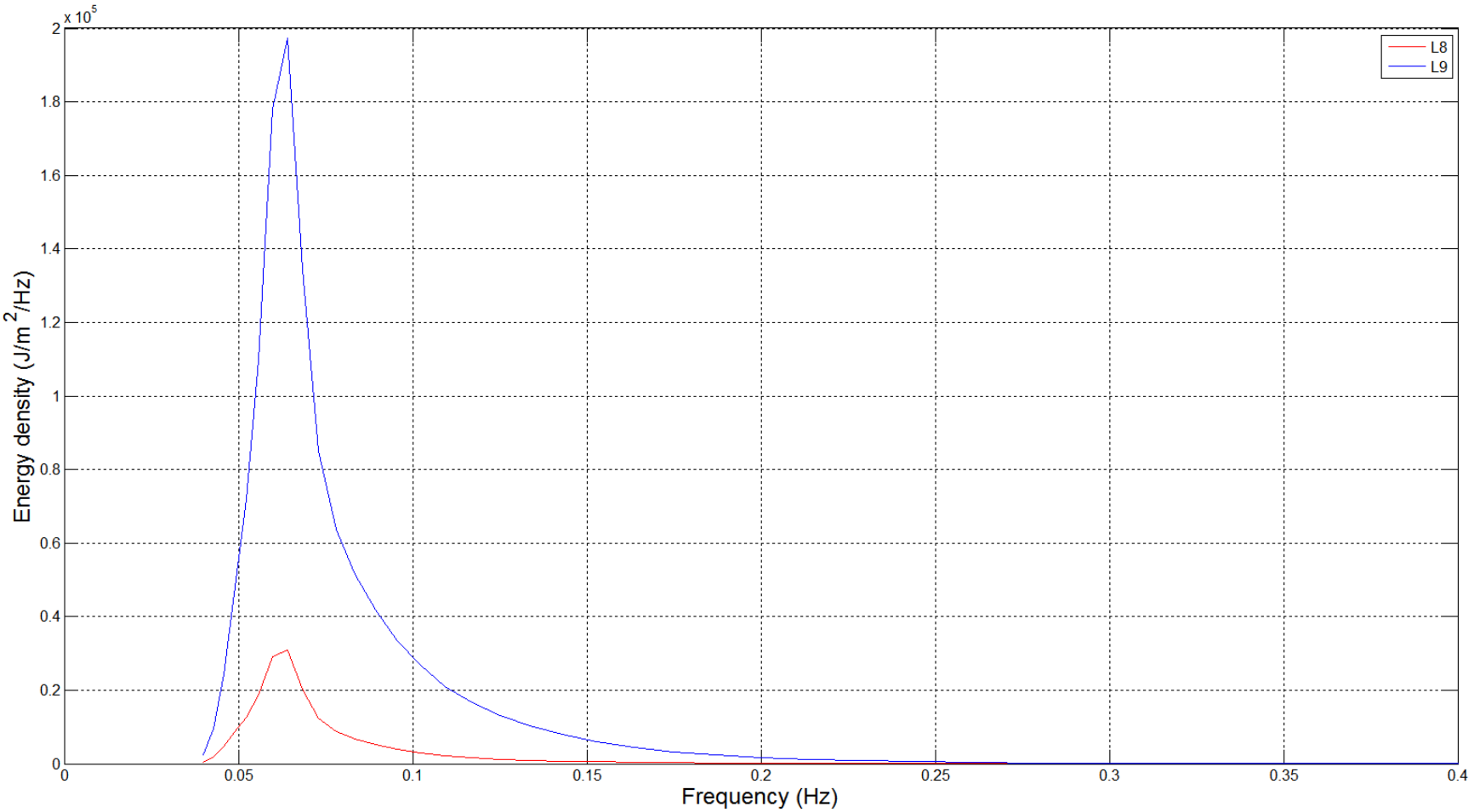

Figure D.18: Wave energy difference for L8 and L9 of condition 8.

List of References

Abanades Tercero, J. (2017). *Beach morphodynamics in the lee of a wave farm: synergies with coastal defence*. Ph.D. thesis, University of Plymouth.

Ailliot, P., Maisondieu, C. and Monbet, V. (2013). Dynamical partitioning of directional ocean wave spectra. *Probabilistic Engineering Mechanics*, vol. 33, pp. 95–102.

Aranuvachapun, S. (1987). Parameters of jonswap spectral model for surface gravity waves ii. predictability from real data. *Ocean engineering*, vol. 14, no. 2, pp. 101–115.

Babarit, A., Hals, J., Muliawan, M., Kurniawan, A., Moan, T. and Krokstad, J. (2012). Numerical benchmarking study of a selection of wave energy converters. *Renewable Energy*, vol. 41, pp. 44–63.

Bahaj, A.S. (2011). Generating electricity from the oceans. *Renewable and Sustainable Energy Reviews*, vol. 15, no. 7, pp. 3399–3416.

Battjes, J.A. and Janssen, J. (1978). Energy loss and set-up due to breaking of random waves. In: *Coastal Engineering 1978*, pp. 569–587.

Beels, C., Troch, P., De Visch, K., Kofoed, J.P. and De Backer, G. (2010). Application of the time-dependent mild-slope equations for the simulation of wake effects in the lee of a farm of wave dragon wave energy converters. *Renewable Energy*, vol. 35, no. 8, pp. 1644–1661.

Behrens, S., Hayward, J., Hemer, M. and Osman, P. (2012). Assesing the wave energy converter potential for australian coastal regions. *Renewable Energy*, vol. 43, pp. 210–217.

Benassai, G. (2006). *Introduction to coastal dynamics and shoreline protection*. Wit Press.

Bento, A.R., Rusu, E., Martinho, P. and Soares, C.G. (2014). Assessment of the changes induced by a wave energy farm in the nearshore wave conditions. *Elsevier*, vol. 71, pp. 50–61.

Bevilacqua, G. and Zanuttigh, B. (2011). Overtopping wave energy converters: general aspects and stage of development.

Booij, N., Ris, R. and Holthuijsen, L.H. (1999). A third-generation wave model for coastal regions: 1. model description and validation. *Journal of geophysical research: Oceans*, vol. 104, no. C4, pp. 7649–7666.

Bosboom, J. and Stive, M.J. (2012). *Coastal Dynamics I: Lectures Notes CIE4305*. VSSD.

Brooke, J. (2003). *Wave energy conversion*, vol. 6. Elsevier.

Carballo, R., Sánchez, M., Ramos, V., Taveira-Pinto, F. and Iglesias, G. (2014). A high resolution geospatial database for wave energy exploitation. *Energy*, vol. 68, pp. 572–583.

Cavaleri, L. and Rizzoli, P.M. (1981). Wind wave prediction in shallow water: Theory and applications. *Journal of Geophysical Research: Oceans*, vol. 86, no. C11, pp. 10961–10973.

CDIP, T.C.D.I.P. (2015). Wave measurement.
Available at: https://cdip.ucsd.edu/?nav=documents&xitem=waves

CEM (2002). Coastal engineering manual. *Engineer Manual*, vol. 1110, pp. 2–1100.

Christensen, L., Friis-Madsen, E. and Kofoed, J.P. (2005). The wave energy challenge: the wave dragon case. In: *POWER-Gen Europe*.

Clément, A., McCullen, P., Falão, A., Fiorentino, A., Gardner, F., Hammarlund, K., Lemonis, G., Lewis, T., Nielsen, K., Petroncini, S., Pontes, M.-T., Schild, P., Sjöström, B.-O., Søresen, H. and Thorpe, T. (2002). Wave energy in europe: current status and perspectives. *Renewable and Sustainable Energy Reviews*, vol. 6, pp. 405–431.

Cooley, J.W. and Tukey, J.W. (1965). An algorithm for the machine calculation of complex fourier series. *Mathematics of computation*, vol. 19, no. 90, pp. 297–301.

CRSES (2015). technologies, ocean.
Available at: http://www.crses.sun.ac.za/technologies-ocean

CSIR (2015). History of ocean wave recording in south africa.
Available at: http://wavenet.csir.co.za/history.htm

Davidson-Arnott, R. (2010). *Introduction to coastal processes and geomorphology*. Cambridge University Press.

Denny, M.W. and Gaines, S.D. (2007). *Encyclopedia of tidepools and rocky shores*. 1. Univ of California Press.

Dhanak, M.R. and Xiros, N.I. (2016). *Springer Handbook of Ocean Engineering*. Springer.

Diaconu, S. and Rusu, E. (2013). The environmental impact of a wave dragon array operating in the black sea. *The Scientific World Journal*, vol. 2013.

Drew, B., Plummer, A. and Sahinkaya, M. (2009). A review of wave energy converter technology. *Power and Energy*, vol. 223, p. 887.

Du Plessis, J. (2012). *A hydraulic wave energy converter*. Ph.D. thesis, Stellenbosch: Stellenbosch University.

EMEC, T.E.M.E.C.L. (2015). Pelamis wave power.
Available at: http://www.emec.org.uk/about-us/wave-clients/pelamis-wave-power

Erselcan, İ.Ö. and Kükner, A. (2014). A review of power take-off systems employed in wave energy converters. *Journal of Naval Science and Engineering*, vol. 10, no. 1, pp. 32–44.

Folley, M. (2016). *Numerical Modelling of Wave Energy Converters: State-of-the-Art Techniques for Single Devices and Arrays*. Academic Press.

Folley, M., Whittaker, T. and Osterried, M. (2004). The oscillating wave surge converter. *Renewable Energy*, vol. 377, pp. 1–5.

Gilhousen, D.B. and Hervey, R. (2002). Improved estimates of swell from moored buoys. In: *Ocean Wave Measurement and Analysis (2001)*, pp. 387–393.

Goda, Y. (2010). *Random seas and design of maritime structures*. World scientific.

Greenwood, C.E., Christie, D. and Venugopal, V. (2013). The simulation of nearshore wave energy converters and their associated impacts around the outer hebrides. In: *10th Eur. Wave Tidal Energy Conf.(EWTEC 2013)*.

Guedes Soares, C., Bhattacharjee, J. and Karmakar, D. (2014). Overview and prospects for development of wave and offshore wind energy. *Brodogradnja*, vol. 65, no. 2, pp. 87–109.

Harris, R.E., Johanning, L. and Wolfram, J. (2004). Mooring systems for wave energy converters: A review of design issues and choices. In: *3rd international conference on marine renewable energy, Blyth, UK*, pp. 180–189.

Hasselmann, K., Barnett, T., Bouws, E., Carlson, H., Cartwright, D., Enke, K., Ewing, J., Gienapp, H., Hasselmann, D., Kruseman, P. *et al.* (1973). Measurements of wind-wave growth and swell decay during the joint north sea wave project (jonswap). Tech. Rep., Deutches Hydrographisches Institut.

He, H., Qu, Q. and Li, J. (2013). Numerical simulation of section systems in the pelamis wave energy converter. *Advances in Mechanical Engineering*.

Holthuijsen, L.H. (2010). *Waves in oceanic and coastal waters*. Cambridge University Press.

Hwang, P.A., Ocampo-Torres, F.J. and García-Nava, H. (2012). Wind sea and swell separation of 1d wave spectrum by a spectrum integration method. *Journal of Atmospheric and Oceanic Technology*, vol. 29, no. 1, pp. 116–128.

Jamasb, T., Nuttall, W.J. and Pollitt, M.G. (2006). *Future electricity technologies and systems*, vol. 67. Cambridge University Press.

Joubert, J. and Van Niekerk, J. (2009). Recent developments in wave energy along the coast of southern africa. In: *European Wave Tidal Energy Conference*, pp. 1096–1100.

Joubert, J.R. (2008). *An investigation of the wave energy resource on the South African coast, focusing on the spatial distribution of the south west coast*. Master's thesis, Mechanical Engineering, University of Stellenbosch, Stellenbosch, South Africa.

Joubert, J.R. (2013). *Design and development of a novel wave energy converter*. Ph.D. thesis, Mechanical Engineering, University of Stellenbosch, Stellenbosch, South Africa.

Kamphuis, J.W. (2010). *Introduction to coastal engineering and management*, vol. 30. World Scientific Publishing Co Inc.

Kofoed-Hansen, H., Kerper, D.R., Sørensen, O.R. and Kirkegaard, J. (2005). Simulation of long wave agitation in ports and harbours using a time-domain boussinesq model. In: *Proceedings of the Fifth International Symposium on Ocean Wave Measurement and Analysis (WAVES)*. *IAHR Secretariat, Madrid, Spain*.

Komen, G., Hasselmann, K. and Hasselmann, K. (1984). On the existence of a fully developed wind-sea spectrum. *Journal of physical oceanography*, vol. 14, no. 8, pp. 1271–1285.

Komen, G.J., Cavaleri, L. and Donelan, M. (1996). *Dynamics and modelling of ocean waves*. Cambridge university press.

Kumar, V.S. and Kumar, K.A. (2008). Spectral characteristics of high shallow water waves. *Ocean Engineering*, vol. 35, no. 8, pp. 900–911.

Lakhan, V.C. (2003). *Advances in coastal modelling*, vol. 67. Elsevier.

Liberti, L., Carillo, A. and Sannino, G. (2013). Wave energy resource in the mediterranean, the italian perspective. *Renewable Energy*, vol. 50, pp. 938–949.

Lucas, C. and Soares, C.G. (2015). On the modelling of swell spectra. *Ocean Engineering*, vol. 108, pp. 749–759.

MacHutchon, K.R. (2006). *The characterisation of South African sea storms*. Master's thesis, Mechanical Engineering, University of Stellenbosch, Stellenbosch, South Africa.

Madsen, P.A. and Sørensen, O.R. (1992). A new form of the boussinesq equations with improved linear dispersion characteristics. part 2. a slowly-varying bathymetry. *Coastal engineering*, vol. 18, no. 3-4, pp. 183–204.

Mansard, E. and Funke, E. (1991). On the fitting of jonswap spectra to measured sea states. In: *Coastal Engineering 1990*, pp. 464–477.

Margheritini, L., Hansen, A.M. and Frigaard, P. (2012). A method for eia scoping of wave energy converters based on classification of the used technology. *Environmental Impact Assessment Review*, vol. 32, no. 1, pp. 33–44.

Marx, C., LW, C., M, R., de Watt, H. and AC Van, W. (1993). Agulhas bank metocean data summary 1993 update of environmental design parameters: Waves. Tech. Rep., CSIR REPORT EMAS-C 93046.

McDonald, D.A. (2012). *Electric capitalism: Recolonising Africa on the power grid*. Routledge.

Miles, J.W. (1957). On the generation of surface waves by shear flows. *Journal of Fluid Mechanics*, vol. 3, no. 02, pp. 185–204.

Miles, J.W. (1981). Hamiltonian formulations for surface waves. *Applied Scientific Research*, vol. 37, no. 1, pp. 103–110.

Millar, D., Smith, H. and Reeve, D. (2007). Modelling analysis of the sensitivity of shoreline change to a wave farm. *Ocean engineering*, vol. 34, no. 5, pp. 884–901.

Mitsuyasu, H., Tasai, F., Suhara, T., Mizuno, S., Ohkusu, M., Honda, T. and Rikiishi, K. (1975). Observations of the directional spectrum of ocean waves using a cloverleaf buoy. *Journal of Physical Oceanography*, vol. 5, no. 4, pp. 750–760.

Ochi, M.K. and Hubble, E.N. (1977). Six-parameter wave spectra. In: *Coastal Engineering 1976*, pp. 301–328.

O'Dea, A.M., Haller, M.C. *et al.* (2014). Analysis of the impacts of wave energy converter arrays on the nearshore wave climate.

Olsson, D.M. and Nelson, L.S. (1975). The nelder-mead simplex procedure for function minimization. *Technometrics*, vol. 17, no. 1, pp. 45–51.

Parente, C.E., Robinson, I.S. and Nunes, L.M.P. (2002). On the growth of wind-generated waves in a swell-dominated region in the south atlantic.

Parry, M.L., Canziani, O., Palutikof, J.P., van der Linden, P.J. and Hanson, C.E. (2007). Contribution of working group ii to the fourth assessment report of the intergovernmental panel on climate change, 2007. *Climate change*.

Pecher, A. and Kofoed, J.P. (2017). Introduction. In: *Handbook of Ocean Wave Energy*, pp. 1–15. Springer.

Phillips, O.M. (1957). On the generation of waves by turbulent wind. *J. Fluid Mech*, vol. 2, no. 5, pp. 417–445.

Phillips, O.M. (1958). The equilibrium range in the spectrum of wind-generated waves. *Journal of Fluid Mechanics*, vol. 4, no. 04, pp. 426–434.

Pierson, W.J. and Moskowitz, L. (1964). A proposed spectral form for fully developed wind seas based on the similarity theory of sa kitaigorodskii. *Journal of geophysical research*, vol. 69, no. 24, pp. 5181–5190.

Pinet, P.R. (2012). *Essential Invitation to Oceanography*. Jones & Bartlett Publishers.

Polinder, H. and Scuotto, M. (2005). Wave energy converters and their impact on power systems. In: *Future Power Systems, 2005 International Conference on*, pp. 9–pp. IEEE.

Radder, A. and Dingemans, M. (1985). Canonical equations for almost periodic, weakly nonlinear gravity waves. *Wave motion*, vol. 7, no. 5, pp. 473–485.

Rashmi, R., Aboobacker, V., Vethamony, P. and John, M. (2013). Co-existence of wind seas and swells along the west coast of india during non-monsoon season. *Ocean Science*, vol. 9, no. 2, p. 281.

Rasmeemasmuang, T. and Weesakul, S. (2009). One-line model using the combination of polar and cartesian coordinates for crenulate shaped bay. In: *Proceedings Of Coastal Dynamics 2009: Impacts of Human Activities on Dynamic Coastal Processes (With CD-ROM)*, pp. 1–14.

Reeve, D., Chadwick, A. and Fleming, C. (2004). *Coastal engineering: processes, theory and design practice*. CRC Press.

Roberts, J.D., Chang, G. and Jones, C. (2014). Investigation of wave energy converter effects on near-shore wave fields: Model generation validation and evaluation-kaneohe bay hi. Tech. Rep., Sandia National Laboratories (SNL-NM), Albuquerque, NM (United States).

Roelvink, D., Reniers, A., Van Dongeren, A., Van Thiel de Vries, J., Lescinski, J. and McCall, R. (2010). Xbeach model description and manual. *Unesco-IHE Institute for Water Education, Deltares and Delft University of Tecnhology. Report June*, vol. 21, p. 2010.

Rossouw, J. (1984). *Review of existing wave data, wave climate and design waves for South African and South West African (Namibian) coastal waters*. CSIR-National Research Institute for Oceanology.

Rossouw, J. (1989). *Design waves for the South African coastline*. Ph.D. thesis, Stellenbosch: University of Stellenbosch.

Rossouw, M., Terblanche, L. and Moes, J. (2013). General characteristics of long waves around the south african coast.

Salimullah, S.M., Rafi, M. and Sheikh, M. (2014). Prospects of wave power in bangladesh. *American Journal of Engineering Research (AJER)*, vol. 3, pp. 29–35.

Saulnier, J.-B. and Le Crom, I. (2013). Peakedness of wave systems observed on the french wave energy test site (sem-rev) using a spectral partitioning algorithm. In: *ASME 2013 32nd International Conference on Ocean, Offshore and Arctic Engineering*, pp. V008T09A096–V008T09A096. American Society of Mechanical Engineers.

Silva, D., Rusu, E. and Soares, C.G. (2013). Evaluation of various technologies for wave energy conversion in the portuguese nearshore. *Energies*, vol. 6, no. 3, pp. 1344–1364.

Smith, E.H. (2013). *Mechanical engineer's reference book*. Butterworth-Heinemann.

Smith, H. (2008). Nearshore model calibration for wave energy resources and impact assessment. 2^{nd} International Conference on Ocean Energy (ICOE), Brest, France.

Smith, H.C., Pearce, C. and Millar, D.L. (2012). Further analysis of change in nearshore wave climate due to an offshore wave farm: An enhanced case study for the wave hub site. *Renewable Energy*, vol. 40, no. 1, pp. 51–64.

Soares, C.G. (1991). On the occurence of double peaked wave spectra. *Ocean Engineering*, vol. 18, no. 1-2, pp. 167–171.

Soares, C.G. (1999). The bivariate distribution of wave heights and periods in mixed sea states.

Soares, C.G. (2015). *Renewable Energies Offshore*. CRC Press.

Soares, C.G. and Nolasco, M. (1992). Spectral modelling of sea states with multiple wave systems. *Journal of Offshore Mechanics and Artic Engineering*, pp. 278–284.

Sorensen, R.M. (2005). *Basic coastal engineering*, vol. 10. Springer Science & Business Media.

Tabak, J. (2009). *Wind and Water*, vol. 6. Infobase Publishing.

Thorpe, T.W. (1999). *A brief review of wave energy*. Harwell Laboratory, Energy Technology Support Unit.

Torsethaugen, K., Haver, S. *et al.* (2004). Simplified double peak spectral model for ocean waves. In: *The Fourteenth International Offshore and Polar Engineering Conference*. International Society of Offshore and Polar Engineers.

Van Ballegooyen, R., Luger, S. and Monteiro, P. (2002). Integrated port design using a suite of coupled numerical models. In: *State of Kuwait*. Proceeedings of the International Conference on Coastal Zone Management and Development.

Van der Borch van Verwolde, E. (2004). *Characteristics of extreme wave events and the correlation between atmospheric conditions along the South African coast*. Master's thesis, Oceanography: University of Cape Town, Cape Town, South Africa.

Van der Westhuysen, A. (2002). *The application of the numerical wind wave model SWAN to a selected field case on the South African coast*. Master's thesis, Mechanical Engineering, University of Stellenbosch, Stellenbosch, South Africa.

Van Tonder, A. (1994). *The development and testing of a system for the measurement of directional wave spectra in the nearshore coastal zone*. Ph.D. thesis, Mechanical Engineering, University of Stellenbosch, Stellenbosch, South Africa.

Veigas, M. and Iglesias, G. (2014). Potentials of a hybrid offshore farm for the island of fuerteventura. *Energy Conversion and Management*, vol. 86, pp. 300–308.

Venugopal, V. and Smith, G. (2007). Wave climate investigation for an array of wave power devices. In: *Proceedings of the 7th European wave and tidal energy conference, Porto, Portugal*, pp. 11–14.

Walker, H.J. (2012). *Artificial structures and shorelines*, vol. 10. Springer Science & Business Media.

Wang, D.W. and Hwang, P.A. (2001). An operational method for separating wind sea and swell from ocean wave spectra. *Journal of Atmospheric and Oceanic Technology*, vol. 18, no. 12, pp. 2052–2062.

Warren, I. and Bach, H. (1992*a*). Mike 21: a modelling system for estuaries, coastal waters and seas. *Environmental Software*, vol. 7, no. 4, pp. 229–240.

Warren, I. and Bach, H. (1992*b*). Mike 21: a modelling system for estuaries, coastal waters and seas. *Environmental Software*, vol. 7, no. 4, pp. 229–240.

Yemm, R., Pizer, D., Retzler, C. and Henderson, R. (2012). Pelamis: experience from concept to connection. *Phil. Trans. R. Soc. A*, vol. 370, no. 1959, pp. 365–380.

Young, I. and Verhagen, L. (1996). The growth of fetch limited waves in water of finite depth. part 2. spectral evolution. *Coastal Engineering*, vol. 29, no. 1-2, pp. 79–99.

Young, I.R. (1999). *Wind generated ocean waves*, vol. 2. Elsevier.

Zanopol, A.T., Onea, F. and Rusu, E. (2014). Studies concerning the influence of the wave farms on the nearshore processes. *International Journal of Geosciences*, vol. 2014.